

257

OXYGEN TRANSFER AND BUBBLE FLOW IN SPLIT-CYLINDER AIRLIFT TOWERS

by

MARK E. ORAZEM

B. S., Kansas State University, 1976

A MASTER'S THESIS

submitted in partial fulfillment of the

requirements for the degree


MASTER OF SCIENCE

Department of Chemical Engineering

KANSAS STATE UNIVERSITY
Manhattan, Kansas

May, 1978

Approved by:



L. E. Erickson, Major Professor

Document
LD
2668
.T4
1978
072
c.2

TABLE OF CONTENTS

Chapter I	INTRODUCTION	1
Chapter II	OXYGEN TRANSFER IN FERMENTATION SYSTEMS	3
	Introduction.	3
	Material Parameters	5
	Process Related Parameters.	6
	Geometric Parameters.	8
	Single Stage Fermentors	8
	Multi-Stage Fermentors.	11
	Notation.	13
	References.	15
Chapter III	OXYGEN TRANSFER RATES AND EFFICIENCIES IN ONE AND TWO STAGE AIRLIFT TOWERS	23
	Introduction	23
	Materials and Methods	25
	Results and Discussion.	28
	Gas Hold-up	28
	Oxygen Transfer Characteristics	29
	Performance Ratio	32
	Comparison with Literature.	33
	Conclusions	35
	Notation.	36
	References.	37
Appendix A:	Sulfite Oxidation Technique.	53
	References.	58
Appendix B:	Data Summary.	60

Chapter IV STATISTICAL ANALYSIS OF BUBBLE FLOW IN THE DOWNFLOW SECTION OF THE AIRLIFT TOWER	71
Introduction	71
Theoretical	73
Experimental	84
Facilities	85
Probe	85
Signal Analysis System	86
Airlift Tower	87
Procedures	87
Verification of Cross-Covariance Technique	88
Analysis of Bubble Flow in the Airlift Tower	88
Results and Discussion	89
Verification of Cross-Covariance Technique	90
Analysis of Bubble Flow in the Airlift Tower	93
Conclusions	98
Notation	100
References	102
Appendix A: Construction of Conductivity Probes	137
Design Factors	137
Procedure	138
Appendix B: Block Diagram of Response Signal Treatment System	143
Appendix C: Data Summary for Airlift Tower	144
Appendix D: Data Summary for Verification of Cross-Covariance Technique	152
Chapter V CONCLUDING REMARKS	153
Conclusions	153
Recommendations	155
References	157
Acknowledgement	160

Chapter I

INTRODUCTION

Gas-liquid contacting with a continuous liquid phase is an essential process in chemical and biochemical industries. Many reactions are controlled by the transfer of a component from the gas phase to the liquid phase. The mass transfer characteristics of gas-liquid contacting devices, therefore, have been extensively studied.

Gas-liquid contacting is traditionally provided by bubble columns and by agitated vessels. Many researchers have shown that separating the bubble column into stages results in improved mass transfer characteristics. Similar results have been presented for the stage-wise separation of agitated vessels.

One of the more promising contactor designs for high mass transfer rates with low power consumption is the airlift tower. The airlift tower is a bubble column divided into two sections. The gas is sparged into one section, causing the dispersion density in that section to be lower than the density in the unsparged section. The resulting pressure difference causes liquid circulation. An upward liquid velocity is observed in the sparged section, and a downward liquid velocity is observed in the unsparged section. The downward liquid flow entrains some gas, therefore mass transfer can take place in all parts of the tower.

A discussion of the effects of material, process related and geometric parameters on mass transfer is presented in Chapter II. The mass transfer coefficients reported for the airlift tower, bubble column, agitated vessel, staged bubble column and staged agitated vessel are compared.

Staging has been shown to improve the mass transfer characteristics of bubble columns and agitated vessels. It is likely, therefore, the

staged airlift tower will exhibit superior mass transfer characteristics as compared to the single stage airlift tower. A comparison of one-stage and two-stage airlift towers is presented in Chapter III. The comparison is based on mass transfer rates and efficiencies at superficial gas velocities ranging from 0.120 m/s to 0.455 m/s.

The optimal design and operation of large scale airlift towers are contingent upon the successful modeling and prediction of performance. An understanding of the gas phase flow is necessary to model the airlift tower. The gas phase in the sparged region (upflow) is present as bubbles in turbulent upward flow. The bubble flow in the unsparged (downflow) region is more complex. The forces acting on a bubble in the downflow region are the buoyant force, acting in the upward direction, and the drag force, acting in the downward direction. The bubble flow in the downflow region, therefore, has both upward and downward components of flow.

In Chapter IV a statistical method is introduced to analyze the bubble flow for an air-water system in the downflow section of a one-stage airlift tower. This method is theoretically developed, experimentally verified and applied to the airlift tower to measure local time averaged bubble velocities and void fractions. The flowrates of the gas phase in the upward and downward direction were determined at two axial positions for superficial gas velocities ranging from 0.0682 m/s to 0.3115 m/s. The bulk liquid circulation rate and regional hold-ups were obtained to characterize the airlift tower.

Chapter V presents conclusions and recommendations for future work.

OXYGEN TRANSFER IN FERMENTATION SYSTEMS

Introduction

Submerged aerobic fermentation has found application in areas ranging from waste treatment to manufacture of pharmaceuticals and food products. Of great interest is the production of single cell protein (SCP) for animal or human consumption⁽¹⁻³⁾. Substrates for SCP production include energy source materials such as petroleum derivatives, waste material such as bagasse and animal manure, and renewable source material such as cellulose and sugar⁽⁴⁾. The economic viability of production of SCP from these substrates hinges in large degree upon the growth rate of the microorganisms employed.

Of the nutrients necessary for microbial growth, oxygen has the lowest solubility in the liquid phase. The design of fermentation equipment is oriented, therefore, toward maximizing the oxygen supply available for cell growth while minimizing the power requirement⁽⁵⁾.

Schlegel⁽⁶⁾ has recently reported that oxygen can be successfully supplied to a culture by adding hydrogen peroxide to a shaking flask under nitrogen blanket. Cell concentrations achieved were comparable to those achieved in shaking flasks under open atmosphere. Most fermentations, however, depend on the mass transfer of oxygen from the gas phase to the liquid to provide the required oxygen.

The fermentation process typically entails a three phase system, containing the cell, medium and gas phases. The mechanism of oxygen transfer in such a system involves three steps in series. The oxygen is transferred from the gas phase to the liquid phase, and then from the liquid phase to the cells. At the cell-liquid interface a chemical reaction takes place with the oxidizable substrates through the respiratory enzymes

of the cell.^(7,8) The oxygen transfer steps may encounter a gas-film resistance and a liquid film resistance at the gas-liquid interface, a liquid film resistance at the liquid-cell interface, as well as a bulk liquid diffusional resistance⁽⁹⁾.

A detailed treatment of the transport equations for multi-phase systems has been presented by Whitaker⁽¹⁰⁾. The treatment associates every point in space with an averaging volume large enough to give rise to a continuous, well-behaved, space-averaged value of a state variable ψ for each phase. For momentum transport, ψ represents the momentum vector, ρv . Whitaker's time smoothed relationship, modified by Gray⁽¹¹⁾ and applied to mass transport in a given phase "i", is

$$\frac{\partial C_i}{\partial t} + v_i \cdot \nabla C_i = \nabla \cdot (D_i \cdot \nabla C_i) - \sum_j K_{ij} a_{ij} (C_i - C_i^o) + R_i \quad (1)$$

where C is the molar concentration, v is the mass average velocity, t is time, D is the mass dispersion tensor, K is the overall mass transfer coefficient, a is the interfacial area between phases i and j , C^o is the equilibrium molar concentration, and R is the molar rate of production due to reaction. This relationship holds under the assumptions that no phase change occurs, the fluid is incompressible, the concentration of the diffusing species is small and the fluctuation terms resulting from time averaging are negligible.

A fermentation system can be described by equation (1) with oxygen as the diffusing species. When the oxygen transfer resistance of the cell is negligible, the cell can be treated as a reacting species. The production term in equation (1) is replaced by the volumetric oxygen consumption rate of the cells as follows:

$$\frac{\partial C_i}{\partial t} + v_i \cdot \nabla C_i = \nabla \cdot (D \cdot \nabla C_i) - \sum_j K_{ij} a_{ij} (C_i - C_i^0) - rX \quad (2)$$

where r is the specific oxygen uptake of the cells and X is the cell concentration. If the fermentor is well mixed the concentration gradients are zero. Thus, we have

$$\frac{\partial C_i}{\partial t} = \sum_j K_{ij} a_{ij} (C_i^0 - C_i) - rX \quad (3)$$

The gas film resistance has been shown to be negligible in fermentation systems⁽¹²⁻¹⁴⁾, and thus, in the liquid phase the relationship becomes

$$\frac{\partial C}{\partial t} = K_L a (C^* - C) - rX \quad (4)$$

where $K_L a$ is the overall oxygen transfer coefficient based on the liquid side resistance controlling, and C^* is the phase equilibrium dissolved oxygen concentration

Mass transfer in a gas-liquid contacting system is affected by a number of parameters which can be classified as material, process related or geometric.

Material Parameters

For low liquid viscosity systems the interfacial properties are the important material parameters. In slow bubble formation at an open vertical tube immersed in a liquid the bubble grows until its buoyancy exceeds the surface tension holding it to the tube. The surface tension in this case controls the bubble size and hence, the interfacial area. In rapid bubble formation, however, the effect of surface tension is less pronounced, and for constant flow conditions with a large pressure drop across the sparger the surface tension becomes insignificant compared to the inertial forces.⁽¹⁵⁾

In pure water, bubbles will coalesce easily after being sparged, but the addition of impurities hinders coalescence. This has been explained

in terms of a change in surface viscosity or elasticity due to the addition of surface active compounds,⁽¹⁵⁾ but such compounds are not the only substances which affect this observation. The addition of electrolytes to water hinders coalescence because of the formation of electrical double layers around gas bubbles which become negatively charged and repel each other.^(16,17) Zlokarnik⁽¹⁶⁾ has shown that a salt concentration of 10 g/l enhances the absorption rate five-fold and its influence increases until at 100 g/l the enhancement is almost seven-fold. The surface pressure, defined as the difference between the surface tension of water and that of the solution, was shown to be an insignificant parameter in the coalescence phenomena.

A surface tension gradient, caused by a temperature or concentration gradient along the interface, can create surface turbulence and increase the interfacial area. This, in turn, increases the mass transfer rates⁽¹⁵⁾. Interfacial properties seem to affect mass transfer primarily through the interfacial area by promoting or hindering coalescence and interfacial turbulence.

Process Related Parameters

The mass transfer coefficients in gas-liquid systems have been empirically or semi-empirically related to process related parameters. The parameters employed include the volume flowrate of gas per unit liquid volume, q/V , and the power consumption per unit liquid volume, P/V .⁽¹⁶⁾ Frequently the power consumed in mixing under ungasged conditions, P_o , is employed.

The oxygen transfer coefficient in a simple bubble column has been related to the superficial gas velocity by an equation of the form

$$K_L a = I v_s^\alpha \quad (5)$$

where C and α are constants that depend on column geometry, sparger design and void fraction⁽¹⁸⁾.

In a bubble column with mechanical agitation the correlation is made in terms of the power of agitation

$$K_L a = I P_m^n \quad (6)$$

where I and n are constants. This works well for the special case where the power consumed in aeration is small. Miller⁽¹⁹⁾ and Tojo⁽²⁰⁾ have recommended consideration of the effective power as

$$P_e = P_m + I_2 P_a \quad (7)$$

where P_e is the effective power consumption, P_m is the power consumed in mixing and P_a is the power consumed in compression of the gas. I_2 is a weighting factor. The oxygen transfer coefficient now becomes

$$K_L a = I_1 (P_m + I_2 P_a)^n \quad (8)$$

where I_1 and n are constants that depend on the type of contacting device. The Miller correlation can be used to describe systems not employing mechanical agitation by assigning a zero value to P_m , making it a general correlation.

The power consumption can be related to material and system parameters such as the Weber number, Aeration number and liquid and dispersion densities. Such a correlation is presented by Hassan and Robinson⁽²²⁾

$$\frac{P_m}{P_o} = I N_{We}^m N_A^n \left(\frac{\rho_L}{\rho_D}\right) \quad (9)$$

where I , and n are functions of impeller size, tank size and electrolytic nature of the aqueous phase.

Geometric Parameters

The primary geometric consideration is the type of contacting device. Some of the fermentors are shown in Tables 1 and 2. They are classified as single and multi-stage fermentors.

Single Stage Fermentors

The fermentors used traditionally in industry are the bubble column and agitated tank, generally operated in a batch mode. The chief advantage of bubble columns is that they have no moving parts, thus eliminating the need for seals and reducing maintenance expense. Bubble columns require a small amount of floor space, and fermentation heat transfer requirements are easily provided through the tower walls. Mashelkar⁽²²⁾ has reported that coalescence will cause a reduction in interfacial area which reduces the oxygen transfer rate in bubble columns with length-to-diameter ratios greater than 12. This effect is dependent upon the material parameters.

Yoshida et al.⁽¹⁴⁾ have reported an oxygen transfer coefficient of 6.7 min^{-1} at a superficial gas velocity of 1333 cm/min for a sodium sulfite-air system. Mashelkar⁽²³⁾ has found a mass transfer coefficient of 7.8 min^{-1} at a superficial gas velocity of 2400 cm/min for absorption of CO_2 in a sodium carbonate, sodium bicarbonate buffer solution. Other representative values of mass transfer rates^(24,25) are shown in Table 1.

The efficiency of oxygen transfer can be shown by the performance ratio defined as the rate of oxygen transfer divided by the power consumed in achieving that transfer rate.⁽¹⁸⁾

$$\xi = \frac{N_{\text{O}_2}}{P} \quad (10)$$

A high value of the performance ratio indicates a high oxygen transfer efficiency. The bubble column typically exhibits a high performance ratio

at low oxygen transfer rates, but as shown in Fig. 1, this value decreases rapidly with an increase in the oxygen transfer rate. This is due primarily to bubble coalescence and inadequate liquid phase mixing.

To increase the oxygen transfer rates, agitation is applied to the bubble column. This agitation increases liquid mixing and the interfacial area. The liquid and gas phases can be considered as completely mixed, and since a high air flow rate is not needed to generate mixing, the gas input to the agitated fermentor can be reduced considerably.

Fukuda et al.⁽²⁶⁾ reports oxygen transfer rates ranging from 2.6 to 13.8 min^{-1} in a turbine agitated sodium sulfite-air system. Their results are reviewed by Hospodka et al.⁽²⁷⁾ Agitated tanks are characterized by higher oxygen transfer rates than found in bubble columns, but the total power consumption is high. The performance ratio can be seen in Fig. 1 to be low for agitated tanks.

Many novel gas-liquid contacting devices have been investigated, including several that depend on gas entrainment to achieve oxygen transfer^(18,27-33). One of the more promising of these designs is the air-lift tower invented by Lefrancois et al.⁽³⁴⁾ in 1954. This device, shown in Fig. 2, can be described as a bubble column divided into two sections. Air is sparged into one of these sections, causing the dispersion in that section to have a lower density than the ungasged section. The resulting pressure difference causes liquid circulation. In essence, the airlift tower provides liquid agitation and mixing by using a high gas flowrate. The airflow rate in the airlift tower is generally larger than that in the agitated tank, and the need for mechanical agitation is eliminated. The airlift tower has been described by Hatch⁽¹⁸⁾ as having

three regions: the upflow region, the downflow region, and the head region consisting of the two phase dispersion above the upflow and downflow regions. It is in the head region that gas disengagement takes place. Gas bubbles are entrained by the downward flow of liquid in the downflow region so oxygen transfer can take place in all parts of the airlift tower.

The airlift tower has no moving parts; therefore, the need for seals is eliminated. Maintenance expenses are low as compared to the agitated tank, and the downward flow of liquid from the head region of the tower reduces some of the foaming problems found in fermentation in bubble columns at similar oxygen transfer rates. The performance of the airlift tower in mass transfer applications is good.

Hatch⁽¹⁹⁾ found oxygen transfer rates of up to 6.3 min^{-1} for a concentric cylinder airlift with candida intermedia on n-alkanes. Gasner⁽³²⁾ investigated a rectangular airlift with a baffle separating the upflow and downflow sections and found a $K_L a$ of 9.7 min^{-1} . He has suggested that the rectangular system inherently has less coalescence than the concentric cylinder airlift due to configurational differences. A further modification of the airlift tower is described by Belfield⁽³³⁾ who found a $K_L a$ of 7.8 min^{-1} in a cylinder split into two equal sections by a baffle. This split cylinder airlift has a lower wetted-surface-to-volume ratio than the concentric cylinder airlift tower which increases the liquid circulation rate and hence the liquid mixing. The ease of construction of the split cylinder airlift makes this fermentor design attractive.

Ho⁽³⁵⁾ has modeled the airlift tower by treating the upflow region as N tanks-in-series, the downflow region as M tanks-in-series and the head region as one completely mixed tank in which gas disengagement takes place.

This approach can be modified to incorporate a dispersion model. The use of such detailed models, however, depends upon further characterization of the airlift tower. The amount of gas entrained in the downflow region as a function of incoming air flowrate, axial position and tower design should be established.

Multi-Stage Fermentors

A number of motivations exist for considering multi-stage operation in a fermentation system. Chen et al.⁽³⁶⁾ and Moo-Young⁽³⁷⁾ have pointed out the value of partial mixing in continuous fermentation. Chen et al.⁽³⁷⁾ found a single stirred tank followed by a plug flow reactor to be optimal in an autocatalytic fermentation with sterile feed and a high desired conversion of substrate to cell mass. Several authors⁽³⁸⁻⁴²⁾ have found multi-stage systems useful in continuous fermentations where more than one biological reaction take place. In batch and continuous operations improved oxygen transfer rates have frequently been found in multi-stage operation.

Various researchers^(14,23,25,43-45) have found good oxygen transfer characteristics in bubble towers filled with ceramic or screen packing. A mass transfer coefficient of 7.8 min^{-1} has been found by Voyer and Miller⁽⁴⁵⁾ for a $\text{CO}_2\text{-H}_2\text{O}$ system in a tower packed with open end cylindrical mesh packing (0.5 inch x 0.5 inch) at a superficial gas velocity of 3658 cm/min. The use of perforated plates in multistage sieve tray bubble towers has been shown to improve mass transfer characteristics as compared to the single stage bubble column^(25,46,47). Hsu et al.^(25,46) have compared the multistage sieve tray tower to a tower packed with Koch motionless mixers and found the Koch mixers to improve the oxygen transfer characteristics.

Oxygen transfer coefficients of 3.33 min^{-1} were found at a superficial gas velocity of 180 cm/min for a mixed culture fermentation.

Falch and Gaden^(48,49) and Paca and Gregr^(50,51) have added mechanical agitation to each stage of the sieve tray bubble tower to further improve the oxygen transfer rates. This type of fermentor could be considered as a multistage agitated tank tower. Paca and Gregr⁽⁵⁰⁾ have found an oxygen transfer coefficient of 18.6 min^{-1} at a superficial gas velocity of 89.3 cm/min and an agitation speed of 800 rpm . Another multi-stage tower investigated was the vibrating disk tower by Tojo et al.⁽⁵²⁾ for low oxygen transfer rates.

Calderbank^(53,54) and Mashelkar⁽²²⁾ have shown that coalescence will occur in tall bubble columns, which in turn reduces the interfacial area. Orazem⁽⁵⁵⁾ has shown that an optimal height exists for oxygen transfer in a split cylinder airlift tower using the sulfite oxidation method. This may also be a result of bubble coalescence. The concept of employing a multi-stage airlift tower to enhance oxygen transfer appears to be valid.

Notation

a	interfacial area
A	cross-sectional area
C	Molar concentration
C°	Equilibrium molar concentration
C*	Saturation liquid phase oxygen concentration
d	impellor diameter
D	Mass dispersion tensor
I	Constant
K	Overall mass transfer coefficient
$K_L a$	Liquid side oxygen transfer coefficient
m	constant
n	constant
N	impellor rotational speed
N_A	Aeration Number, Q/Nd^3
N_{O_2}	Oxygen transfer rate
N_{We}	Weber Number, $N^2 d^3 \rho_L / \sigma$
P	Total power consumption
P_a	Power consumed in aeration
P_e	Effective power consumption
P_m	Power consumed in mixing in a gassed system
P_0	Power consumed in mixing in an ungassed system
Q	Volumetric gas sparge rate
r	Specific oxygen uptake of the cells
R	molar rate of production due to reaction
t	Time
v	Velocity

v_s	Superficial gas velocity, Q/A
X	Cell concentration

Subscripts

L	Liquid
D	Dispersion

Greek

α	Constant
ξ	Performance ratio
ρ	Density
σ	Surface tension

References

1. Litchfield, J. H., "Single Cell Protein," Food Technology, p. 175, May (1977).
2. Moo-Young, M., "A Survey of SCP Production Facilities," Proc. Biochem., 11, 32 (1976).
3. Gaden, E. L., "Biotechnology - An Old Solution to New Problems," Chem. Eng. Ed., p. 40, Winter (1975).
4. Humphrey, A. E., "Product Outlook and Technical Feasibility of SCP," in Single Cell Protein II, (eds). Tannenbaum, S. R. and D.I.C. Wang, p. 1, The M.I.T. Press, Cambridge, Mass. (1975).
5. Hatch, R. T., "Fermentor Design," in Single Cell Protein II, (eds). Tannenbaum, S. R. and D.I.C. Wang, p. 46, The M.I.T. Press, Cambridge, Mass.(1975).
6. Schlegel, H. G., "Aeration Without Air: Oxygen Supply by Hydrogen Peroxide," Biotech. and Bioengg., 19, 413 (1977).
7. Blakebrough, N., "Mass Transfer in Aerobic Microbial Systems," Brit. Chem. Engr., 12, [38], 78 (1967).
8. Hixson, A. W., and E. L. Gaden, Jr., "Oxygen Transfer in Submerged Fermentation," Ind. and Eng. Chem., 42, 1792 (1950).
9. Bartholemew, W. H., E. O. Karow, M. R. Stat and R. H. Wilhelm, "Oxygen Transfer and Agitation in Submerged Fermentations - Mass Transfer of Oxygen in Submerged Fermentation of Streptomyces Griseus," Ind. and Eng. Chem., 42, 1801 (1950).
10. Whitaker, S., "The Transport Equations for Multi-Phase Systems," Chem. Eng. Sci., 28, 139 (1973).
11. Gray, W., "A Derivation of the Equations for Multiphase Transport," Chem. Eng. Sci., 30, 229 (1975).
12. Calderbank, P. H., "Physical Rate Processes in Industrial Fermentation. II, Mass Transfer Coefficients in Gas-Liquid Contacting with and without Mechanical Agitation," Trans, Instn, Chem, Eng., 37, 173 (1959).
13. Westerterp, K. P., "Design of Agitators for Gas-Liquid Contacting," Chem. Eng. Sci., 18, 495 (1963).
14. Yoshida, F. and K. Akita, "Performance of Gas Bubble Columns," A.I.Ch.E. J., 11, 9 (1965).

15. Valentin, F. H. H., "Absorption in Gas-Liquid Dispersions", E. & F. N. Spon Ltd., London, (1967).
16. Zlokarnik, M., "Influence of Some Important Geometric, Material and Process Parameters on Mass Transfer in Gas-Liquid Contacting," Presented at Engineering Foundation Conference on "Mass Transfer and Scale-Up of Fermentations," Hennicker, N. H., July (1977).
17. Berg, J. C. and D. R. Woods, "Principles of Surface and Colloid Chemistry," American Society for Engineering Education, Chemical Engineering Division Summer School for Chemical Engineering Faculty, Snowmass, Col., Aug. (1977).
18. Hatch, R. T., "Experimental and Theoretical Studies of Oxygen Transfer in the Air-Lift Fermentor," Ph.D. Thesis, M.I.T. (1973).
19. Miller, D. N., "Scale-Up of Agitated Vessels Gas-Liquid Mass Transfer," A.I.Ch.E. J., 20, 445, (1974).
20. Tojo, K., personal communication (1977).
21. Hassan, I. T. M. and C. W. Robinson, "Stirred-Tank Mechanical Power Requirements and Gas Hold-Up in Aerated Aqueous Phases," A.I.Ch.E. J. 23, 49, (1977).
22. Mashelkar, R. A., "Bubble Columns," Brit. Chem. Eng., 15, 1297 (1970).
23. Mashelkar, R. A. and M. M. Sharma, "Mass Transfer in Bubble and Packed Bubble Columns," Trans. Instn. Chem. Eng., 48, T 162 (1970).
24. Jackson, M. L., D.R. James and B. P. Leber, Jr., "Oxygen Transfer in a 23-Meter Bubble Column; AIChE Symposium Series - Water 1975, 71, 151 (1975).
25. Hsu, K. H., L. E. Erickson and L. T. Fan, "Pressure Drop, Gas Hold-up and Oxygen Transfer in Tower Systems," Biotech. and Bioengg., 19, 247 (1977).
26. Fukuda, H., Y. Sumino and T. Kanzaki, "Scale-Up of Fermentors," J. Ferm. Tech. 46, 829 (1968).
27. Hospodka, J., Z. Caslousky, K. Beran and F. Stros, in "Continuing Cultivation of Microorganisms," I. Malek, K. Beran and J. Hospodka, eds., Publishing House of the Czechoslovak Academy of Science, Prague, 1964, p. 353.
28. Akiba, J. and T. Fukimbara, "A Tower Type Fermentor with a Gas Entrainment Process. V. Oxygen Transfer Characteristics," J. Ferm. Tech., 50, 414 (1972).
29. Lin, C. H. et al., "Oxygen Transfer and Mixing in a Tower Cycling Fermentor," Biotech and Bioengg., 18, 1557 (1976).
30. Russell, T. W. F. and I. J. Dunn, "The Tubular Batch Fermentor: Basic Concepts," Biotech. and Bioengg., 17, 1261, (1975).

31. Ziegler, H., D. Mesiter, I. S. Dunn, H. W. Blanch and T.W.F. Russell, "The Tubular Loop Fermentor: Oxygen Transfer, Growth Kinetics and Design," *Biotech. and Bioengg.*, 19, 507 (1977).
32. Gasner, L., "Development and Application of the Thin Channel Rectangular Air-Lift Mass Transfer Reactor to Fermentation and Waste Water Treatment Systems," *Biotech. and Bioengg.*, 16, 1179 (1974).
33. Belfield, A. R., "Experimental Studies of Oxygen Transfer in a Split Cylinder Airlift," M.S. Thesis, Univ. of Maryland (1976).
34. Lefrancois, L., C. G. Mariller and J. V. Mejane, "Effectonnements aux procedes de Cultures Fongiques et de Fermentations Industrielles," Brevet D'Invention, France #1.102.200, Delivree le 4 Mai, 1955.
35. Ho, C. S., "Modeling and Simulation of Mass Transfer in Airlift Fermentors," M.S. Thesis, Kansas State University (1976).
36. Chen, G.K.C., L. T. Fan and L. E. Erickson, "On the Merits of Partial Fluid Mixing in the Biochemical Reactor," *Can. J. Chem. Eng.*, 50, 157 (1972).
37. Moo-Young, M., "Microbial Reactor Design for Synthetic Protein Production," *Can. J. Chem. Eng.*, 53, 113 (1975).
38. Fenc1, Z., J. Ricica and J. Kodesova, "The Use of the Multi-Stage Chemo-stat for Microbial Product Formation," *J. Appl. Chem. Biotech.*, 22, 405 (1972).
39. Jensen, D. E., "Continuous Production of Extracellular Protease by *Bacillus Subtilis* in a Two Stage Fermentor," *Biotech. and Bioengg.*, 14, 647 (1972).
40. Pilat, P., A. Prokop and Z. Fenc1, "Multi-Stage Continuous Cultivation of *Candida Lipolytica* on Mineral Oil," *J. Ferm. Tech.*, 51, 249 (1973).
41. Camhi, J. D. and P. L. Rogers, "Multistage Cultivation of *Candida Utilis* on Spent Sulfite Liquor," *J. Ferm. Tech.*, 54, 437 (1976).
42. Camhi, J. D. and P. L. Rogers, "Continuous Cultivation of Bacteria (*Pseudomonas* sp.) on Spent Sulfite Liquore," *J. Ferm. Tech.*, 54, 450 (1976).
43. Carleton, A. J., R. J. Flain, J. Rennie, and F.H.H. Valentin, "Some Properties of a Packed Column," *Chem. Eng. Sci.*, 22, 1839 (1967).
44. Fan, L. T., H. H. Hsu and K. B. Wang, "Mass Transfer Coefficient and Pressure Drop Data of Two-Phase Oxygen-Water Flow in Bubble Column Packed with Static Mixers," *J. Chem. Eng. Data*, 20, 26 (1975).
45. Voyer, R. D. and A. I. Miller, "Improved Gas-Liquid Contacting in Co-Current Flow," *Can. J. Chem. Eng.*, 46, 335 (1968).

46. Hsu, K., L. E. Erickson and L. T. Fan, "Oxygen Transfer to Mixed Cultures in Tower Systems," *Biotech. and Bioengg.*, 17, 449 (1975).
47. Kitai, A., H. Tone and A. Ozaki, "Performance of a Perforated Plate Column as a Multistage Continuous Fermentor," *Biotech. and Bioengg.*, 11, 911 (1969).
48. Falch, E. A. and E. L. Gaden, Jr., "A Continuous Multistage Tower Fermentor. I. Design and Performance Tests," *Biotech. and Bioengg.*, 11, 927 (1969).
49. Falch, E. A. and E. L. Gaden, Jr., "A Continuous Multistage Tower Fermentor. II. Analysis of Reactor Performance," *Biotech. and Bioengg.*, 12, 465 (1970).
50. Paca, J. and Y. Gregr, "Design and Performance Characteristics of a Continuous Multistage Tower Fermentor," *Biotech. and Bioengg.*, 18, - 1075 (1976).
51. Paca, J. and Y. Gregr, "Growth Characteristics of *Candida Utilis* on Volatile Substrates in a Multistage Tower Fermentor," *Biotech. and Bioengg.*, 19, 539 (1977).
52. Tojo, K., K. Miyanami and T. Yano, "Mass Transfer in a Multistage Vibrating Disk Column with Co-current Liquid-Gas Flow," *J. Chem. Engg. (Japan)*, 1, 126 (1974).
53. Calderbank, P. H., M. B. Moo-Young and R. Bibby, "Coalescence in Bubble Reactors and Absorbers," *Chem. Reaction Engg. Symp.*, p. 91 (1964).
54. Calderbank, P. H., "Gas Absorption from Bubbles," *Chem. Engr.*, 45, CE 209 (1967).
55. Orazem, M. E., "Effect of Column Height on Oxygen Transfer in Airlift Systems," Proceedings of the Sixth Biochemical Engineering Symposium, Iowa State Univ. (1976).

Table 1
Oxygen Transfer Characteristics of Single Stage Fermentors

Fermentor	System	Superficial Gas Velocity, cm/min	$K_L a$, min^{-1}	Reference
Bubble Column	air - Na_2SO_3	1333	6.7	Yoshida, and Akita (14)
Bubble Column	CO_2 - Na_2CO_3 , NaHCO_3 buffer soln.	900 - 2400	3.6 - 7.8	Malshelkar and Sharma (23)
Bubble Column	air - Na_2SO_3	0 - 73	0 - 0.67	Jackson et. al. (24)
Bubble Column	O_2 - water	20 - 200	0.13 - 1.50	Hsu et. al. (25)
Turbine	air - Na_2SO_3		2.6 - 7.1	Fukuda et. al. (26)
Turbine	air - Na_2SO_3		6.2 - 13.8	Hospodka et. al. (27)
Waldhof	yeast		1.0 - 1.7	Hospodka et. al. (27)
Phrix	yeast		1.3 - 2.6	Hospodka et. al. (27)
Vogelbusch	yeast		1.6 - 2.7	Hospodka et. al. (27)
Gas entrainment Tower	air - H_2O		0.6 - 6.0	Akiba and Fukimbara (28)
Cycling Tower	yeast	90 - 540	0.3 - 1.7	Lin et. al. (29)
Tubular Loop	yeast		3.10	Russell and Dunn (30)
Tubular Loop	yeast	16.5 - 165	1.39 - 9.07	Ziegler et. al. (31)
Thin Channel	air - Na_2SO_3	0 - 400	0 - 9.7	Casner (32)
Rectangular Concentric Cylinder Air-Lift	yeast	740-1340	3.3 - 6.3	Hatch (18)
Split Cylinder Air-Lift	air - Na_2SO_3	150-1200	1.8 - 7.8	Belfield (33)

Table 2
Oxygen Transfer Characteristics of Multistage Fermentors

Fermentor	System	Superficial Gas Velocity, cm/min	$K_L a$, min^{-1}	Reference
Packed Column (Raschig Rings)	$\text{CO}_2 - \text{H}_2\text{O}$	120 - 360	2.10	Carleton et. al. (43)
Packed Column(Koch)	$\text{O}_2 - \text{H}_2\text{O}$	350 - 2100	3.90 - 15.0	Fan et. al. (44)
Packed Column	$\text{CO}_2 - \text{Na}_2\text{CO}_3$, NaHCO_3 buffer soln.	600 - 1620	4.20 - 7.20	Mashekar and Sharma(23)
Packed Column	$\text{CO}_2 - \text{H}_2\text{O}$	550 - 4938	7.80	Voyer and Miller (45)
Packed Column	$\text{CO}_2 - \text{H}_2\text{O}$		0.03 - 1.0	Yoshida and Akita (14)
	$\text{CO}_2 - \text{KOH}$		0.07 - 10.0	
Packed Column (Koch static mixers)	$\text{O}_2 - \text{H}_2\text{O}$	20 - 200	0.33 - 2.53	Hsu et. al. (25)
	air - waste water (mixed culture)	20 - 176	0.42 - 3.33	Hsu et. al. (46)
Sieve Tray	$\text{O}_2 - \text{H}_2\text{O}$	20 -200	0.25 - 2.50	Hsu et. al. (25)
	air - waste water (mixed culture)	20 - 176	0.33 - 2.33	Hsu et. al. (46)
Sieve Tray	air - Na_2SO_3	24 - 600	0.33 - 6.67	Kitai et. al. (47)
4-Stage CSTR	air - Na_2SO_3	13-41(320 rpm)	1.92 - 3.66	Falch and Gaden (48,49)
4-Stage CSTR	air - Na_2SO_3	27-41(510 rpm)	6.39 - 7.56	Paca and Cregr (50)
vibrating disk	air - Na_2SO_3	38-112(600rpm)	0.62 - 18.6	Tojo et. al. (52)
	$\text{CO}_2 - \text{H}_2\text{O}$	60-360	1.8 - 6.0	

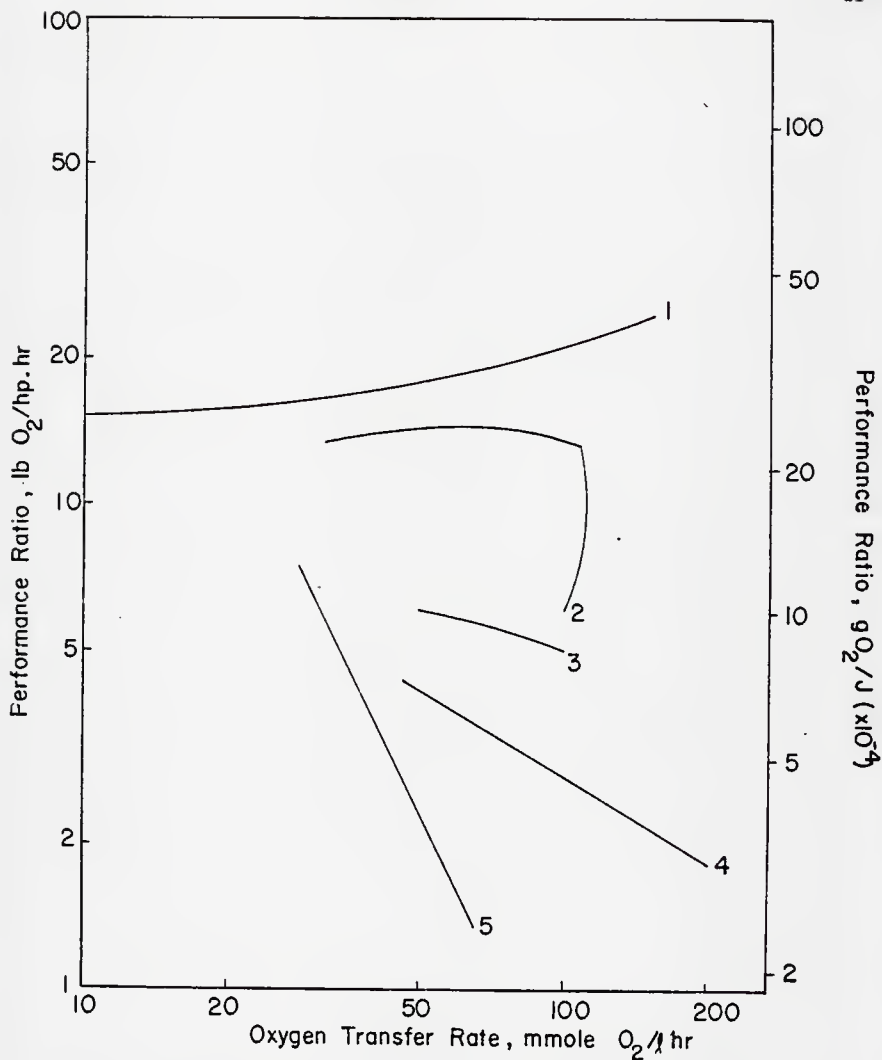


Fig. 1. Performance Ratio as a Function of Oxygen Transfer Rate; 1. rectangular airlift (32), 2. one stage split cylinder airlift (33), 3. concentric cylinder airlift (18), 4. agitated tank (26), 5. aeration tower (5).

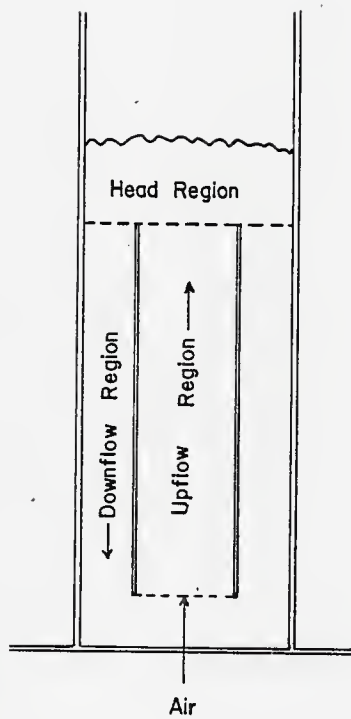


Fig. 2. Concentric Cylinder Airlift Tower.

OXYGEN TRANSFER RATES AND EFFICIENCIES IN ONE AND TWO STAGE AIRLIFT TOWERS

Introduction

Submerged aerobic fermentation has found application in areas ranging from waste treatment to manufacture of pharmaceuticals and food products. Of great interest is the production of single cell protein (SCP) for animal or human consumption (1-3). Substrates considered for SCP production include energy source materials such as petroleum derivatives, waste materials such as bagasse and animal manure, and renewable source material such as cellulose and sugar (4). The economic viability of production of SCP from these substrates hinges in large degree upon the growth rate of the microorganisms employed.

Of the nutrients necessary for the growth of microorganisms, oxygen has the lowest solubility in the liquid phase. The design of fermentation equipment is geared, therefore, toward maximizing the oxygen supply available for cell growth while minimizing the power requirement (5).

Schlegel (6) recently reported that oxygen can be successfully supplied to a culture by adding hydrogen peroxide to a shaking flask under nitrogen blanket. Cell concentrations achieved were comparable to those achieved in shaking flasks under open atmosphere. Most fermentation equipment, however, depend on the mass transfer of oxygen from the gas phase to the liquid. The bubble column and the agitated tank are traditional gas-liquid contacting devices.

High oxygen transfer rates were found by Hatch (5,7) in a concentric cylinder airlift tower with low power requirements. The airlift tower provides liquid agitation through the use of a large gas flow rate. Belfield (8) described an airlift tower which consists of a cylinder divided into two sections by a baffle. The reduced wetted surface area to volume ratio and its ease of construction make the split cylinder airlift tower attractive.

Multistage systems have been shown to have good mass transfer characteristics. Various researchers⁽⁹⁻¹³⁾ have found improved mass transfer characteristics in bubble towers filled with random ceramic or screen packing. Mass transfer coefficients of 7.80 min^{-1} were found by Voyer and Miller⁽¹³⁾ for a $\text{CO}_2 - \text{H}_2\text{O}$ system in a tower packed with open end cylindrical mesh packing (0.5 inch x 0.5 inch) at a superficial gas velocity of 3658 cm/min. The use of perforated plates in multistage sieve tray bubble towers was shown to improve mass transfer characteristics as compared to the single stage bubble column⁽¹⁴⁻¹⁶⁾. Hsu et al.^(14,15) compared the multistage sieve tray tower to a tower packed with Koch motionless mixers and found the Koch mixers to improve the oxygen transfer characteristics. Oxygen transfer coefficients of 3.33 min^{-1} were found at a superficial gas velocity of 180 cm/min for a mixed culture fermentation.

Falch and Gaden^(17,18) and Paca and Gregr⁽¹⁹⁾ added mechanical agitation to each stage of the sieve tray bubble tower to further improve the oxygen transfer rates. This type of fermentor could be considered as a multistage agitated tank tower. Paca et al.⁽¹⁹⁾ found an oxygen transfer coefficient of 18.6 min^{-1} at a superficial gas velocity of 89.3 cm/min and an agitation speed of 800 rpm for a sulfite-air system. Another multistage tower investigated was the vibrating disk tower by Tojo et al.⁽²⁰⁾

In an investigation preceding the work presented here, the effect of column height on oxygen transfer in a split cylinder airlift tower was studied for a sodium sulfite-air system⁽²¹⁾. An optimal baffle height for a 15.24 cm diameter column was found to be near 60 cm for a baffle placed 6.20 cm above the base. It was concluded that a multi-stage airlift tower would merit further consideration as a means of increasing oxygen transfer rates.

The objective of this study was to determine the applicability of a multistage split cylinder airlift tower for gas-liquid mass transfer such as expected in fermentation systems. The range of superficial gas velocities studied was 735 cm/min to 2728 cm/min. The volume of gas per volume liquid per minute (vvm) ranged from 3.28 min⁻¹ to 12.21 min⁻¹. This range was chosen to provide good data for scale-up. The volumetric gas flow rate can be described as the product of the superficial gas velocity and the cross-sectional area.

$$Q = v_g \cdot A \quad (1)$$

The vvm ratio is seen to be

$$\text{vvm} = \frac{Q}{Ah} \quad (2)$$

where h is the tower height. Thus

$$\text{vvm} = \frac{v_g}{h} \quad (3)$$

Industrial fermentations are typically conducted with a vvm ratio of approximately three. In order to keep superficial velocities constant in tower scale-up the studies at low tower height must be conducted at high vvm values. Thus studies in a one-meter tall tower with a vvm of twelve can be related to a four-meter tall tower with a vvm ratio of three.

Materials and Methods

Two split cylinder airlift towers were employed in this study. They are shown in Fig. 1. Each tower held a liquid volume of 20.5 l and had an inside diameter of 15.24 cm. The single stage tower had a baffle height of 107.1 cm and the gap between the lower edge of the baffle and the bottom of the column was 5.5 cm. The cross sectional area allowed for flow between the bottom of the column and the baffle was equal to the upflow and downflow

cross sectional areas. Air was sparged into the upflow section of the column through a 0.95 cm I.D. plexiglas tube which was level with the lower edge of the baffle.

The two stage airlift was composed of two sections, each with a 50.8 cm high baffle. The distance between the lower edge of the baffle and the bottom of the tower section was 5.5 cm, as in the single stage tower. The two sections were divided by a plate with a sparger identical to the one used in the single stage tower. The sections were designed so as to allow a large range of superficial gas velocities without restricting the head region volume for the lower stage. To provide a level control for the upper stage an external downcomer was placed at an adjustable height at the top of the head region. The lower stage level control was provided by pumping continuously from the desired liquid level to the upper stage. The total circulation between the two stages provided in this manner was 27 ml/min for a volume exchange time of 6.3 hours. Air was filtered and the flowrate was monitored by a Fisher and Porter (T2-1308/2) rotameter which had been calibrated by use of a wet test meter.

Open end manometers were used to obtain pressure drop and local hold up data. These manometers were located at the bottom and the top of each baffle on the upflow and downflow sections of the towers. The overall gassed liquid level was measured to determine the overall gas holdup.

The oxygen transfer characteristics were found through use of the sodium sulfite oxidation method by Cooper et al.⁽²²⁾. This method can be safely employed in a direct comparison of fermentation equipment. A one weight percent solution of technical grade sodium sulfite was used with one part per million cobaltous catalyst. The measured solution pH was 10.0 as recommended by Fan and Wang⁽²³⁾.

The sodium sulfite and the catalyst CoSO_4 were allowed to dissolve thoroughly in a large tank. The solution was then pumped into the tower being used. The sparging of air at the desired flowrate began at a recorded time. Fifty milliliter samples were withdrawn at regular intervals and from each sample a 10 ml. aliquot was titrated using the iodometric analysis for sodium sulfite concentration⁽²⁴⁾. The reaction of sodium sulfite to form sodium sulfate is zero order with respect to sodium sulfite under the conditions used, so the zero order reaction rate constant could be used to determine the amount of oxygen transferred under pseudo steady state conditions with regard to the liquid oxygen concentration. The liquid oxygen concentration was assumed to be negligible and the apparent $K_L a$ was calculated assuming perfect liquid mixing.

The comparative oxygen transfer characteristics of the one stage and two stage towers were found for gas superficial velocities ranging from 720 cm/min to 2728 cm/min. The liquid was at an average temperature of 18°C and the literature values used for the saturated oxygen concentration were adjusted for temperature variation⁽²⁵⁾.

Results and Discussion

Gas Hold-up

The overall gas hold-up was determined for the two-stage tower, the single stage tower, and the single stage tower packed with three Koch LY static mixers and packed with seven Koch LY static mixers. The static mixers consisted of three one-inch corrugated plastic sheets glued together and cut so as to fit inside the upflow section of the airlift tower. The direction of mixing was tangential to the baffle. The Koch mixers⁽²⁶⁾ are described by Hsu et al.⁽¹⁴⁾ and Hsu et al.⁽²⁷⁾. The overall gas hold-up is shown in Fig. 2. The values for the two-stage tower are the arithmetic average values for both stages. The gas hold-up in the single stage tower is seen to be much lower than in the two stage tower for high superficial gas velocities. At a superficial gas velocity of 2262 cm/min the gas hold-up in the two stage tower is 40 percent higher than in the one stage tower. This could be attributed to increased coalescence in the single stage tower, causing the bubbles to increase in size and escape more quickly from the dispersion. A reduced gas residence time would result.

The gas holdup in the head region, upflow region and downflow region are shown in Fig. 3 for the upper stage of the two-stage tower and in Fig. 4 for the single stage tower. Results for the lower stage are similar to those shown in Fig. 3. The very high hold-up in the head region of the two stage tower, 0.575 at a superficial gas velocity of 2778 cm/min, could be partly due to entrainment of surface air. Calderbank⁽²⁸⁾ found surface aeration to be important in agitated gas liquid contacting systems. The entrainment of surface air due to the intense turbulence, as well as the downward velocity of the liquid, could play an important role in mass transfer.

The hold-up in the head region of the single stage tower was not as high as that in the two stage tower. At a superficial gas velocity of 2262 cm/min the observed hold-up was 0.355. The agitation in the single stage tower was observed not to be as intense as in the two stage tower, and the carry-through of entrained air in the downflow section was not as large. Coalescence and the resulting rapid escape from the system would account for these observations.

Oxygen Transfer Characteristics

Under the assumptions that the content of the aqueous phase is completely mixed and the oxygen content in gaseous phase remains invariant with respect to the spatial position, an oxygen balance over the aqueous phase in each stage of the airlift tower gives

$$\frac{dC}{dt} = -N_A + K_L a (C^* - C) \quad (4)$$

Under a pseudo-steady state condition, this reduces to

$$N_A = K_L a (C^* - C) \quad (5)$$

The $K_L a$ to be determined here is on a liquid volume basis, i.e., the concentrations are in units of milligrams O_2 per unit liquid volume and not per unit dispersion volume.

$$K_L a = \frac{N_A}{C^* - C} \quad (6)$$

The saturated liquid oxygen concentration value was found from the literature⁽¹⁷⁾ for a 1 wt percent salt solution at the dispersion temperature and atmospheric pressure. The effect of pressure on the saturated liquid oxygen concentration was neglected for the short towers used, since the pressure recorded at the bottom of the towers was close to atmospheric. The liquid oxygen concentration was assumed to be zero. This assumption of a maximum oxygen

transfer driving force leads to a conservative estimate of the apparent oxygen transfer coefficient.

The oxygen transfer coefficient, $K_L a$, was based on the liquid film resistance controlling. This assumption is reasonable for oxygen transfer in gas-liquid contacting systems (28,29).

$K_L a$ is shown in Fig. 5 as a function of superficial gas velocity for the two-stage and one-stage towers. At a superficial gas velocity of 2262 cm/min the $K_L a$ was 54 percent higher in the two-stage tower than in the single stage. Reproducibility of the data was within a standard deviation of six percent. The rise in $K_L a$ begins to fall off at high gas velocities for the one stage tower. This is probably due to the effect of coalescence, and, while $K_L a$ is a linear function of superficial gas velocity for the two stage tower at the velocities studied, a leveling can be expected at some yet undetermined higher gas velocity. The $K_L a$ found in the lower stage in the two-stage tower matched consistently that found in the upper stage within experimental accuracy. This could be due to the relatively small consumption of the available oxygen in the sparged air. The calculated oxygen mole fraction in the exit gas stream at a superficial gas velocity of 2400 cm/min was 0.198. That in the gas entering the second stage 0.204. An inlet oxygen mole fraction of 0.21 was assumed in these calculations.

The oxygen transfer coefficient is shown in Fig. 6 for the single stage tower packed with three Koch LY static mixers and with seven Koch LY static mixers. The effect of the mixing elements was to reduce the liquid

circulation rate and to decrease the oxygen transfer. Under the conditions investigated, the empty airlift tower was found to have better oxygen transfer characteristics than the airlift tower with packing in the upflow section. The static mixers did increase the interfacial area by reducing coalescence but this effect was overshadowed by the decrease in liquid velocities.

It must be noted that the static mixers employed were not of optimal configuration. The mixing was not three-dimensional and the corrugation was coarse relative to the column diameter. These results should not be interpreted to imply that packing, or Koch mixers, are not desirable under any conditions in airlift or split cylinder airlift towers.

As samples were withdrawn from the tower during the course of a run, the total liquid volume decreased by two percent, corresponding to an ungasged liquid level change of 2.2 cm in the one-stage tower. The effect on $K_L a$ of varying the ungasged liquid level from 9 cm above the baffle to 9 cm below is shown in Fig. 7. The effect of a variation of 2 cm in liquid level can be seen to be negligible.

Oxygen transfer is enhanced in the two stage tower as compared to the single stage at large superficial gas velocities. An important consideration in the evaluation of the data presented is the total volume occupied by the aeration equipment. The oxygen transfer characteristics were adjusted to a dispersion volume basis by the relation

$$K_L a' = K_L a (1-H) \quad (7)$$

where $K_L a'$ is the oxygen transfer coefficient on a dispersion volume basis and H is the overall gas hold-up. The comparison of oxygen transfer coefficients on a dispersion volume basis is more reasonable than a similar

comparison on a tower volume basis. The two-stage tower was designed to allow a large void volume between the first and second stages. This void volume can be greatly reduced in tower design for a specific gas flowrate, while the volume occupied by the liquid-gas dispersion cannot be reduced without changing the system flow characteristics.

The oxygen transfer coefficient based on a dispersion volume basis is shown in Figure 8 for the two-stage and one-stage towers. The $K_L a'$ values for the two stage tower still exceed those of the one-stage tower at high superficial gas velocities but the $K_L a'$ is not a linear function of gas velocity as it was for the liquid volume based $K_L a$. At 2000 cm/min the $K_L a'$ rises less rapidly with gas velocity. The $K_L a'$ based on dispersion volume was 27 percent higher in the two-stage tower than in the one stage tower at a superficial gas velocity of 2262 cm/min.

Performance Ratio

As stated in the introductory section, the design of fermentation equipment hinges on maximizing the oxygen transfer rates while minimizing the power requirements. The performance ratio defined by Hatch⁽⁷⁾ is a measure of the oxygen transferred per unit of power required to transfer that oxygen. The adiabatic power of compression for air is⁽³⁰⁾

$$P = 0.0153 Q_1 P_1 \left[\left(\frac{P_2}{P_1} \right)^{0.286} - 1 \right] \quad (8)$$

where P is the power requirement, hp, Q is the gas flowrate, SCFM, P_1 is the atmospheric pressure, and P_2 is the pressure at the gas sparger, psia. The power term obtained is characteristic of the tower only and not of the air line between the compressor and the tower.

The performance ratio, ξ , is

$$\xi = N_A/P \quad (10)$$

The performance ratio is shown in Fig. 9 for the one- and two-stage towers. The towers are comparable at low oxygen transfer rates but at a transfer rate of 180 m mole O_2/ℓ hr the two-stage tower becomes clearly more efficient. The performance ratio has its highest values at low oxygen transfer rates in the two-stage tower and an optimal value near 150 m mole O_2/ℓ hr for the one-stage tower.

Figure 10 displays the performance ratio for the packed one-stage airlift tower. The results for the two stage tower are also shown in this figure for reference.

Comparison with Literature

The oxygen transfer coefficient as a function of superficial gas velocity is presented in Fig. 11 for various airlift tower systems. Values were adjusted to a liquid temperature of 18°C. The physical characteristics and dimensions of the various towers studied are shown in Table 1. It is important to note that while our work and those of Belfield⁽⁸⁾ and Gasner⁽³¹⁾ utilized a sulfite-air system, the work presented by Hatch⁽⁷⁾ made use of a fermentation system. Thus, the K_L values obtained by Hatch are not directly comparable to those obtained through the use of the sulfite oxidation method.

Both curves 2 and 4 represent single stage split cylinder airlift towers. Flooding, or the appearance of a coalescence effect occurs in

Belfield's tower at a superficial gas velocity of 600 cm/sec while in the smaller tower it occurs at roughly 1200 cm/sec. This discrepancy may be due in part to the lack of an optimal baffle height in the larger tower.

The results from Gasner clearly show the merit of using a wide baffle in an airlift system. Large oxygen transfer coefficients were obtained at low gas velocities. This may have been due in part to the use of a multiple hole sparger as compared to the single open tube sparger used in Belfield's and our work. The use of a similar sparger or a perforated plate should be considered in the split cylinder airlift. The rectangular airlift should be investigated at higher gas velocities and in a multiple stage combination.

The performance ratios are shown in Fig. 12 for various systems. The airlift towers are clearly superior to the bubble column and agitated tank fermentors. The application of the multi-stage concept to the split cylinder airlift tower yields a high efficiency at high oxygen transfer rates. The performance ratio of a small system will be smaller than that of a large system due to a larger surface-area-to-volume ratio of the small system. Therefore, the performance ratios of lines 4 and 5 may be expected to increase if scaled up to the size of systems 1, 2 or 3.

Conclusions

The use of a multi-stage airlift tower has merit in gas-liquid contacting. Oxygen transfer coefficients ($K_L a$) of over 25 min^{-1} (or 1500 hr^{-1}) were obtained at a superficial gas velocity of 2728 cm/min for a sodium sulfite-air system in a two-stage tower. At a superficial gas velocity of 2262 cm/min the $K_L a$ for the two-stage tower was 54 percent higher than in the one-stage system.

The use of a multi-stage tower requires more reactor volume than the single stage tower of equal liquid volume, but the oxygen transfer coefficient based on the total dispersion volume is still 27 percent higher than in the one stage tower at a superficial gas velocity of 2262 cm/min.

At low gas velocities, the two-stage and one-stage towers have equivalent mass transfer characteristics. At 1300 cm/min the $K_L a$ begins to level off for the one-stage system while the $K_L a$ for the two stage tower increases linearly with superficial gas velocity in the range studied.

The two-stage tower becomes considerably more efficient than the single stage tower at oxygen transfer rates larger than 180 m mole/2 hr.

Notation

A	cross sectional area, cm^2
C	liquid oxygen concentration, mg/ℓ
H	gas holdup based on dispersion volume
h	tower height, cm
$K_{L,a}$	oxygen transfer coefficient based on liquid volume, min^{-1}
$K_{L,a}'$	oxygen transfer coefficient based on dispersion volume, min^{-1}
N_A	rate of oxygen consumption, $\text{mg}/\ell \text{ min}$
P	adiabatic power of compression, hp
Q	volumetric gas flowrate, SCFM
t	time, min
V_S	superficial gas velocity, cm/min
vvm	volume of gas per volume of liquid per minute, min^{-1}

Superscript

* saturation

Greek letter

ξ performance ratio, $\text{lb O}_2/\text{hp hr}$ (or) $\text{g O}_2/\text{J}$

References

1. Litchfield, John H., "Single Cell Proteins," Food Technology, May (1977), p. 175.
2. Moo-Young, M., "A Survey of SCP Production Facilities," Proc. Biochem. 11, 32 (1976).
3. Gaden, E. L., "Biotechnology - An Old Solution to New Problems," Chem. Eng. Ed., Winter (1975), p. 40.
4. Humphrey, A. E., "Product Outlook and Technical Feasibility of SCP," in Single Cell Protein II, (eds.) Tannenbaum, S. R. and C.I.C. Wang, p. 1, The M.I.T. Press, Cambridge, Mass. (1975).
5. Hatch, R. T., "Fermentor Design," in Single Cell Protein II, (eds.) Tannenbaum, S. R. and D.I.C. Wang, P. 46, The M.I.T. Press, Cambridge, Mass. (1975).
6. Schlegel, H. G., "Aeration Without Air: Oxygen Supply by Hydrogen Peroxide," Biotech. and Bioengg., 19, 413 (1977).
7. Hatch, R. T., "Experimental and Theoretical Studies of Oxygen Transfer in the Airlift Fermentor," PhD Thesis, M.I.T. (1973).
8. Belfield, A. R., "Experimental Studies of Oxygen Transfer in a Split Cylinder Airlift," M.S. Thesis, Univ. of Maryland (1976).
9. Carleton, A. J., R. J. Flain, J. Rennie and F.H.H. Valentin, "Some Properties of a Packed Bed Column," Chem. Eng. Sci., 22, 1839 (1967).
10. Mashelkar, R. A., and M. M. Sharma, "Mass Transfer in Bubble and Packed Bubble Columns," Trans. Instn. Chem. Engrs., 48, T162 (1970).
11. Mashelkar, R. A., "Bubble Columns," Brit. Chem. Eng., 15, 1297 (1970).
12. Yoshida, F. and Y. Miura, "Effective Interfacial Area in Packed Columns for Absorption with Chemical Reaction," A.I.Ch.E. J., 9, 333 (1963).
13. Voyer, R. D. and A. I. Miller, "Improved Gas-Liquid Contacting in Co-Current Flow," Can. J. Chem. Eng., 46, 335 (1968).
14. Hsu, K., L. E. Erickson and L. T. Fan, "Oxygen Transfer to Mixed Cultures in Tower Systems," Biotech. and Bioeng., 17, 499 (1975).
15. Hsu, K., L. E. Erickson and L. T. Fan, "Pressure Drop, Gas Hold-Up, and Oxygen Transfer in Tower Systems," Biotech. and Bioeng., 19 247 (1977).
16. Kitai, A., H. Tone, and A. Ozaki, "Performance of a Perforated Plate Column as a Multistage Continuous Fermenter," Biotech. and Bioeng. 11, 911 (1969).

17. Falch, E. A. and E. L. Gaden, Jr., "A Continuous Multistage Tower Fermentor. I. Design and Performance Tests," *Biotech. and Bioengg.*, 11, 927 (1969).
18. Falch, E. A. and E. L. Gaden, Jr., "A Continuous Multistage Tower Fermentor. II. Analysis of Reactor Performance," *Biotech. and Bioengg.*, 12, 465 (1970).
19. Paca, J. and Y. Gregr, "Design and Performance Characteristics of a Continuous Multistage Tower Fermentor," *Biotech. and Bioengg.*, 18, 1075 (1976).
20. Tojo, K., K. Miyanami and T. Yano, "Mass Transfer in a Multistage Vibrating Disk Column with Co-current Liquid-Gas Flow," *J. Chem. Engg. (Japan)*, 1, 126 (1974).
21. Orazem, M. E., "Effect of Column Height on Oxygen Transfer in Airlift Systems," Proceedings of the Sixth Biochemical Engineering Symposium, Iowa State Univ. (1976).
22. Cooper, C. M., G. A. Fernstrom and S. A. Miller, "Performance of Agitated Gas Liquid Contactors," *Ind and Eng Chem*, 36, 504 (1944).
23. Fan, L. T. and K. B. Wang, "Oxidation of Sulfite in an Air Lift Reactor Packed with Motionless Mixers," presented at 81st Nat. Meeting AIChE, Kansas City, Mo. (1976).
24. Taras, M. J., et al., (eds.) Standard Methods for the Examination of Water and Wastewater, 13th ed. American Public Health Assoc., Washington D. C. (1971).
25. Precision Scientific Company, "G.C.O.A. Tables: Temperature Correction, Solubility Correction, Dissolved Oxygen," Chicago, Ill. (1966), p. 88.
26. Koch Static Mixers, Bulletin KSM-2, Koch Engineering Company, Wichita, Kansas.
27. Hsu, H. H., K. B. Wang and L. T. Fan, "Mass Transfer Coefficient and Pressure Drop Data of Two-Phase Oxygen-Water Flow in Bubble Column Packed with Static Mixers," *J. Chem. Eng. Data*, 20, 26 (1975).
28. Calderbank, P. H., "Physical Rate Processes in Industrial Fermentation. Part II: Mass Transfer Coefficients in Gas-Liquid Contacting with and without Mechanical Agitation," *Trans. Instn. Chem. Engrs.*, 37, 173 (1959).
29. Yoshida, F. and K. Akita, "Performance of Gas Bubble Columns: Volumetric Liquid-Phase Mass Transfer Coefficient and Hold-Up," *A.I.Ch.E. J.*, 11, 9 (1965).
30. Perry, R. H. (ed.) "Chemical Engineers Handbook," 5th ed., McGraw Hill, New York (1973), P. 6-16.
31. Gasner, L., "Development and Application of the Thin Channel Rectangular Air Lift Mass Transfer Reactor to Fermentation and Waste-Water Treatment Systems," *Biotech. and Bioengg.*, 16, 1179 (1974).

32. Fukuda, H., Y. Sumino, and T. Kanzaki, "Scale-up of Fermentors," J. Ferm. Tech., 46, 829 (1968).

Table 1. Physical Characteristics and Dimensions of Air Lift Towers

Plot Number	Type of Fermentor	Process	Reactor Volume	Sparger	Baffle Height	Reference
1	rectangular airlift	Sodium Sulfite Oxidation	90.9 l	48 ports 0.159 cm I.D.	61.0 cm	Gasner (31)
2	one stage split cylinder airlift	Sodium Sulfite Oxidation	200 l	1 open tube 1.58 cm I.D.	182,8 cm	Belfield (8)
3	concentric cylinder airlift	Candida Intermedia on n-alkanes	200 l	multiple hole	260 cm	Hatch (7)
4	one stage split cylinder airlift	Sodium Sulfite Oxidation	20.5 l	1 open tube 0.95 cm I.D.	107.1 cm	
5	two stage split cylinder airlift	Sodium Sulfite Oxidation	20.5 l	2(1 open tube 0.95 cm I.D.)	2(50.8 cm)	

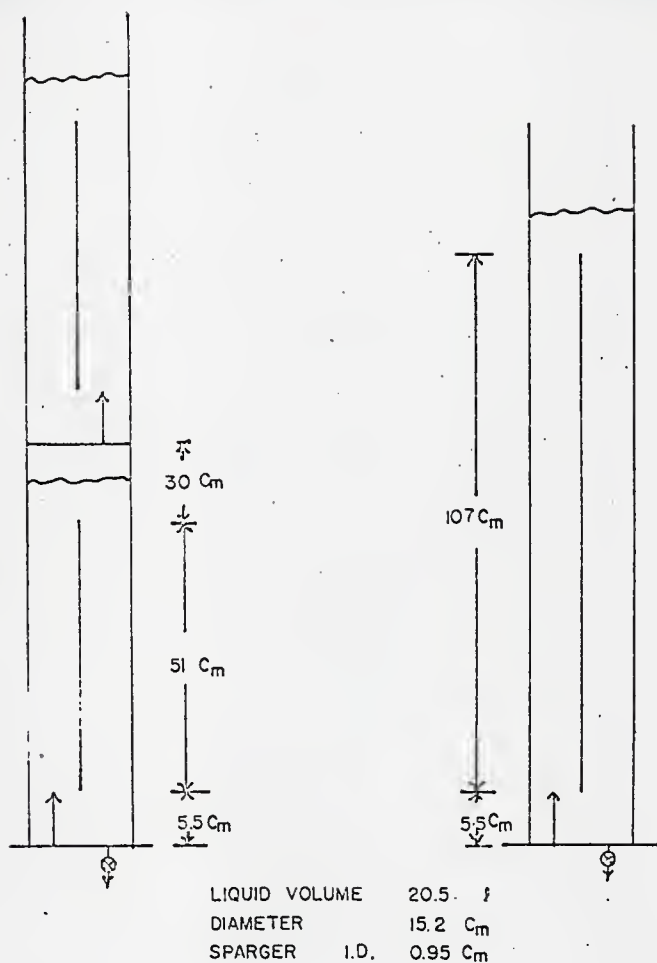


Fig. 1. Schematic Diagram of Single Stage and Two Stage Tower.

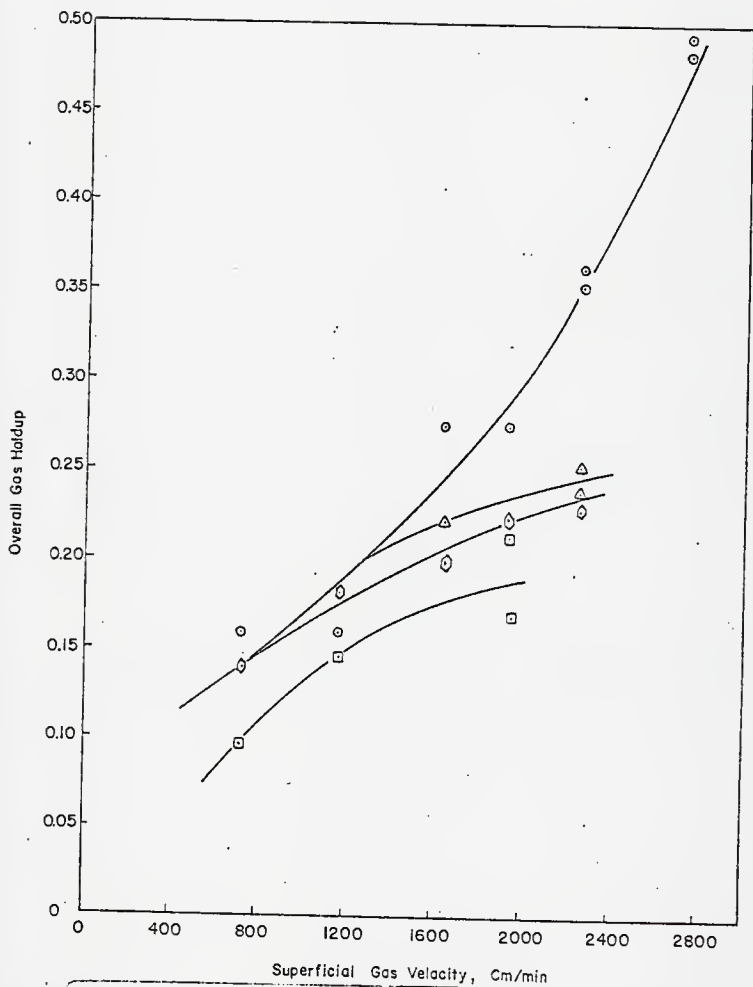


Fig. 2. Overall Gas Hold-Up as a Function of Superficial Gas Velocity; ○ Two Stage Tower, △ One Stage Tower, ◇ One Stage Tower with Three Koch LY Mixers, □ One Stage Tower with 7 Koch LY Mixers.

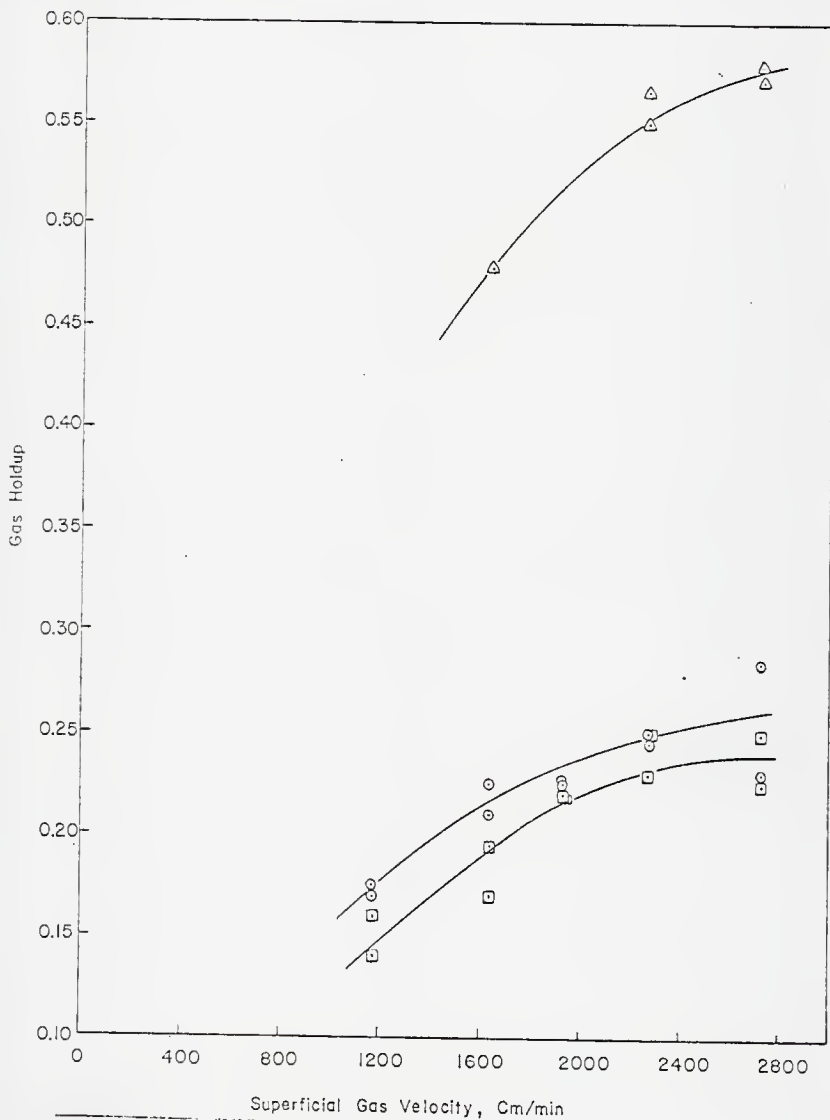


Fig. 3. Gas Holdup as a Function of Superficial Gas Velocity for a Two-Stage Airlift Tower in the Upper Stage; Δ Head Region, \circ Upflow Region, \square Downflow Region.

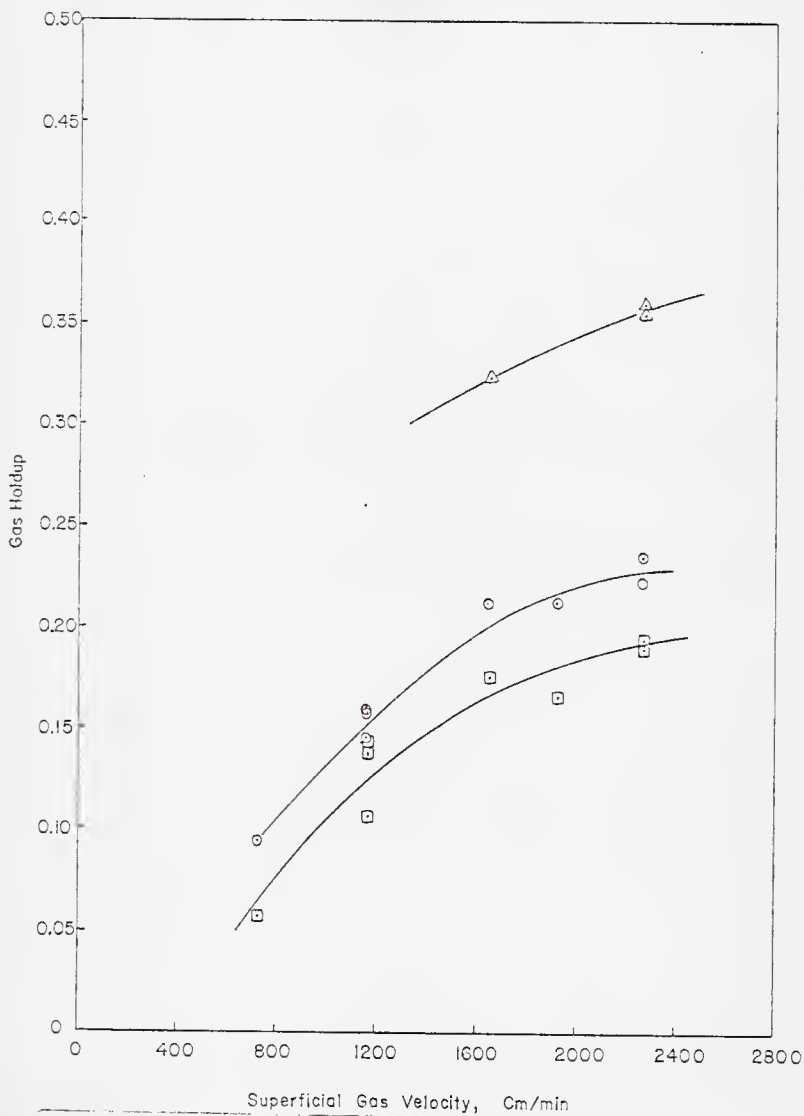


Fig. 4. Gas Holdup as a Function of Superficial Gas Velocity for a One-Stage Airlift Tower; Δ Head Region, \circ Upflow Region, \square Downflow Region.

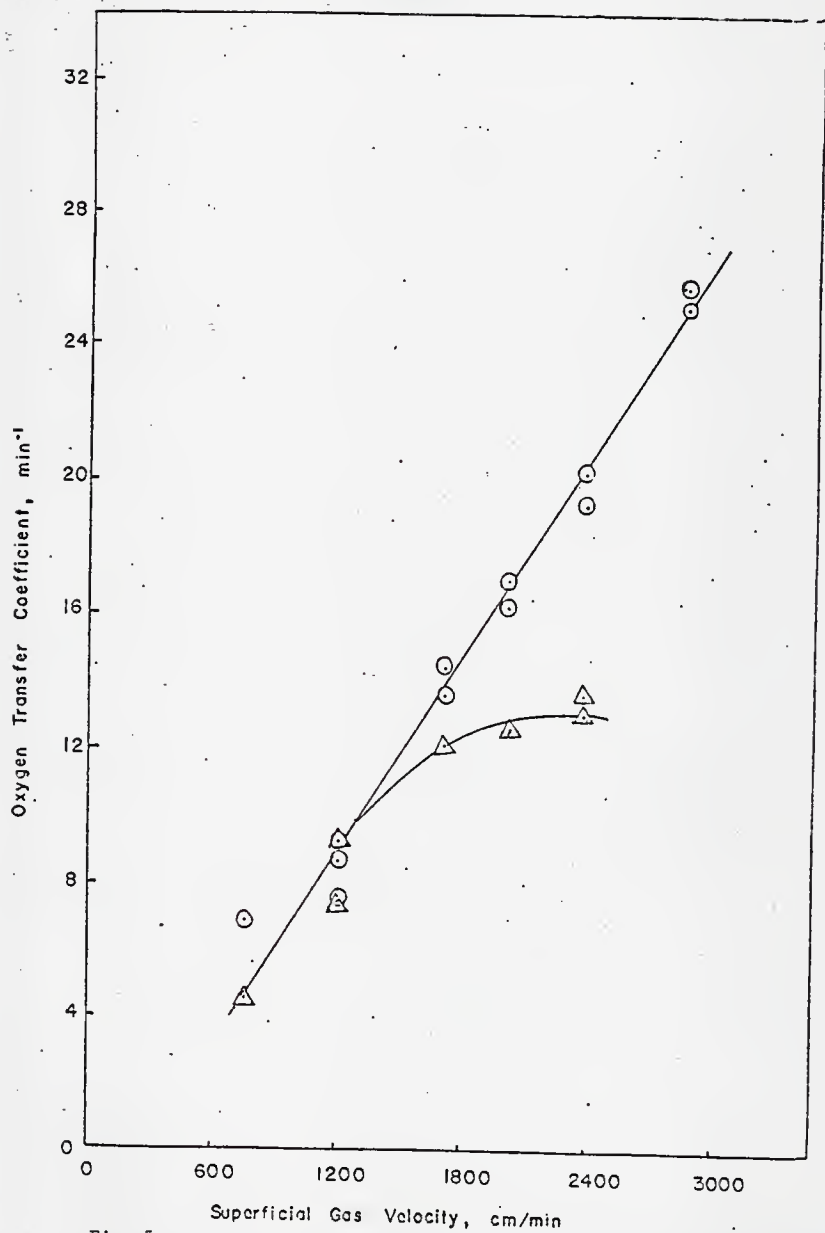


Fig. 5. Oxygen Transfer Coefficient as a Function of Superficial Gas Velocity; ○ Two Stage Tower. △ One Stage Tower.

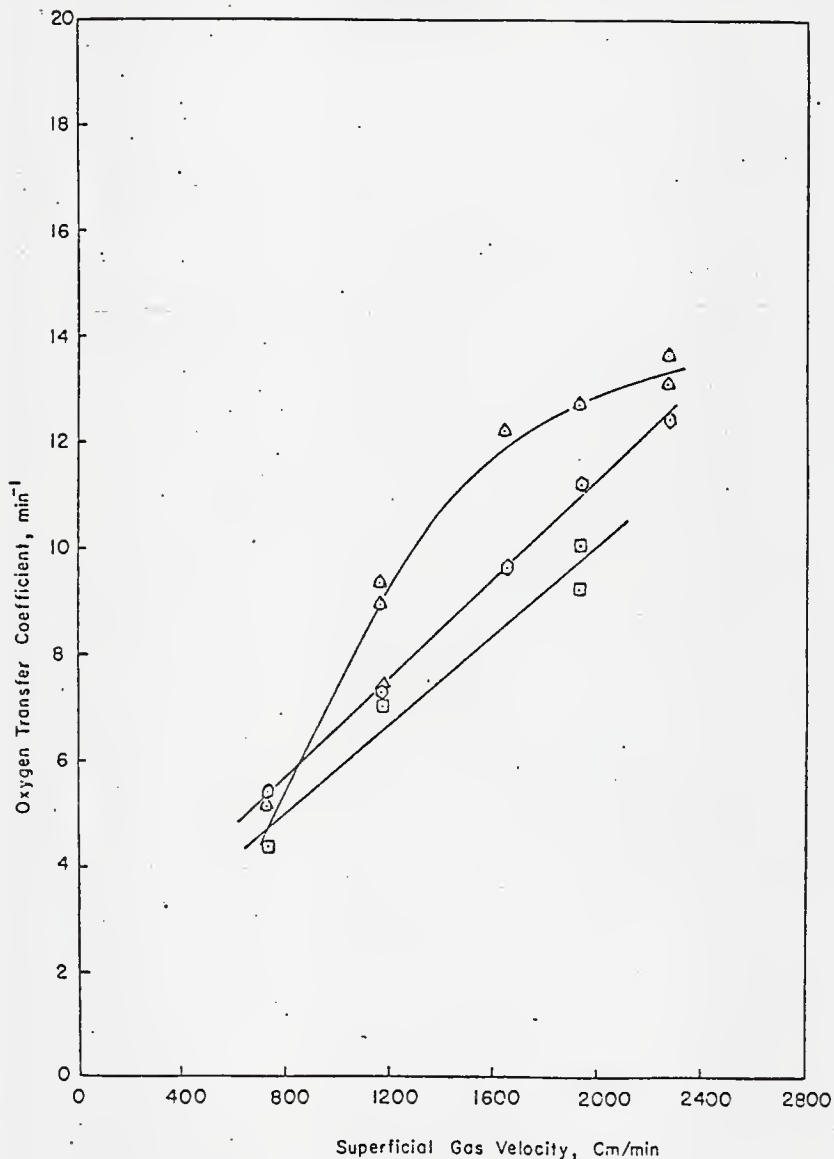


Fig. 6. Oxygen Transfer Coefficient as a Function of Superficial Gas Velocity for a One-Stage Airlift Tower; Δ Empty Tower, \circ Packed with 3 Koch LY Mixers. \square Packed with 7 Koch LY Mixers.

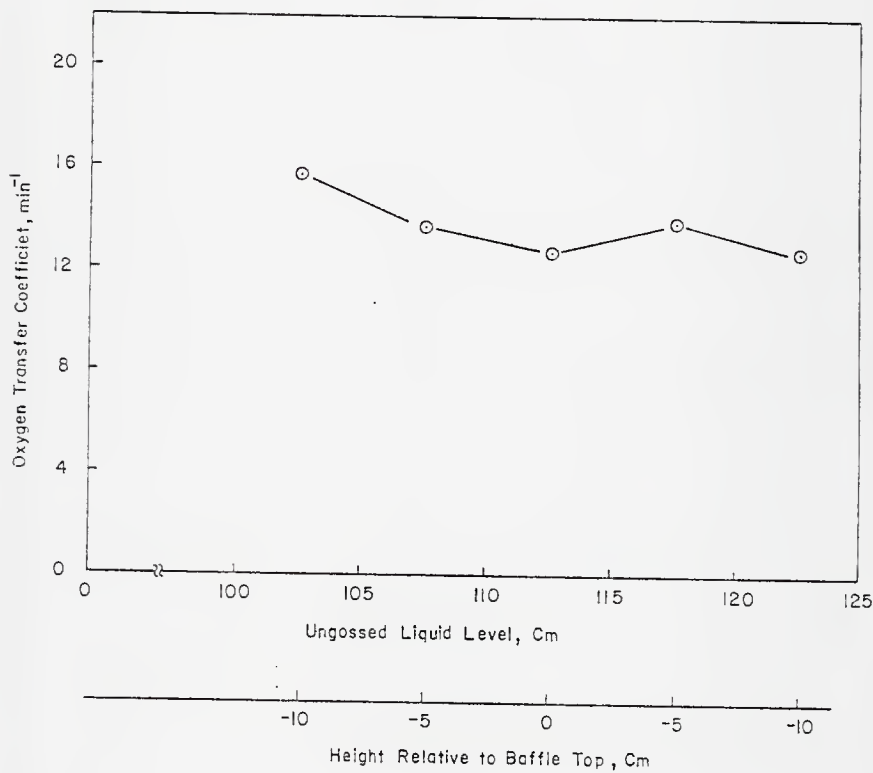


Fig. 7. Oxygen Transfer Coefficient as a Function of Ungassed Liquid Level in a One Stage Tower at a Superficial Gas Velocity of 1929 cm/min.

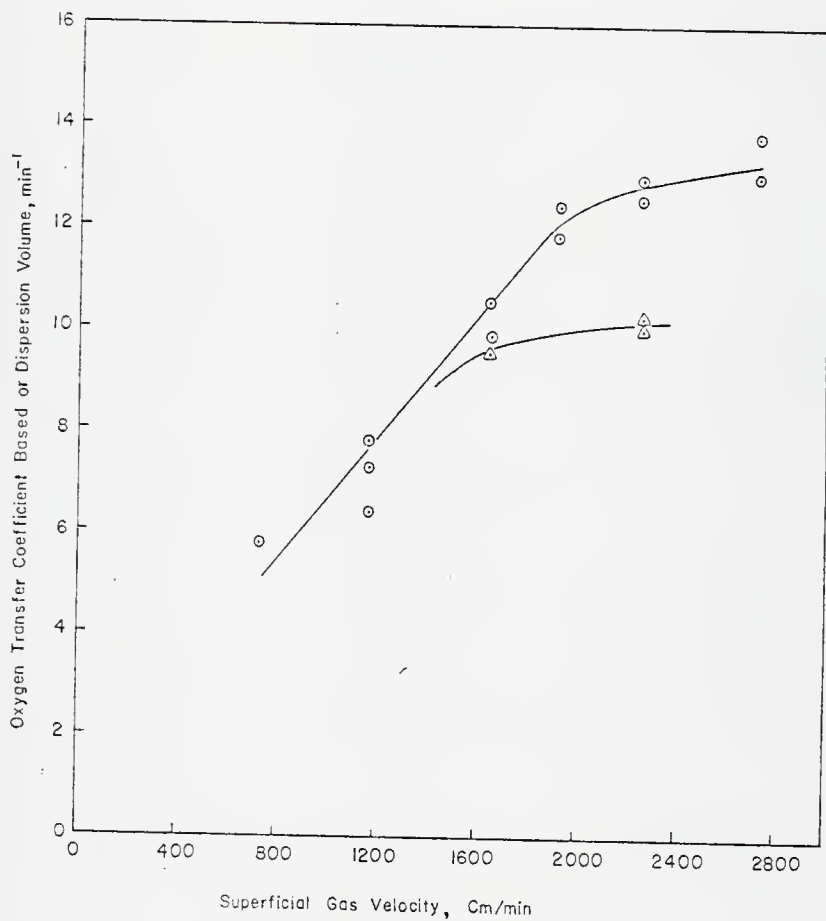


Fig. 8 The Oxygen Transfer Coefficient based on Dispersion Volume as a Function of Superficial Gas Velocity; ○ Two Stage Tower, △ One Stage Tower.

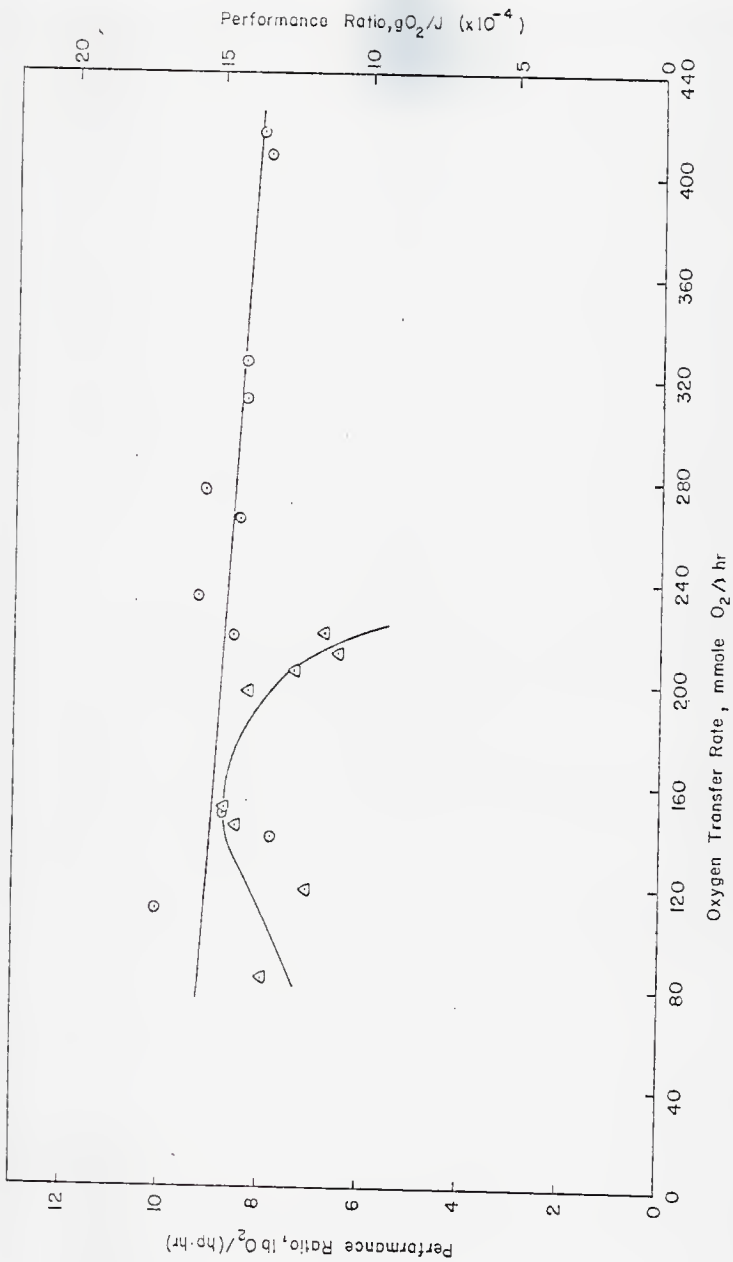


Fig. 9. Performance Ratio as a Function of Oxygen Transfer Rate;
 O Two Stage Tower, Δ One Stage Tower.

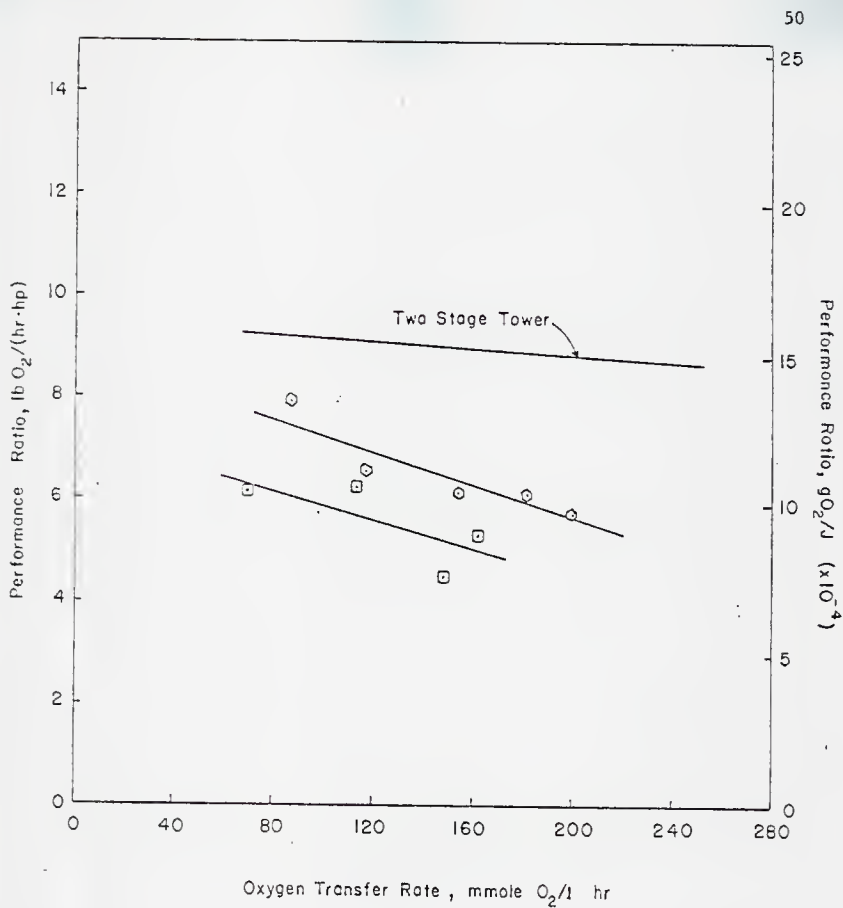


Fig. 10. Performance Ratio as a Function of Oxygen Transfer Rate for the Single Stage Tower; ○ Packed with 3 Koch LY Mixers, □ Packed with 7 Koch LY Mixers.

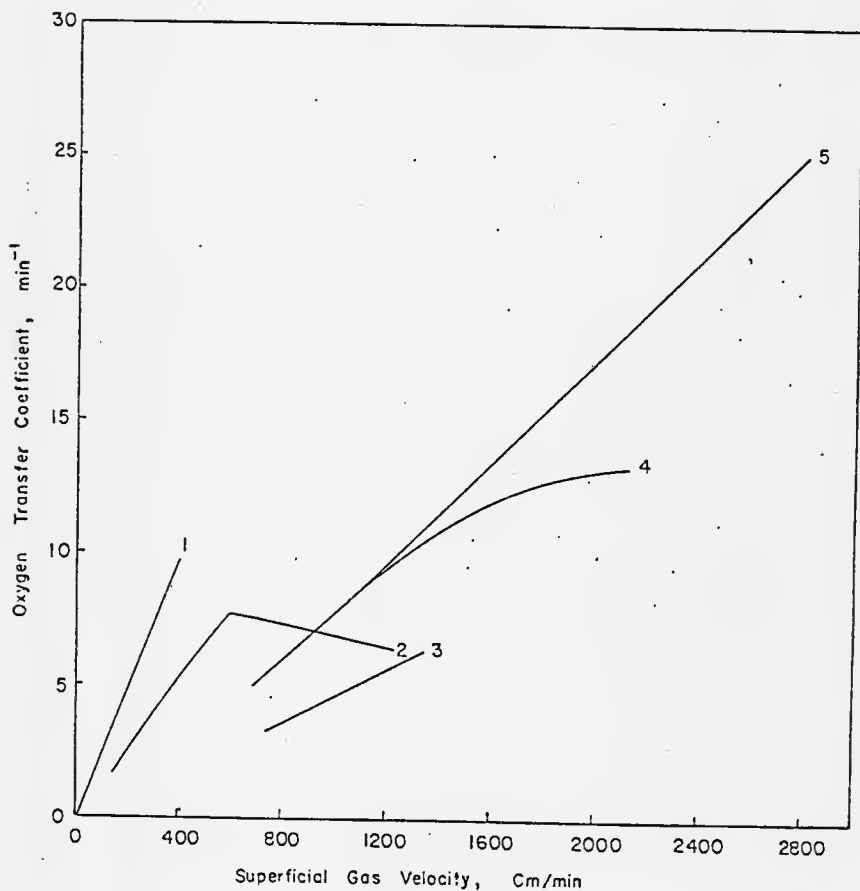


Fig. 11. Oxygen Transfer Coefficient as a Function of Superficial Gas Velocity; 1. rectangular airlift (31), 2. one stage split cylinder airlift (8), 3. concentric cylinder airlift (7), 4. one stage split cylinder airlift, 5. two stage split cylinder airlift.

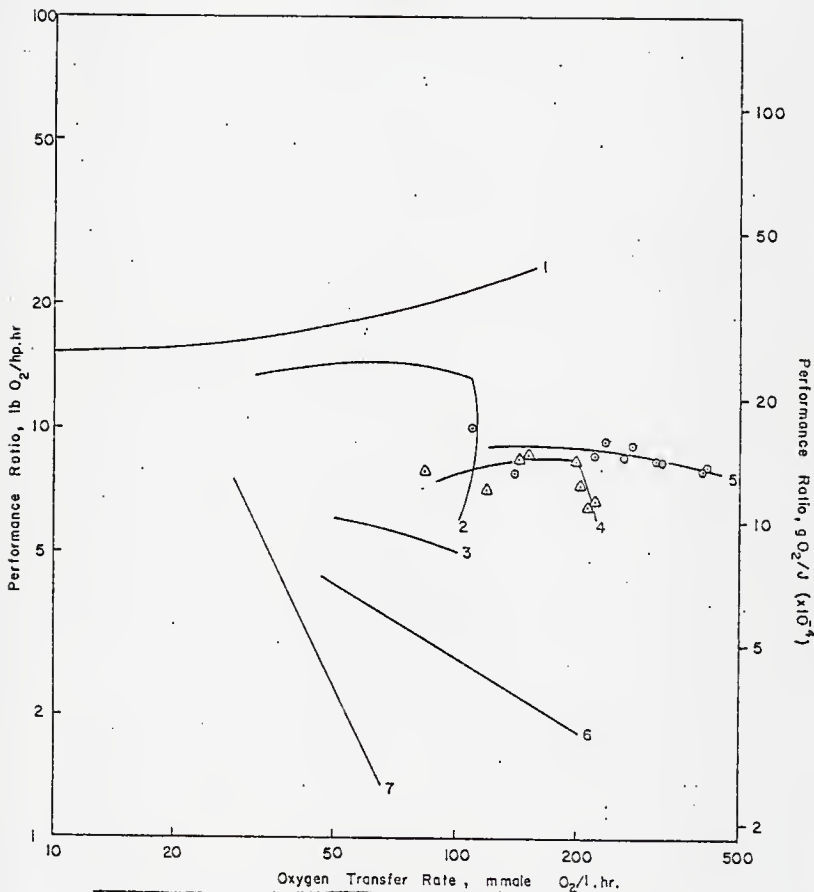


Fig. 12. Performance Ratio as a Function of Oxygen Transfer Rate; 1. rectangular airlift (31), 2. one stage split cylinder airlift (8), 3. concentric cylinder airlift (7), 4. One stage split cylinder airlift, 5. two stage split cylinder airlift, 6. agitated tank (32), 7. aeration tower (5).

APPENDIX A: Sulfite Oxidation Technique

The use of sulfite oxidation to characterize the oxygen transfer of aeration equipment was proposed by Cooper et al.⁽¹⁾ in 1944. This method utilizes the very rapid reaction of sulfite with oxygen in the presence of copper or cobalt catalyst to form sulfate. The oxygen consumption may be determined directly through analysis of incoming and exiting gas streams for oxygen or through reaction stoichiometry. Although the reaction has been studied extensively for the last two decades, considerable confusion still exists as to the reaction kinetics⁽²⁻⁵⁾. This confusion seems to be due to the apparent complexity of the reaction kinetics. According to Astarita⁽⁶⁾ et al., when the reaction is catalyzed by cobalt, it is zero order with respect to oxygen at a sulfite concentration of 0.06 M, first order at 0.25 M, and second order at 0.25 M to 1.0 M. The reaction is zero order with respect to sulfite for a 5 wt% Na_2SO_3 solution⁽²⁾.

Fan and Wang⁽²⁾ have found that the reaction proceeds most rapidly in a pH range of 9 to 11, and the reaction rate is fastest at a temperature of 90°C. The existence of an optimal temperature was attributed to the increase of reaction rate with temperature coupled with a decrease of oxygen solubility in the sulfite solution with increasing temperature. They would not identify explicitly the dependence of the reaction rate on the cobalt catalyst concentration from 1 ppm to 10 ppm CoSO_4 . Fan and Wang⁽²⁾ report reaction rate constants exceeding $0.063 \text{ gmole Na}_2\text{SO}_3/(\text{m}^3\text{s})$, and Orazem and Erickson⁽⁷⁾ report reaction rates up to $0.182 \text{ gmole Na}_2\text{SO}_3/(\text{m}^3\text{s})$ using 1 ppm cobaltous catalyst. Robinson and Engel⁽⁸⁾ and Finn⁽⁹⁾ have recommended the use of cobalt as a catalyst over copper. Pirt et al.⁽¹⁰⁾ found that oxygen absorption rates were two to five times higher when the

reaction was catalyzed by cobaltous ions than when it was catalyzed by Cupric ions.

Maxon and Johnson⁽¹¹⁾ claimed that the absorption of oxygen by a sulfite solution catalyzed by copper must be gas film controlled. Schultz and Gaden⁽¹²⁾ studied oxygen transfer through a stagnant air-sulfite solution interface. Agitation of the gas phase did not increase the oxygen transfer rate; therefore, they concluded that the gas-film was not controlling.

Under the assumptions that the content of the liquid phase is completely mixed and the oxygen content of the gaseous phase remains invariant with respect to the spatial position, an oxygen balance over the aqueous phase yields

$$\frac{dC}{dt} = -N_A + K_L a (C^* - C) \quad (1)$$

where N_A is the rate of oxygen consumption by reaction, $K_L a$ is the oxygen transfer coefficient, C^* is the saturation liquid phase oxygen concentration, and C is the liquid phase oxygen concentration. Since the oxidation of sulfite is very rapid, the reaction is mass transfer controlled, and the bulk oxygen concentration can be assumed negligible.

Thus, a pseudo steady state condition is attained, in which the rate of oxygen consumption by reaction is balanced by the rate of oxygen transfer from the gas phase to the liquid, i.e.,

$$N_A = K_L a C^* \quad (2)$$

The oxygen transfer coefficient, $K_L a$, can be found by measuring the rate of oxygen consumption.

$$K_L a = \frac{N_A}{C^*} \quad (3)$$

The sulfite oxidation reaction is zero order with respect to the sodium sulfite concentration. Thus, equation (3) becomes

$$K_L a = - \frac{K}{C^*} \frac{\Delta C_{\text{Na}_2\text{SO}_3}}{\Delta t} \quad (4)$$

where $\Delta C_{\text{Na}_2\text{SO}_3}$ is the change in sodium sulfite concentration, mg $\text{Na}_2\text{SO}_3/\ell$, in the time interval Δt , min, C^* is in units mg O_2/ℓ , and K is the stoichiometric conversion factor, 0.127 mg $\text{O}_2/\text{mg}/\text{mg Na}_2\text{SO}_3$. The value of C^* can be found in the literature, or can be determined with a dissolved oxygen probe. The rate of oxygen consumption can also be determined through comparison of the mole fraction of oxygen in the inlet and exit gas streams.

The value of $K_L a$ determined through sulfite oxidation usually differs from values found under fermentation conditions. Greenhalgh et al.⁽¹³⁾ found that for low cell concentrations the oxygen transfer coefficient under fermentation conditions was lower than the oxygen transfer coefficient determined through sulfite oxidation. At high cell concentrations the $K_L a$ under fermentation conditions was higher than that determined through sulfite oxidation. The presence of microbial cells as a solid phase has been shown to enhance oxygen transfer⁽¹⁴⁻¹⁶⁾.

Benedek and Bennett⁽¹⁷⁾ note that the $K_L a$ found through sulfite oxidation is not equivalent to that found for an air-water system. This is attributed to the difference in liquid properties between the sulfite solution and water and to the enhancement of mass transfer by the reaction. The addition of electrolytes to water results in the formation of electrical double layers around gas bubbles which become negatively charged and repel each other. This effect prevents coalescence and can also significantly increase oxygen transfer. Zlokarnik⁽¹⁸⁾ reports a seven-fold increase in

$K_L a$ for a 5 wt. percent Na_2SO_3 solution when compared to water. The sulfite method, therefore, can be used safely only as a means of comparing the relative oxygen transfer efficiencies of two systems.

In utilizing the sulfite oxidation technique for a comparison of oxygen transfer devices, a number of precautions should be followed.

1. The solution properties must be constant from experiment to experiment. The addition of a sulfite salt, as noted by Benedek and Bennett⁽¹⁷⁾, can greatly change the viscosity, density, surface charge and interfacial tension of the liquid-gas dispersion. A change in salt concentration will also affect the saturation value of the dissolved oxygen concentration, which then changes the driving force for mass transfer.

If not stored in an airtight container, solid sulfite will slowly react with the oxygen in the air to form sulfate. Constant initial sodium sulfite concentrations in repeated experiments can be attained by adding increasing amounts of solids to compensate for the sulfite degradation. This, however, makes comparison from experiment to experiment difficult since the fluid and interfacial properties are highly dependent upon salt concentration^(17,18). Since the zero order reaction rate constant is to be determined, the maintenance of a constant initial sulfite concentration is not necessary. The total salt concentration is the parameter which should be held constant for all experiments to be carried out for comparisons.

2. The assumption of a negligible liquid oxygen concentration results in a maximum oxygen transfer driving force and the $K_L a$ determined will be conservative. If an actual dissolved oxygen concentration exists, the measured $K_L a$ will be low. It is important to allow the reaction to proceed under near optimal conditions. The pH should be between 9 and 11⁽²⁾ and a

cobaltous catalyst should be employed. Liquid mixing also should be such that no strong sulfite concentration gradient exists as this could result in a non-zero oxygen concentration at some point in the contactor.

The assumption of a negligible oxygen concentration in the liquid phase can be checked by the use of a dissolved oxygen probe.

3. Liquid samples should be analyzed as quickly as possible after being withdrawn from the contactor. Samples should be stabilized immediately, as described by "Standard Methods for the Examination of Water and Wastewater"⁽¹⁹⁾.

References

1. Cooper, C. M., G. A. Fernstrom, and S. A. Miller, "Performance of Agitated Gas-Liquid Contactors," *Ind. Eng. Chem.*, 36, 504 (1944).
2. Fan, L. T., and K. B. Wang, "Oxidation of Sulfite in an Air Lift Reactor Packed with Motionless Mixers," presented at 81st A.I.Ch.E. National Meeting, Kansas City, Mo. (1976).
3. Yagi, S. and H. Inove, "The Absorption of Oxygen into Sodium Sulfite Solution," *Chem. Eng. Sci.*, 17, 411 (1962).
4. Barron, C. H., and H. A. O'Hern, "Reaction Kinetics of Sodium Sulfite Oxidation by the Rapid Mixing Method," *Chem. Eng. Sci.*, 21, 397 (1966).
5. Sawicki, J. E. and C. H. Barron, "On the Kinetics of Sulfite Oxidation in Heterogeneous Systems," *Chem. Eng. J.*, 5, 153 (1973).
6. Astarita, G., G. Marucci, and L. Coletti, "*Chimica Ind., Milano*, 46, 1021 (1964).
7. Orazem, M. E. and L. E. Erickson, "Oxygen Transfer Rates and Efficiencies in One and Two Stage Airlift Towers," submitted *Biotech. and Bioengg.*, 1977.
8. Robinson, R. G., and A. J. Engel, "An Analysis of Controlled-Cycling Mass Transfer Operations," *Bio. Eng. Food Process, Chem. Eng. Prog. Symp. Series*, 69, 129 (1966).
9. Finn, R. K., "Agitation - Aeration in the Laboratory and in Industry," *Bacterial Review*, 18, 254 (1954).
10. Pirt, S. J., D. S. Callow and W. A. Gillett, "Oxygen Absorption Rates in Sodium Sulfite Solutions. Comparison of Cupric and Cobaltous Ions as Catalysts," *Chem. Ind. (London)*, 730 (1957).
11. Maxon, W. D., and M. J. Johnson, "Aeration Studies on Propagation of Bakers Yeasts," *Ind. Eng. Chem.*, 45, 2554 (1953).
12. Shultz, J. S., and E. L. Gaden, Jr., "Sulfite Oxidation as a Measure of Aeration Effectiveness," *Ind. Eng. Chem.*, 48, 2209 (1956).
13. Greenhalgh, S. H., W. J. McManamey, and K. E. Porter, "A Comparison of Oxygen Mass Transfer into Sodium Sulfite Solution and a Bacteriological System," *J. Appl. Chem. Biotechnol.*, 25, 143 (1975).
14. Tsao, G.T.N., "Simultaneous Gas-Liquid Interfacial Mass Transfer and Uptake by Small Particles," *Biotech. and Bioengg.*, 11, 1071 (1969).
15. Van Der Kroon, G.T.M., "The Influence of Suspended Solids on the Rate of Oxygen Transfer in Aqueous Solutions," *Water Research*, 2, 27 (1968).

16. Yagi, H. and F. Yoshida, "Oxygen Absorption in Fermenters - Effects of Surfactants, Antifoaming Agents and Sterilized Cells, J. Ferm. Tech., 52, 905 (1974).
17. Benedek, A., and G. F. Bennett, "Aeration and the Sulfite Oxidation Test," A.I.Ch.E. Symposium Series, No. 145, 71 (1975).
18. Zlokarnik, M., "Influence of Some Important Geometric, Material and Process Parameters on Mass Transfer in Gas-Liquid Contacting," Presented at Engineering Foundation Conference on "Mass Transfer and Scale-Up of Fermentations," Hennicker, N. H., July (1977).
19. Taras, M. J., et al., (eds.) Standard Methods for the Examination of Water and Wastewater, 13th ed., American Public Health Assoc., Washington, D. C. (1971).

APPENDIX B: Data Summary

Table B1. General Tower Characteristics

	One Stage		Two Stage		
Liquid Volume	20.50		20.50		
Diameter	15.20 cm		15.20 cm		
Baffle Height	107.00 cm		(2) 51.00 cm		
Distance from Stage Bottom to Bottom Edge of Baffle	5.50 cm		(2) 5.50 cm		
Sparger Tube Height	5.50 cm		(2) 5.50 cm		
Sparger Tube I. D.	0.95 cm ²		(2) 0.95 cm ²		
Upflow Cross-sectional Area	90.70 cm ²		90.70 cm ²		
Pressure Tap Number and Location	Section	Baffle Edge	Section	Baffle Edge	Stage
0	UP	L	UP	L	lower
1	UP	U	UP	U	lower
2	DN	L	DN	L	lower
3	DN	U	DN	U	lower
4					
5			DN	L	upper
6			DN	U	upper
7			UP	L	upper
8			UP	U	upper

UP upflow section

DN downflow section

L lower edge of baffle (5.5 cm above bottom of stage)

U upper edge of baffle

Table B2. Two-Stage Airlift Tower - No Packing

Run Number	1	2	3	4	5	6	16	17
Rotameter Reading	0.7	0.7	0.7	0.5	1.0	1.0	1.0	1.1
Air Pressure (psig)	5	5	5	0	12	12	9.2	16
Air Flow Rate (std. m ³ /min)	0.106	0.106	0.106	0.0668	0.176	0.176	0.150	0.207
Superficial Gas Velocity (cm/min)	1167	1167	1167	735	1929	1929	1645	2266
vvm (min ⁻¹)	5.23	5.23	5.23	3.28	8.63	8.63	7.36	10.14
Liquid Temperature (°C)	21.7	21.7	22.2	20.0	16.0	17.0	18.0	18.0
Salt Concentration (wt %)	1.0	1.0	1.0	1.0	2.0	1.0	1.0	1.0
Reaction Rate (MgNa ₂ SO ₃ /l min)	-550	-476	-584	-449	-1027	-1049	-983	-1375
K _L a (min ⁻¹)	8.67	7.56	9.27	6.87	16.3	17.1	14.52	20.31
K _L a' (min ⁻¹)	7.29	6.36	7.80	5.78	11.82	12.40	10.53	12.94
Power Consumption (W)	18.8	3.90	17.9	3.55	32.4	31.4	26.4	40.2
Oxygen Transfer Rate (g O ₂ /l hr)	4.48	3.90	4.77	3.55	8.42	8.83	7.49	10.46
Performance Ratio (g O ₂ /J *10 ⁶)	13.6	15.2	15.2	15.2	14.8	16.0	16.1	14.8
Hold Up:								
Overall	0.159	0.159	0.159	0.159	0.275	0.275	0.275	0.363
Lower Stage								
upflow								
downflow								
Upper Stage	0.150	0.150	0.165	0.165	0.225	0.230	0.210	0.250
head								
upflow	0.347	0.430	0.430	0.430	0.366	0.466	0.479	0.569
downflow	0.170	0.175	0.175	0.175	0.225	0.225	0.225	0.250
downflow	0.140	0.160	0.160	0.160	0.220	0.220	0.170	0.250

Table B2 continued

Run Number	18	19	29	30
Rotameter Reading	0.9	1.1	1.18	1.18
Air Pressure (psig)	9.2	16	23.9	23.9
Air Flow Rate (std. m ³ /min)	0.150	0.207	0.249	0.249
Superficial Gas Velocity (cm/min)	1645	2266	2728	2728
vvm (min ⁻¹)	7.36	10.14	12.21	12.21
Liquid Temperature (°C)	15.0	15.4	16.0	16.4
Salt Concentration (wt %)	1.0	1.0	2.0	2.0
Reaction Rate (mg Na ₂ SO ₃ /l min)	-975	-1371	-1593	-1629
K _{L,a} (min ⁻¹)	13.61	19.35	25.29	25.86
K _{L,a'} (min ⁻¹)	9.87	12.52	13.00	13.81
Power Consumption (W)	26.7	39.0	53.3	53.3
Oxygen Transfer Rate (g O ₂ /l hr)	7.01	9.98	13.06	13.34
Performance Ratio (g O ₂ /J x 10 ⁴)	14.9	14.6	14.0	14.3
Hold Up:				
Overall	0.275	0.353	0.486	0.466
Lower Stage				
upflow	0.205	0.245	0.250	0.275
downflow	0.180	0.245	0.250	0.275
Upper Stage				
head	0.479	0.550	0.572	0.579
upflow	0.210	0.245	0.285	0.230
downflow	0.195	0.230	0.250	0.225

Table B3. Pressure Data for the Two-Stage Airlift Tower

Run No.	Tap No.	Pressure (cm H ₂ O gauge)								Head Height (cm)	
		0	1	2	3	4	6	7	8	Lower stage	upper stage
1		111.2	107.4	111.9	119.6	146.0	153.1	145.2	153.9		
2		106.1	114.5	106.1	114.5	143.7	151.8	143.7	152.6		
5		116.3	127.7	117.0	127.4	145.2	156.4	145.0	156.4		
6		113.2	124.9	112.7	124.9	143.2	154.4	142.9	154.4		
16		111.2	121.8	111.7	121.8	142.9	151.6	142.7	154.1	20.3	20.3
17		124.6	137.3	122.6	134.0	143.9	156.6	143.9	156.6	30.5	30.5
18		112.5	122.9	113.2	122.4	143.7	153.6	143.4	154.1	20.3	20.3
19		119.6	132.0	120.1	132.5	144.7	156.4	144.2	156.6	29.2	29.2
29		136.6	149.3	136.6	149.3	146.7	159.4	145.7	160.2	31.8	31.8
30		136.6	150.6	136.6	150.6	148.0	159.4	148.0	159.7	31.8	38.1

Table B4. One-Stage Airlift Tower - No Packing

Run Number	7	8	9	10	11	25	26	27
Rotameter Reading	0.5	0.7	1.0	0.7	0.7	0.9	1.1	1.1
Air Pressure (psig)	0	5	12	5	5	9.2	15.9	15.9
Air Flow Rate (std. m ³ /min)	0.0668	0.106	0.176	0.106	0.106	0.150	0.207	0.207
Superficial Gas Velocity (cm/min)	735	1167	1929	1167	1167	1645	2266	2266
vvm (min ⁻¹)	3.28	5.23	8.63	5.23	5.23	7.36	10.14	10.14
Liquid Temperature (°C)	23.0	23.0	19.0	19.5	19.0	19.0	15.0	16.0
Salt Concentration (wt %)	1.0	1.0	2.0	2.0	1.0	1.0	1.0	1.0
Reaction Rate (mg Na ₂ SO ₃ /ℓ min)	-326	-459	-761	-545	-600	-818	-942	-969
K _L a (min ⁻¹)	5.18	7.38	12.72	9.35	8.96	12.22	13.15	13.67
K _L a' (min ⁻¹)								
Power Consumption (W)	11.1	17.7	29.4	18.0	17.8	9.51	10.02	10.21
Oxygen Transfer Rate (g O ₂ /ℓ hr)	2.69	3.81	6.56	4.83	4.61	25.1	34.5	34.6
Performance Ratio (g O ₂ /J)	13.7	12.2	12.7	15.3	14.7	6.30	6.78	7.04
Hold Up:						14.3	11.2	11.6
Overall						0.222	0.238	0.253
head		0.147	0.213	0.159	0.161	0.323	0.355	0.360
upflow	0.095	0.107	0.166	0.138	0.145	0.213	0.223	0.235
downflow	0.057					0.176	0.190	0.194

Table B5. Pressure Data for the One-Stage Airlift Tower - Unpacked

Run No.	Pressure (cm H ₂ O gauge)				Head Height (cm)	
	Tap No.	0	1	2		3
7		104.3	114.5	106.4	112.5	
8		104.3	120.1	106.1	117.5	
9		104.8	127.7	106.9	124.6	
10		106.4	123.4	107.4	122.1	
11		105.3	122.6	106.4	121.8	
25		104.8	127.7	106.4	125.2	30.5
26		104.8	128.7	106.4	126.7	33.5
27		105.1	130.2	106.9	127.7	36.2

Table B6. One-Stage Airlift Tower - Packed with Three Six Inch Koch LY Mixers in Upflow Section with Six Inch Spacers.

Run Number	20	21	22	23	24
Rotameter Reading	0.9	1.1	1.0	0.7	0.5
Air Pressure (psig)	9.2	15.9	12	5	0
Air Flow Rate (std. m ³ /min)	0.150	0.207	0.176	0.106	0.0668
Superficial Gas Velocity (cm/min)	1645	2266	1929	1167	735
vvm (min ⁻¹)	7.36	10.14	8.63	5.23	3.28
Liquid Temperature (°C)	18.5	18.6	15.0	15.0	18.0
Salt Concentration (wt %)	1.0	1.0	1.0	1.0	1.0
Reaction Rate (mg Na ₂ SO ₃ /l min)	-647	-840	-807	-523	-366
K _L a (min ⁻¹)	9.61	12.49	11.26	7.30	5.40
Power Consumption (W)	26.4	36.7	31.2	18.7	11.7
Oxygen Transfer Rate (g O ₂ /l hr)	4.96	6.43	5.82	3.78	2.78
Performance Ratio (g O ₂ /J × 10 ⁴)	10.7	10.0	10.6	11.5	13.6
Hold Up:					
Overall	0.199	0.229	0.224	0.184	0.139
Head	0.370	0.366	0.375	0.345	0.335

Table B7. Pressure Data for the One-Stage Airlift Tower Packed with Three Koch LY Static Mixers in the Upflow Section with 6 Inch Spacers

Run No.	Pressure (cm H ₂ O gauge)				Head Height (cm)
	Tap No. 0	1	2	3	
20	110.9	123.9	111.9	123.6	26.7
21	112.2	127.2	113.0	127.2	31.8
22	117.7	126.4	113.2	126.4	31.0
23	110.7	122.9	111.4	122.6	24.1
24	110.2	118.5	110.9	118.3	17.3

Table B8. One-Stage Airlift Tower - Packed with Seven Six Inch Koch LY Mixers
in Upflow Section with No Spacers.

Run Number	12	13	14	15
Rotameter Reading	0.5	1.0	0.7	1.0
Air Pressure (psig)	0	12	5	12
Air Flow Rate (std. m ³ /min)	0.0668	0.176	0.106	0.176
Superficial Gas Velocity (cm/min)	735	1929	1167	1929
vvm (min ⁻¹)	3.28	8.63	5.23	8.63
Liquid Temperature (°C)	18.0	19.0	16.5	16.5
Salt Concentration (wt %)	1.0	1.0	1.0	1.0
Reaction Rate (mg Na ₂ SO ₃ /l min)	-295	-675	-494	-648
K _L a (min ⁻¹)	4.36	10.09	7.05	9.25
K _L 'a (min ⁻¹)				
Power Consumption (W)	12.11	32.2	19.1	32.2
Oxygen Transfer Rate (g O ₂ /l hr)	2.24	5.22	3.65	4.77
Performance Ratio (g O ₂ /J x 10 ⁴)	10.53	9.23	10.9	8.43
Hold Up:				
Overall	0.096	0.214	0.146	0.169
Head	0.307	0.485	0.358	0.312

Table B9. Pressure Data for the One-Stage Airlift Tower Packed with Seven Koch LY Static Mixers in the Upflow Section

Run No.	Pressure (cm H ₂ O gauge)			Head Height (cm)
	Tap No. 0	1	2 3	
12	113.2	114.5	114.0 115.0	11.4
13	115.5	121.3	116.8 122.1	29.2
14	113.5	118.3	114.0 118.8	18.3
15	115.8	121.6	116.5 122.1	21.8

Table B10. One-Stage Airlift Tower-No Packing

	31	32	33	34
Run Number	121.5	103.5	117.0	108
Liquid Level (cm)	1.0	1.0	1.0	1.0
Rotameter Reading	13.9	13.9	13.9	13.9
Air Pressure (psig)	0.176	0.176	0.176	0.176
Air Flow Rate (std. m ³ /min)	1929	1929	1929	1929
Superficial Gas Velocity (cm/min)	8.63	8.63	8.63	8.63
vvm (min ⁻¹)	22.0	22.2	17.0	17.2
Liquid Temperature (°C)	1.0	1.0	1.0	1.0
Salt Concentration (wt %)	-804	-989	-967	-952
Reaction Rate (MgNa ₂ SO ₃ /l min)	12.76	15.70	13.96	13.74
K _L a (min ⁻¹)				

STATISTICAL ANALYSIS OF BUBBLE FLOW IN THE DOWNFLOW SECTION OF THE AIRLIFT TOWER

Introduction

Gas-liquid contacting with a continuous liquid phase is an important operation in chemical and biochemical industries. The bubble column and stirred tank are traditionally employed in gas-liquid mass transfer. One of the more promising contactor designs for high mass-transfer applications is the airlift tower invented by Lefrancois et al.⁽¹⁾ in 1954. This device, shown in Fig. 1, can be described as a bubble column divided into two sections. Air is sparged into one of these sections, causing the dispersion in that section to have a lower density than that in the ungasged section. The resulting pressure difference causes a liquid circulation. Liquid agitation is provided, therefore, by the gas supply.

The airlift tower has been described by Hatch⁽²⁾ as having three regions: the upflow, downflow and head regions. The head region, where gas disengagement takes place, is the two phase dispersion above the upflow and downflow regions. Gas bubbles are entrained by the liquid flow in the downflow region; therefore, both phases are present in all parts of the airlift tower.

Ho et al.⁽³⁾ has modeled the airlift tower by treating the upflow region as N tanks-in-series, the downflow region as M tanks-in-series and the head region as one completely mixed tank. This approach can be modified to incorporate dispersion models. The gas phase in the upflow region consists of bubbles in turbulent upward flow. The flow in the downflow section of the tower is more complex. The forces on a bubble in the downflow section are the buoyant force and the drag force, acting in opposite directions. The net direction of flow for a large bubble will be upward and that for a small bubble will be downward. There are, therefore, significant upward

and downward components of gas flow in the downflow section of the airlift tower. The proportion of the incoming gas entrained in the downflow section of the airlift tower needs to be established as a function of spatial position, incoming gas flow rate and system parameters for use in detailed models, such as that proposed by Ho et al.⁽³⁾.

The two-phase flow in the airlift tower is turbulent, and, therefore, a stochastic analysis is often more appropriate than a deterministic approach for the airlift tower⁽⁴⁾. Analyses of turbulence have long used statistical techniques, employing time smoothing to obtain mean values of state variables, autocorrelation to identify the cyclical nature of a process, and cross-correlation to find the time lag between dependent signals generated by the turbulent flow^(5,6).

Mesch et al.⁽⁷⁾ describe the use of correlation methods to measure the velocity of moving surfaces. Ong and Beck⁽⁸⁾ found bulk slurry velocities in turbulent slurry flow by finding the cross correlation between signals from pressure transducers placed a known distance apart. The signals were generated by the pressure variation inherent in turbulent flow. Ong and Beck⁽⁸⁾ reported a measurement accuracy of two percent. Beck et al.⁽⁹⁾ and Mesch and Kipphan⁽¹⁰⁾ measured bulk particle velocities in pneumatic conveyors by obtaining the cross correlation of naturally occurring flow noise, measured by two capacitance transducers placed a known distance apart along the axis of the conveyor. Mesch and Kipphan⁽¹⁰⁾ also employed optical techniques. Lassahn⁽¹¹⁾ measured the flow velocities of two-phase fluids by using radiation beams as sensors to detect the passing of inhomogeneities. Fourier spectrum analysis of the resulting signals was used to extract the velocity information.

Cross-correlation techniques may be used to extract time lag information from two related signals. The method used to generate these signals determines the interpretation of the results as a local or bulk phenomenon. Oki et al.⁽¹²⁾ developed an optical probe which could be inserted into a bed to find local solid particle velocities. Heringe and Davis⁽¹³⁾ used the cross-correlation technique to determine local bubble velocities in air-water mixtures. The signals were generated by two resistivity probes. A single resistivity probe will yield local void fractions and bubble sizes as functions of time^(13,14). The time averaged value is used to characterize these parameters.

Cross-correlation techniques have been shown to be useful for velocity measurement in stationary stochastic systems with a single average velocity. Haines et al.⁽¹⁵⁾ have presented bimodal cross-correlation functions, indicating the presence of two average solid velocities in a fluidized bed. The cross-correlation of signals obtained from the downflow section of the airlift tower can be expected, therefore, to be bimodal since two significant velocity components are present.

The intent of this work was to develop a technique capable of extracting the time lag and the time fraction of flow associated with each velocity component from a bimodal cross-correlation function. A further objective of the work was to experimentally verify the validity of the technique, and to demonstrate its use in the complex two-phase flow of the downflow section of the airlift tower.

Theoretical

A point in a two-phase flow field can only be occupied by one phase at a time. At any time, t , therefore, the void fraction at a point in a gas-liquid system can only have a value of unity or zero. The void fraction

at a point as a function of time will take the form of a square wave with values of one or zero⁽¹⁶⁾. The expectation, or mean, of this function is the time-averaged void fraction.

Each point in the gas-liquid flow field has associated with it a void fraction as a function of time. Suppose that two points are parallel to the net direction of flow and are separated by a short distance so that a bubble passing through one point can reasonably be expected to pass through the other. Then, the respective void fractions as functions of time will be related, and the cross correlation between these two functions will give rise to the time lag between them. If the distance between the two points is known, the bubble velocity can be determined.

Suppose that the gas phase flow in the gas-liquid flow field has significant upflow and downflow components. If point X is above point Y, a bubble moving downward will pass first through X and then Y. Similarly, a rising bubble will pass first through Y and then through X. The cross correlation between the void fraction at X and that at Y is bimodal. Each peak of the cross-correlation function is characterized by a time lag. The time lag corresponding to a downward velocity is positive and that corresponding to an upward velocity is negative. A time fraction, χ , of the bubbles passing through the two points is associated with the downward velocity, and a time fraction $1-\chi$, is associated with the upward velocity.

The void fraction at point X can be represented as the time series, $X(t)$, with the upward component, $X_{up}(t)$, and the downward component $X_{dn}(t)$, i.e.,

$$X(t) = X_{up}(t) + X_{dn}(t) \quad (1)$$

The relationship among $X(t)$, $X_{up}(t)$ and $X_{dn}(t)$ can be seen in Fig. 2. Similarly, the void fraction at Y can be expressed as

$$Y(t) = Y_{up}(t) + Y_{dn}(t) \quad (2)$$

When a bubble is present at point X, $X(t)$ has a value of one, and when the liquid phase is present, $X(t)$ has a value of zero. A bubble rising and a bubble moving downward cannot simultaneously occupy a given point; therefore, the upward and downward components cannot simultaneously have a value of one. The components can, however, simultaneously have a value of zero.

The sample means of $X(t)$ and $Y(t)$ converge to constant values, and therefore, the series $X(t)$ and $Y(t)$ can be considered stationary. The presence of bubbles at point X or Y can be considered to be a random occurrence. The time series representing bubbles moving upward at X is assumed independent of the time series representing bubbles moving downward at Y, and similarly, the series representing bubbles moving downward at X is assumed independent of the series representing bubbles moving upward at Y. The time series representing the bubbles in upward flow at points X and Y, however, are not independent since the bubbles in upward flow will pass through point Y before passing through point X. These series, $X_{up}(t)$ and $Y_{up}(t)$, are related by a time lag which can be determined through correlation techniques. The series $X_{dn}(t)$ and $Y_{dn}(t)$ are similarly related by a time lag.

The cross-covariance function, $\gamma_{WZ}(\tau)$, for two stationary time series, $W(t)$ and $Z(t)$, is a function of time lag, τ ⁽¹⁷⁾, i.e.,

$$\gamma_{WZ}(\tau) = E\{[W(t) - E[W(t)]] [Z(t + \tau) - E[Z(t + \tau)]]\} \quad (3)$$

Equation (3) can be expanded to yield

$$\begin{aligned} Y_{WZ}(\tau) = & E\{W(t)Z(t + \tau) - W(t)E[Z(t + \tau)] - Z(t + \tau)E[W(t)] \\ & + E[W(t)] E[Z(t + \tau)]\} \end{aligned} \quad (4)$$

The expectation of a sum is equal to the sum of the expectations⁽¹⁸⁾; therefore,

$$\begin{aligned} Y_{WZ}(\tau) = & E[W(t)Z(t + \tau)] - E[W(t)] E[Z(t + \tau)] \\ & - E[Z(t + \tau) E[W(t)]] + E[E[W(t)] E[Z(t + \tau)]] \end{aligned} \quad (5)$$

Since

$$E[E[W(t)]] = E[W(t)], \quad (6)$$

equation (5) becomes

$$Y_{WZ}(\tau) = E[W(t)Z(t + \tau)] - E[W(t)] E[Z(t + \tau)] \quad (7)$$

The cross-correlation function is found by normalizing the cross-covariance function as

$$\rho_{WZ}(\tau) = \frac{Y_{WZ}(\tau)}{[Y_{WW}(0) Y_{ZZ}(0)]^{1/2}} \quad (8)$$

where $Y_{WW}(0)$ and $Y_{ZZ}(0)$ are, respectively, the autocovariance functions of $W(t)$ and $Z(t)$ at $\tau = 0$. The autocovariance function of $W(t)$ is given by

$$Y_{WW}(\tau) = E[W(t)W(t + \tau)] - E[W(t)]E[W(t + \tau)] \quad (9)$$

and the autocorrelation function is defined as

$$\rho_{WW}(\tau) = \frac{Y_{WW}(\tau)}{Y_{WW}(0)} \quad (10)$$

The time series $W(t)$ can be discretized to form the discrete series $W(k)$ where k is an integer value corresponding to a sample number. Time, t , is the product of the sample increment, Δt , and the sample number, k . Time lag, τ , can be expressed as the product of the sample increment Δt and the lag, h , defined by

$$h = \frac{\tau}{\Delta t}$$

The cross-correlation and autocorrelation functions for discrete stationary series are functions of h . An estimator of the autocorrelation function of $W(k)$, $\rho_{WW}(h)$, is given by

$$\hat{\rho}_{WW}(h) = \frac{\sum_{k=1}^{K-h} [(W(k) - \bar{W})(W(k+h) - \bar{W})]}{\sum_{k=1}^K (W(k) - \bar{W})^2} \quad (11)$$

where K is the total number of observations, and \bar{W} is the estimated mean of $W(t)$. The estimator of the autocorrelation function $\rho_{WW}(h)$, approaches the true autocorrelation function value as the sample number increases according to ⁽¹⁹⁾

$$\hat{\rho}_{WW}(h) = \rho_{WW}(h) + O_p(K^{-1/2}). \quad (12)$$

The calculation of the autocorrelation function value can be viewed as the matching of a discrete function $W(k)$ with another function

identical to $W(k)$, but shifted by some lag, h . This second function is $W(k + h)$. Suppose that $W(k)$ is a discrete series of random pulses with only one observation for every pulse. Clearly, the matching at a zero lag of $W(k)$ with $W(k + 0)$ is one to one. As shown in Fig. 3a, the matching is not one to one for $W(k)$ and $W(k + 1)$. The autocorrelation function for this series is shown to have a value of one at $h = 0$, and zero at $h \neq 0$ (Fig. 3b). Suppose that the function, $W(k)$, is again a discrete series of random pulses, but now with three observations for every pulse. Even in this case the matching of $W(k)$ with $W(k + 0)$ is one to one; however, the correlation of $W(k)$ with $W(k + 1)$ has a value, as does the correlation of $W(k)$ with $W(k + 2)$, as shown in Fig. 4a. The autocorrelation of $W(k)$ with three observations for every pulse still has a value of one at $h = 0$, but, as shown in Fig. 4b, the peak is spread.

The form of the autocorrelation and the cross-correlation functions is dependent upon the number of observations for each pulse, ℓ . The autocorrelation function of $W(k)$ is intuitively assumed to be described by

$$\hat{\rho}_{WW}(h) = \left(\frac{\ell - 1}{\ell}\right)^{|d-h|} \quad (13a)$$

where d is the theoretical lag. For the autocorrelation function the theoretical lag is zero. The cross-correlation function is assumed to follow equation (13a), but in this case the theoretical lag may be nonzero.

$$\hat{\rho}_{WZ}(h) = \left(\frac{\ell - 1}{\ell}\right)^{|d-h|} \quad (13b)$$

The empirical justification of equations (13a) and (13b) will be examined later.

The time series defined in equations (1) and (2) can be discretized to become functions of the sample number. The cross-covariance function is given by a discrete version of equation (7) which is

$$\begin{aligned} \gamma_{XY}(h) = & E[(X_{up}(k) + X_{dn}(k)) (Y_{up}(k+h) + Y_{dn}(k+h))] \\ & - E[X_{up}(k) + X_{dn}(k)] E[Y_{up}(k+h) + Y_{dn}(k+h)] \quad (14) \end{aligned}$$

Equation (14) can be expanded and rearranged to obtain

$$\begin{aligned} \gamma_{XY}(h) = & E[X_{up}(k) Y_{up}(k+h)] - E[X_{up}(k)] E[Y_{up}(k+h)] \\ & + E[X_{up}(k) Y_{dn}(k+h)] - E[X_{up}(k)] E[Y_{dn}(k+h)] \\ & + E[X_{dn}(k) Y_{up}(k+h)] - E[X_{dn}(k)] E[Y_{up}(k+h)] \\ & + E[X_{dn}(k) Y_{dn}(k+h)] - E[X_{dn}(k)] E[Y_{dn}(k+h)] \quad (15) \end{aligned}$$

or

$$\gamma_{XY}(h) = \gamma_{X_{up} Y_{up}}(h) + \gamma_{X_{up} Y_{dn}}(h) + \gamma_{X_{dn} Y_{up}}(h) + \gamma_{X_{dn} Y_{dn}}(h) \quad (16)$$

The cross covariance, therefore, is additive. Since X_{up} and Y_{dn} are assumed independent, as are X_{dn} and Y_{up} , this relationship becomes

$$\gamma_{XY}(h) = \gamma_{X_{up} Y_{up}}(h) + \gamma_{X_{dn} Y_{dn}}(h) \quad (17)$$

From equation (8), the cross-covariance function becomes

$$\begin{aligned} \gamma_{XY}(h) = & \rho_{X_{up} Y_{up}}(h) [\gamma_{X_{up} X_{up}}(0) \gamma_{Y_{up} Y_{up}}(0)]^{\frac{1}{2}} \\ & + \rho_{X_{dn} Y_{dn}}(h) [\gamma_{X_{dn} X_{dn}}(0) \gamma_{Y_{dn} Y_{dn}}(0)]^{\frac{1}{2}} \end{aligned} \quad (18)$$

By the nature of the one-zero square wave series, we have

$$[X(k)]^2 = X(k) \quad (19)$$

Thus, from equation (9),

$$\gamma_{X_{up} X_{up}}(0) = \mu_{X_{up}} - \mu_{X_{up}}^2, \quad (20)$$

$$\gamma_{X_{dn} X_{dn}}(0) = \mu_{X_{dn}} - \mu_{X_{dn}}^2, \quad (21)$$

$$\gamma_{Y_{up} Y_{up}}(0) = \mu_{Y_{up}} - \mu_{Y_{up}}^2, \quad (22)$$

$$\gamma_{Y_{dn} Y_{dn}}(0) = \mu_{Y_{dn}} - \mu_{Y_{dn}}^2 \quad (23)$$

Introducing equation (13b) and equations (20) through (23) into equation (18)

the cross-covariance function becomes

$$\begin{aligned} \gamma_{XY}(h) = & \left(\frac{\ell-1}{\ell}\right)^{|d_{up}-h|} [(\mu_{X_{up}} - \mu_{X_{up}}^2)(\mu_{Y_{up}} - \mu_{Y_{up}}^2)]^{\frac{1}{2}} \\ & + \left(\frac{\ell-1}{\ell}\right)^{|d_{dn}-h|} [(\mu_{X_{dn}} - \mu_{X_{dn}}^2)(\mu_{Y_{dn}} - \mu_{Y_{dn}}^2)]^{\frac{1}{2}} \end{aligned} \quad (24)$$

where d_{up} represents the theoretical lag corresponding to the upward velocity component, and d_{dn} is the theoretical lag corresponding to the downward velocity component. The lags, d_{up} and d_{dn} , are opposite in sign and, in this study, have a magnitude between 50 and 150 in units of h. The value of the cross-covariance function at a lag of d_{up} is, from equation (24),

$$\begin{aligned} \gamma_{XY}(d_{up}) = & \left[(\mu_{X_{up}} - \mu_{X_{up}}^2) (\mu_{Y_{up}} - \mu_{Y_{up}}^2) \right]^{\frac{1}{2}} \\ & + \left(\frac{\ell - 1}{\ell} \right)^{|d_{dn} - d_{up}|} \left[(\mu_{X_{dn}} - \mu_{X_{dn}}^2) (\mu_{Y_{dn}} - \mu_{Y_{dn}}^2) \right]^{\frac{1}{2}} \quad (25a) \end{aligned}$$

A similar expression can be found for d_{dn} .

$$\begin{aligned} \gamma_{XY}(d_{dn}) = & \left(\frac{\ell - 1}{\ell} \right)^{|d_{up} - d_{dn}|} \left[(\mu_{X_{up}} - \mu_{X_{up}}^2) (\mu_{Y_{up}} - \mu_{Y_{up}}^2) \right]^{\frac{1}{2}} \\ & + \left[(\mu_{X_{dn}} - \mu_{X_{dn}}^2) (\mu_{Y_{dn}} - \mu_{Y_{dn}}^2) \right]^{\frac{1}{2}} \quad (25b) \end{aligned}$$

The cross-covariance function for the combined upward and downward component will have local maxima at d_{up} and d_{dn} , respectively, just as the individual cross-covariance functions for unidirectional upward and downward flow will exhibit maxima at d_{up} and d_{dn} , respectively.

Even though the cross covariance at $h = 0$ is, from equation (24),

$$\begin{aligned} \gamma_{XY}(0) = & \left(\frac{\ell - 1}{\ell} \right)^{|d_{up}|} \left[(\mu_{X_{up}} - \mu_{X_{up}}^2) (\mu_{Y_{up}} - \mu_{Y_{up}}^2) \right]^{\frac{1}{2}} \\ & + \left(\frac{\ell - 1}{\ell} \right)^{|d_{dn}|} \left[(\mu_{X_{dn}} - \mu_{X_{dn}}^2) (\mu_{Y_{dn}} - \mu_{Y_{dn}}^2) \right]^{\frac{1}{2}} \quad (26) \end{aligned}$$

it is reasonable to assign a value of zero to $\gamma_{XY}(0)$. The reason is that zero time lag corresponds to an infinite bubble velocity, which is improbable in the present system. The cross-covariance function, therefore, is linearly translated so that the value of $\gamma_{XY}(0)$ is zero. The value of the cross-covariance function at d_{up} relative to $\gamma_{XY}(0)$ is

$$L_{up} = \gamma_{XY}(d_{up}) - \gamma_{XY}(0), \quad (27)$$

or

$$\begin{aligned} L_{up} = & [(\mu_{X_{up}} - \mu_{X_{up}}^2)(\mu_{Y_{up}} - \mu_{Y_{up}}^2)]^{1/2} [1 - (\frac{\ell-1}{\ell}) |d_{up}|] \\ & + [(\mu_{X_{dn}} - \mu_{X_{dn}}^2)(\mu_{Y_{dn}} - \mu_{Y_{dn}}^2)]^{1/2} [(\frac{\ell-1}{\ell}) |d_{dn} - d_{up}| \\ & - (\frac{\ell-1}{\ell}) |d_{dn}|] \end{aligned} \quad (28)$$

Similarly at d_{dn} , we have

$$L_{dn} = \gamma_{XY}(d_{dn}) - \gamma_{XY}(0), \quad (29)$$

or

$$\begin{aligned} L_{dn} = & [(\mu_{X_{up}} - \mu_{X_{up}}^2)(\mu_{Y_{up}} - \mu_{Y_{up}}^2)]^{1/2} [(\frac{\ell-1}{\ell}) |d_{up} - d_{dn}| - (\frac{\ell-1}{\ell}) |d_{up}|] \\ & + [(\mu_{X_{dn}} - \mu_{X_{dn}}^2)(\mu_{Y_{dn}} - \mu_{Y_{dn}}^2)]^{1/2} [1 - (\frac{\ell-1}{\ell}) |d_{dn}|] \end{aligned} \quad (30)$$

The peak fraction at d_{up} is defined as

$$\Omega_{up} = \frac{L_{up}}{L_{up} + L_{dn}} \quad (31)$$

Since d_{up} , d_{dn} and $(d_{up} - d_{dn})$ are large in this study, we have

$$\begin{aligned} \left(\frac{\ell - 1}{\ell}\right) |d_{dn}| &\approx 0 \\ \left(\frac{\ell - 1}{\ell}\right) |d_{dn}| &\approx 0 \\ \left(\frac{\ell - 1}{\ell}\right) |d_{up} - d_{dn}| &\approx 0 \end{aligned} \quad (32)$$

These assumptions will be experimentally justified later.

From equations (28), (30), (31) and (32), the peak fraction becomes

$$\Omega_{up} = \frac{[(\mu_{X_{up}} - \mu_{X_{up}}^2)(\mu_{Y_{up}} - \mu_{Y_{up}}^2)]^{\frac{1}{2}}}{[(\mu_{X_{up}} - \mu_{X_{up}}^2)(\mu_{Y_{up}} - \mu_{Y_{up}}^2)]^{\frac{1}{2}} + [(\mu_{X_{dn}} - \mu_{X_{dn}}^2)(\mu_{Y_{dn}} - \mu_{Y_{dn}}^2)]^{\frac{1}{2}}} \quad (33)$$

If every bubble which passes through point X also passes through point Y,

$$\mu_{X_{up}} = \mu_{Y_{up}} = \mu_{up}, \quad (34)$$

and similarly,

$$\mu_{X_{dn}} = \mu_{Y_{dn}} = \mu_{dn} \quad (35)$$

The peak fraction at d_{up} can then be expressed as

$$\Omega_{up} = \frac{(\mu_{up} - \mu_{up}^2)}{(\mu_{up} - \mu_{up}^2) + (\mu_{dn} - \mu_{dn}^2)} \quad (36)$$

or

$$\Omega_{up} = \frac{\mu_{up}}{\mu_{up} + \mu_{dn} \left(\frac{1 - \mu_{dn}}{1 - \mu_{up}}\right)} \quad (37)$$

When μ_{dn} and μ_{up} are small, equation (37) becomes

$$\Omega_{up} = \frac{\mu_{up}}{\mu_{up} + \mu_{dn}} \quad (38a)$$

A similar expression results for the peak fraction at d_{dn} as

$$\Omega_{dn} = \frac{\mu_{dn}}{\mu_{dn} + \mu_{up}} \quad (38b)$$

As mentioned previously, the means, μ_{dn} and μ_{up} , are respectively the time averaged void fractions resulting from the downward and upward components of flow. Hence, equations (38a) and (38b) become respectively

$$\Omega_{up} = \frac{\phi_{up}}{\phi_{up} + \phi_{dn}} = 1 - \chi \quad (39a)$$

$$\Omega_{dn} = \frac{\phi_{dn}}{\phi_{dn} + \phi_{up}} = \chi \quad (39b)$$

where the total void fraction at a point, ϕ_T , is expressed as the sum of its upward component, ϕ_{up} , and its downward component, ϕ_{dn} . The peak fraction corresponding to a given component of bubble flow resulting from a bimodal cross-covariance function is equal to the corresponding time fraction of bubble flow.

Experimental

The relationship developed in the preceding section between the cross-covariance peak fraction and the time fraction of bubble flow was used to analyze the bimodal cross-covariance functions characteristic of bubble flow in the downflow section of the airlift tower. This section describes the facilities and procedures used to generate these functions.

Facilities

The description of the experimental equipment consists of three parts: the probe, the signal analysis system and the airlift tower.

Probe: The presence of a gas or liquid phase at two points in the flow system was detected by a two needle resistivity probe, which used the change in electrical conductivity between the phases to detect bubbles. The probe design is shown in Fig. 5. The two needles were fashioned from Platinum 10% Rhodium wire with 0.02 cm O.D. The wire was honed to a 0.0012 cm tip radius and inserted into a stainless steel tube body with 0.635 cm O.D. The needles were insulated with a fast drying varnish such that only the tip was exposed. The tube served as a common return electrode for the needles.

The tube was flattened near the needle end to accommodate the needles and to present the least resistance to flow. Frictional resistance to bubble flow was minimized by angling the needles away from the detection path as shown in Fig. 5. In the airlift tower bubbles were detected flowing in both the upward and downward directions. The needles were angled against the downward direction of flow to ensure the piercing and detection of bubbles moving downward. Independent tests in a bubble column indicated that, given the same bubble flow, the probe with needles angled against the flow, as shown in Fig. 5, detected 25 percent more bubbles than the probe with needles angled away from the flow.

Herringe and Davis ⁽¹³⁾ used stainless steel suture needles for resistivity probes. Stainless steel needles were used in the initial phases of this work but severe corrosion problems made their use

unacceptable. Platinum 10% Rhodium alloy and Platinum needles both performed well, and Platinum 10% Rhodium was selected because of its durability.

The distance between the two needles of the probe was determined by photographing the probe tips with a known reference length. A 35 mm camera with a 50 mm lens was used with a macro +10 lens added to increase the size of the image on the negative. Comparative lengths were measured from 11 cm x 17 cm prints. The distance between probe tips varied from probe to probe, and ranged from 0.41 cm to 0.51 cm.

Signal Analysis System: The block diagram of the resistivity probe system is shown in Fig. 6. A 10 kHz alternating current was supplied to the common electrode by an Interstate Electronics Corporation F-74 signal generator. The conductivity of the X and Y electrical circuits changed instantaneously when bubbles enveloped the respective probe tips. The resulting signal was a 10 kHz current with reduced amplitude coinciding with the presence of a bubble at the electrode. (see "Raw Signal" in Fig. 5). This signal was passed through a comparator which grounded the signal with amplitudes greater than a variable reference voltage (see "After Comparator" in Fig. 5). The frequency of this signal divided by the input signal frequency yields the fraction of time the needle was enveloped by bubbles. A Fluke 1900A Multi-counter was used to obtain frequencies of the processed signal averaged over one second. The average of this value over a 40 second period of time was used to obtain the time averaged void fraction.

After the comparator, the signal was treated by a frequency to voltage converter. The signals generated here were square wave forms (see "After Frequency to Voltage Converter" in Fig. 5). These were treated by a Honeywell Model SAI-43A Correlator and Probability Analyzer. The analyzer

discretized the signals with a selected sample time increment. The analysis was conducted in real time, and over 450,000 observations were taken. The sampling time was over 90 seconds which was sufficient to ensure reproducibility of the results.

Autocovariance and cross-covariance functions were viewed on an oscilloscope, and a marker pulse was employed to locate the value of h corresponding to the covariance peaks. The values of h ranged from -200 to 200, and the sample time increment, Δt , was chosen in such a way that the peak value of h was near plus or minus 100. The analysis was conducted in the clip mode of the correlator which transforms the incoming signals into a ± 1 square wave. Since the input to the correlator was of the square wave form, the use of the clip mode did not affect the signal form and made the most efficient use of the correlator. Cross correlation with and without the clip mode yielded identical time lag information.

Airlift Tower: The split cylinder airlift tower⁽²¹⁾ studied held a liquid volume of 10.25 l and had a 15.24 cm I.D. The baffle height was 50.8 cm and the distance from the lower edge of the baffle to the bottom of the tower was 5.5 cm. The ungasged liquid was level with the top of the baffle. Air was filtered and the flowrate was monitored by a Fisher and Porter (T2-1308/2) rotameter which had been calibrated with a wet test meter.

Procedures

Since the cross-covariance analysis technique presented in this work is relatively unknown, an investigation of the validity of the technique for slug bubble flow through a tube was conducted. The method used to verify the

technique and the procedures used in studying the downflow section of the airlifts tower are presented.

Verification of Cross-Covariance Technique: Slug bubble flow in a 0.5 cm I.D. latex tube was examined to identify the cross-covariance functions for a simple unidirectional flow system. A constant liquid head and gas entrainment as shown in Fig. 7 provided constant gas-liquid flow conditions. The probe was inserted into a latex tubing and the response signals were recorded on a Hewlett Packard tape recorder.

The cross-covariance function of the response signals recorded on tape was obtained for a given period of time. The tape direction was then reversed and the correlation resumed. The resulting cross-covariance function was bimodal and approximated that found for two-directional bubble flow. Since the signals correlated in the forward and reverse directions were identical, the time fraction of correlation conducted in the forward tape direction corresponded directly with the time fraction of downward bubble flow. If equation (38) is valid, the peak fraction of downward bubble flow will be equal to the corresponding time fraction of flow. The autocorrelation functions of the response signals were obtained to verify the random nature of the appearance of bubbles at points X and Y.

Analysis of Bubble Flow in the Airlift Tower: The airlift tower was studied with an air-water system at superficial gas velocities ranging from 0.0683 m/s to 0.3115 m/s. The liquid temperature was $17.4 \pm 2.7^\circ\text{C}$ and the air temperature was 21°C .

Open end manometers were used to obtain pressure drop and regional hold-up data. These manometers were located at the bottom and top of each baffle on the upflow and downflow sections of the tower. The overall gassed liquid level was measured to determine the overall gas hold-up.

The average liquid circulation rate was determined by hot water tracer analysis⁽²¹⁾ in the downflow section of the tower. The responses from Copper-Constantan thermocouples centered in the tower and 43.9 cm apart were recorded on a Honeywell Electronite 19 two-pen stripchart recorder. The distance between peak centers was converted into real time. The resulting liquid velocity is a cross-sectional averaged quantity found from the average time of fluid travel between two points in the tower. The velocity changes inversely with the local void fraction. Therefore, the value of interest is the liquid circulation rate, found as the product of the bulk liquid velocity and the average cross-sectional area occupied by the liquid:

$$Q_L = v_L (1 - H_d) A \quad (41)$$

where A is the cross sectional area, m^2 , and H_d is the hold-up in the downflow section of the airlift tower.

The bubble flow was examined at two levels in the downflow section of the airlift tower. Level 1 corresponded to the plane perpendicular to the baffle and 4.5 cm below the upper edge of the baffle. Level 2 was located 1.8 cm above the lower edge of the baffle. Both levels were assumed to be normal to the net bubble flow. At each level the flow field was examined at four radial positions for each of four angular positions. The flow field was examined, therefore, at a total of sixteen positions for each level.

Results and Discussion

This section contains two parts. The first part examines the validity of the cross-covariance analysis technique described in the theoretical section. The second part presents and analyzes the results obtained by applying this technique to the airlift tower.

Verification of Cross-Covariance Technique.

Inherent in the derivation of equation (38) was the assumption that the presence of a bubble at a point in a flow field is a random occurrence. The presence of cyclic phenomena in a time series can be detected through the autocovariance function. The autocovariance function has a maximum value at a lag of zero and is symmetric about zero. The presence of harmonic peaks at $h \neq 0$ indicates the presence of a cyclic process. The autocovariance functions for the two electrode response signals, shown in Fig. 8, indicate that the bubbles occur randomly with respect to time. The spread of the peak at zero lag is due to the fact that more than one sample observation were taken for each pulse, as discussed previously. The autocorrelation function is approximated by equation (13a) with $d = 0$. A comparison of equation (13a) with an experimental autocorrelation function is presented in Fig. 9 with $\lambda = 18$. The agreement is good.

The cross-correlation function is approximated by equation (13b). This equation with $d = 72$ and $\lambda = 20$ is compared to an experimental cross-correlation function in Fig. 10. The spread of the experimental cross-correlation function is greater than that predicted by equation (13b). This can be explained by observing that the theoretical lag, d , has a constant value of zero in the case of autocorrelation. This is not true for cross-correlation, and indeed, the theoretical lag for many systems can be expected to be a function of time with constant mean, as explained below.

The cross-correlation function, by analogy with Eq. (13), can be approximated by

$$\hat{\rho}_{wz}(h) = \frac{1}{K} \sum_{k=1}^K \left(\frac{\lambda - 1}{\lambda} \right)^{|d(k) - h|} \quad (41)$$

where d as a function of k is to be determined. If $d(k)$ has a skewed distribution the modal value of $\hat{\rho}_{wz}(h)$ will be at a lag, h , between the mean of $d(k)$ and the modal value of $d(k)$. The time lag indicated by an experimentally obtained cross-correlation function can be considered as a mean value contingent upon the assumption that the mean time lag and modal time lag are close. The distribution of instantaneous velocities, therefore, is assumed normal. Since the theoretical lag as a function of time is unknown, the cross-correlation function was approximated by equation (13b), under the assumption that the velocity distribution is symmetric about the mean.

The theoretical time lag can be expressed as

$$d = \frac{P}{\Delta t} \quad (42)$$

where ℓ is the theoretical time lag in units of time. The number of observations per pulse can be expressed similarly as

$$\ell = \frac{m}{\Delta t} \quad (43)$$

where m is the length of time a bubble is detected at a point. Equation (32) can now be expressed as

$$R = \left(\frac{\ell - 1}{\ell}\right) |d| = \left[\frac{\frac{m}{\Delta t} - 1}{\frac{m}{\Delta t}} \right] \frac{P}{\Delta t} \quad (44)$$

where P represents the upflow theoretical time lag, the downflow theoretical time lag or the difference between them [see equation (32)].

In order that ℓ be greater than one the constraint is added that $0 < m \leq \Delta t$. R has a minimum value at $\Delta t = m$ and a maximum value in the limit

as Δt approaches zero. From L'Hopitals rule,

$$\lim_{t \rightarrow 0} \left[\frac{\frac{m}{\Delta t} - 1}{\frac{m}{\Delta t}} \right]^{\frac{P}{\Delta t}} = e^{-\frac{P}{m}} \quad (45)$$

Since velocity can be expressed as

$$v = \frac{B}{P} = \frac{D}{m} \quad (46)$$

where B is the distance between points X and Y and D is the chord of the bubble seen by the probe, the ratio P/m can be expressed as B/D .

Four operational constraints now become apparent. The sample increment, Δt , should be chosen large enough to minimize R, but small enough to maintain the sensitivity of the technique to signal variations. The distance between points X and Y should be sufficiently large to maximize the ratio B/D , but sufficiently small to ensure the correlation between $X(t)$ and $Y(t)$.

Representative parameter values for slug bubble flow in a tube were $m = 1.5$ ms, $\Delta t = 0.1$ ms and $P = 7.9$ ms, and the resulting value of R was 0.0043. This apparently can be neglected when compared to unity. The assumptions expressed as equation (32) are, therefore, empirically justified.

A typical bimodal cross-covariance function found from the slug bubble flow in a tube (see Procedures - Verification of Techniques) is presented in Fig. 11. The time fraction of upward bubble flow is 0.625. If equation (38) is valid, the cross-covariance peak fraction of downward bubble flow will be equal to the corresponding time fraction of flow. Fig. 12 shows that the peak height fraction yields a reasonable approximation of the time fraction of bubble flow in the corresponding direction.

The lags obtained from the bimodal cross-covariance function were identical to those obtained from the individual cross-covariance functions for unidirectional flow.

Analysis of Bubble Flow in the Airlift Tower

The experimentally determined gas hold-ups in the upflow, downflow and head regions of the airlift tower for the air-water system are presented as functions of superficial gas velocity based on the upflow cross-sectional area in Fig. 13. The high hold-up in the head region was probably due to entrainment of surface air. The overall hold-up is shown in Fig. 14 as a function of the superficial gas velocity.

In Fig. 15 the cross-sectional average linear liquid velocity in the downflow section is shown as a function of the superficial gas velocity. This was determined from the average time of fluid travel between two points in the tower as described in the Section: Experimental. In Fig. 16 the liquid circulation rate is shown as a function of the superficial gas velocity. It can be seen that the liquid circulation rate increased approximately linearly with the superficial gas velocity.

The autocovariance of typical pair of response signals from the downflow section of the airlift tower, shown in Fig. 17, indicates that the bubble flow in the airlift tower is essentially random. A typical cross-covariance function generated from the downflow section of the airlift tower is shown in Fig. 18. The bimodal characteristic of the function is apparent, with one dominant peak appearing on each side of the zero lag. The lowest value of the cross-covariance function occurs at a zero lag. This observation is consistent with the assignment of a zero value to the cross-covariance function at a zero lag, as explained in the theoretical section.

The total time averaged void fraction at a point was found using the procedure described in the experimental section. The validity of using

cross-covariance peak fractions to estimate the time fraction of bubble flow in a given direction was shown in the preceding section. The time fraction, found in this manner, was used to separate the void fraction into its upward and downward components as

$$\phi_T = \phi_{up} + \phi_{dn} \quad (48)$$

From the location of the cross-covariance peaks the positive and negative mean lags were obtained. This results in downward and upward velocities. The overall time-averaged bubble velocity, $(v\phi)_0$, can be found from

$$(v\phi)_0 = v_{up}\phi_{up} - v_{dn}\phi_{dn} \quad (49)$$

where v_{up} and v_{dn} are positive quantities with direction indicated by the subscript. The overall time-averaged bubble velocity at level 1 is shown as a function of the dimensionless radius in Fig. 19. The parameters are the superficial gas velocity, v_g , and the angular position, θ . The bubble velocity and void fraction were assumed to be zero at the walls. The outer wall was located at a dimensionless radius of one, and the inner wall was located at a dimensionless radius of 0.044 or 0.071, depending on angular position. The dimensionless radius at the baffle wall was not zero due to the thickness of the baffle plate. The overall time-averaged gas velocity was downward at the outer wall and upward near the baffle. The downward liquid velocity at level 1, therefore, must be greatest near the outer wall. The gas phase flow field was essentially symmetric with respect to angular position, normal to the baffle wall, θ .

The void fraction at level 1 is shown as a function of the dimensionless radius in Fig. 20. Again, the superficial gas velocity and angular position are parameters. The largest void fraction is observed at a dimensionless radius greater than 0.5. This is due, in part, to the inability of the probe to detect all rising bubbles as explained previously. The separation of the

total void fraction into its upward and downward components should be viewed, therefore, as leading to a correction of downward bubble flow rate measurements. The upward bubble flow rate can be determined through mass balance over the downflow region.

The void fraction, ϕ_T , can be found as

$$\phi_T = \frac{1}{A} \int_0^\pi \int_0^R \phi_T r \, dr \, d\theta \quad (50)$$

where integration is performed over the plane normal to the flow. The downward and upward flow rates of air through that plane are found, respectively, as

$$Q_{A_{dn}} = \int_0^\pi \int_0^R v_{dn} \phi_{dn} r \, dr \, d\theta \quad (51a)$$

$$Q_{A_{up}} = \int_0^\pi \int_0^R v_{up} \phi_{up} r \, dr \, d\theta \quad (51b)$$

Integration of equations (50) and (51) was performed graphically through the use of a planimeter. Values of $v_{dn} \phi_{dn} r$, $v_{up} \phi_{up} r$ and $\phi_T r$ are presented as functions of the dimensionless radius with the angular position, θ , as a parameter, in Figs. 21, 22 and 23, respectively.

The integral of $v_{dn} \phi_{dn} r$ with respect to r is shown as a function of the angular position in Fig. 24. Maxima are observed at an angle of 0.5π corresponding to the line perpendicular to the baffle wall. In Fig. 25 the integral of the upward velocity, $v_{up} \phi_{up} r$, with respect to r is presented as a function of the angular position. This function appears to be bimodal with maximum values at $\theta = 0.2\pi$ and 0.8π and local minima at $\theta = 0$, 0.5π and π . The integral of $\phi_T r$ with respect to r is shown as a function of the angular position in Fig. 26. The values presented Fig. 24, 25 and 26 were

graphically integrated to obtain the downward air flow rate, upward air flow rate and void fraction at level 1. A similar analysis was conducted at level 2, located 1.8 cm above the lower edge of the baffle. The conductivity probe was able to detect bubble flow only at the highest superficial gas velocity studied, 0.3115 m/s. Values of $v_{up} \phi_{up} r$, $v_{dn} \phi_{dn} r$ and $\phi_T r$ are presented, respectively, in Figs. 27, 28 and 29. The integrals of these quantities with respect to the radius are shown as functions of the angular position in Figs. 30 and 31.

The gas flow rates so determined are presented in Fig. 32. The downward flow of air at level 1 with a superficial gas velocity of 0.3115 m/s based on the upflow cross-section area was $2.88 \times 10^{-4} \text{ m}^3/\text{s}$. This is 10.2 percent of the incoming air flow rate. The downward flow of air at level 2 can be considered as the flow of air carried into the upflow section by the liquid circulation. This was found to be $0.2508 \times 10^{-4} \text{ m}^3/\text{s}$ (0.9 percent of the incoming gas flow rate). A mass balance on the downflow section at the superficial gas velocity of 0.3115 m/s yielded the gas flow rate in the upward direction at level 1 as $2.63 \times 10^{-4} \text{ m}^3/\text{s}$. The value determined through integration was $0.875 \times 10^{-4} \text{ m}^3/\text{s}$, and therefore, only one third of the bubbles moving in the upward direction was detected.

It is important to note that uncertainty is present in the integrated results due to the paucity of data points obtained at each level. The void fractions found through integration at levels 1 and 2 are compared in Fig. 33 to the gas hold-up determined through pressure drop measurement in the downflow region. In this integration the void fraction was assumed to be zero at the wall as previously discussed. If a non-zero void fraction at the walls is assumed the average void fraction becomes larger by 30 to 50 percent. These results are also presented in Fig. 33 as functions of superficial gas velocity. It can be noted that the void fraction at

level 1 is much larger relative to the gas hold-up at low superficial gas velocities than it is at higher superficial gas velocities. This is expected, since the region in which a larger concentration of gas bubbles is observed increases with superficial gas velocity. The void fractions presented in this work are low since two thirds of the bubbles moving in upward flow were not detected due to the bias of the probe to detecting bubbles in the downward flow.

Conclusions

Bubble flow in the downflow section of the airlift tower has net upward and downward components. A technique based on time series analysis was developed to obtain the velocity and time fraction of bubble flow for each component. Resistivity probes were employed to obtain dependent time series indicating the presence of the gas or liquid phase at a point. The cross-covariance function of these series was bimodal with local maxima giving rise to the time lag characteristics of each component of flow. The time fraction of flow was found to be equal to the peak fraction of the bimodal cross-covariance function, linearly translated so that the function at zero lag has a value of zero. This technique was developed theoretically and verified experimentally. A number of significant conclusions can be drawn concerning the technique.

1) The appearance of bubbles at a point in a gas-liquid flow field is a random occurrence.

2) The autocorrelation function for random bubble flow is modeled by equation (13).

3) The cross-correlation function is distinguished from the autocorrelation function in that the theoretical lag may be non zero and is not constant. A reasonable model for the cross-correlation function is presented as equation (41).

The technique developed was employed in a study of the downflow section of the airlift tower. The significant conclusions are:

1) Bubble flow in the downflow section of the airlift tower has upward and downward components of velocity.

2) The downflow of air at a level of 4.5 cm below the top edge of the baffle ranged from $1.23 \times 10^{-4} \text{ m}^3/\text{s}$ at a superficial gas velocity of 0.0683 m/s to $2.88 \times 10^{-4} \text{ m}^3/\text{s}$ at a superficial gas velocity of 0.3115 m/s.

3) The flowrate of air carried from the downflow section into the upflow section was $0.2508 \times 10^{-4} \text{ m}^3/\text{s}$ at a superficial gas velocity of 0.3115 m/s.

4) The bubble flow field was essentially symmetric about the angular position.

5) The bubble flow at the upper level of the airlift tower was downward at a large radius and upward near the center of the tower.

The velocities and time fractions of flow in complex two phase flow systems can be found through an analysis of the cross-covariance functions characteristic of the flow field. The techniques developed in this work to extract this information from bimodal cross-covariance functions are general, and should be employed in other multi-phase systems.

Notation

A	Cross-Sectional area
B	Distance between points X and Y
D	Chord of bubble seen by probe
d	Theoretical lag
E	Expectation
H_d	Hold-up in the downflow section of the airlift tower
h	Lag
k	Sample number
K	Total number of observations
L	Height of cross-covariance function peak relative to the value of cross-covariance function at zero lag
l	Number of observations per pulse
m	Length of time the gas phase occupies a point, s
O_p	Order of probability
P	Theoretical time lag, s
Q_A	Flow rate of gas phase, m^3/s
Q_L	Flow rate of liquid phase, m^3/s
r	Radial position
t	Time, s
Δt	Sample increment, s
v	Local bubble velocity, m/s
v_L	Bulk liquid velocity, m/s
v_s	Superficial gas velocity, m/s
$W(t)$	Stationary time series
X	Upper probe point position
$X(t)$	Time series corresponding to void fraction at X
Y	Lower probe point position

Y(t) Time series corresponding to void fraction at Y
 Z(t) Stationary time series

Greek

$\gamma_{XY}(h)$ Cross covariance function of X(t) and Y(t)
 $\gamma_{XX}(h)$ Autocovariance function of X(t)
 θ Angular position, rad.
 μ Mean
 $\rho_{XY}(h)$ Cross-correlation function of X(t) and Y(t)
 $\hat{\rho}_{XY}(h)$ Estimated cross-correlation function of X(t) and Y(t)
 $\rho_{XX}(h)$ Autocorrelation function of X(t)
 $\hat{\rho}_{XX}(h)$ Estimated autocorrelation function of X(t)
 τ Time lag, s
 ϕ Local time averaged void fraction
 Φ Integrated void fraction for a given level
 χ Time fraction of flow
 Ω Peak fraction

Subscripts

dn Downward component
 T Total
 up Upward component
 W Corresponding to W(t)
 X Corresponding to X(t)
 Y Corresponding to Y(t)
 Z Corresponding to Z(t)

References:

1. Lefrancois, L., C. G. Mariller and J. V. Mejane, "Effectionnements aux procedes de Cultures Fongiques et de Fermentations Indistrielles," Brevet D'Invention, France #1.102.200, Delivree le 4 Mai, 1955.
2. Hatch, R. T., "Experimental and Theoretical Studies of Oxygen Transfer in the Air lift Fermentor, " Ph.D. Thesis, M.I.T. (1973).
3. Ho, C. S., L. E. Erickson and L. T. Fan, "Modeling and Simulation of Oxygen Transfer in Airlift Fermentors," Biotech. and Bioengg., 19, 1503 (1977)
4. King, R. P., "Continuous Flow systems with Stochastic Transfer Functions," Chem. Engg. Sci., 23, 1035 (1968).
5. Friedlander, S. K. and L. Topper, (eds.), Turbulence: Classical Papers on Statistical Theory, Interscience Pub., New York, 1961.
6. Panchev, S., Random Functions and Turbulence, Pergamon Press, New York, 1971.
7. Mesch, F., R. Fritsche and H. Kipphan, "Transit Time Correlation-A Survey on its Applications to Measuring Transport Phenomena," Trans. ASME, Dec. 1974, p. 414.
8. Ong, K. H. and M. S. Beck, "Slurry Flow Velocity, Concentration and Particle Size Measurement Using Flow Noise and Correlation Techniques," Measurement and Control, 8, 453 (1975).
9. Beck, M. S., J. Drane, A. Ploskowski and N. Wainwright, "Particle Velocity and Mass Flow Measurement in Pneumatic Conveyors," Powder Technol., 2, 269 (1968/69).
10. Mesch, F. and H. Kipphan, "Solids Flow Measurement by Correlation Methods," Opto-electronics, 4, 451 (1972).
11. Lassahn, G. D., "Two Phase Flow Velocity Measurement Using Radiation Intensity Correlation," I.S.A. Trans., 15, 297 (1976).
12. Oki, K., T. Akehata and T. Shirai, "A Method for Measuring the Velocity of Solid Particles with Fiber Optic Probe," Kagaku Kogaku, 37, 965 (1973).
13. Herringe, R. A. and M. R. Davis, "Structural Development of Gas-Liquid Mixture Flows," J. Fluid Mech., 73, 97 (1976).
14. Koide, K. and H. Kubota, "Gas Holdup Distribution and Liquid Velocity Distribution on Bubble Flow in Vertical Column," Kagaku Kogaku, 5, 77 (1967).
15. Haines, A. K., R. P. King and E. T. Woodburn, "The Interrelationship between Bubble Motion and Solids Mixing in a Gas Fluidized Bed," AIChE J., 18, 591 (1972).

16. Nguyen, V. T. and P. L. Spedding, "Hold-up in Two-Phase, Gas-Liquid Flow - I," Chem. Engg. Sci., 32, 1003 (1977).
17. Jenkins, G. M. and D. G. Watts, Spectral Analysis and Its Applications, Holden-Day, San Francisco, 1968.
18. Fisz, M., Probability Theory and Mathematical Statistics, 3rd ed., John Wiley and Sons, New York, 1963.
19. Fuller, W. A., Introduction of Statistical Time Series, John Wiley and Sons, New York, 1976.
20. Chatfield, C., The Analysis of Time Series: Theory and Practice, Halstead Press, New York, 1975.
21. Belfield, A. R., "Experimental Studies of Oxygen Transfer in a Spilt Cylinder Airlift," M.S. Thesis, Univ. of Maryland (1976).

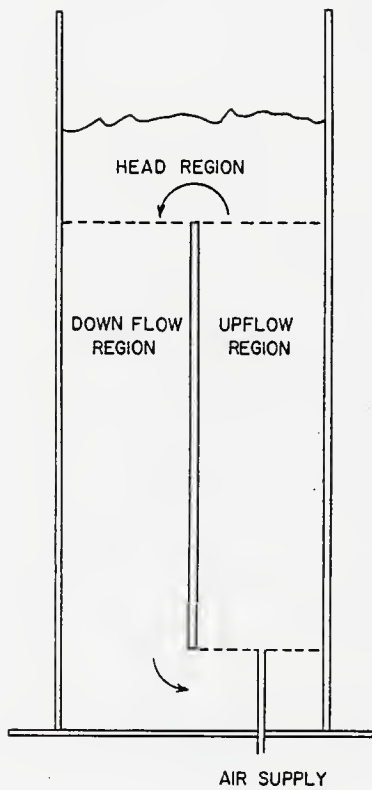


Fig. 1. The Airlift Tower

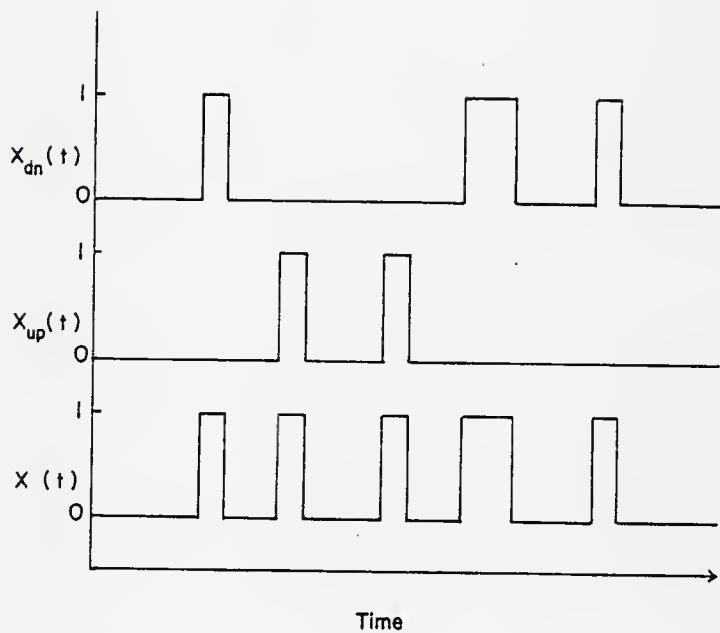


Fig. 2. The Void Fraction at a Point as a Function of Time.

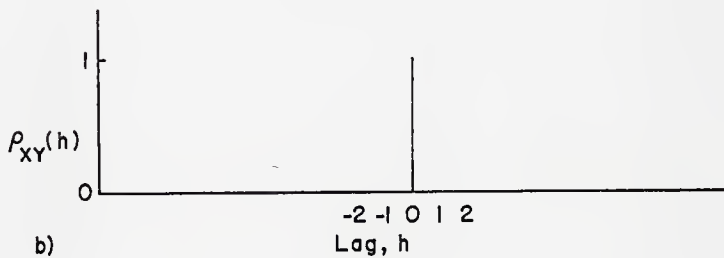
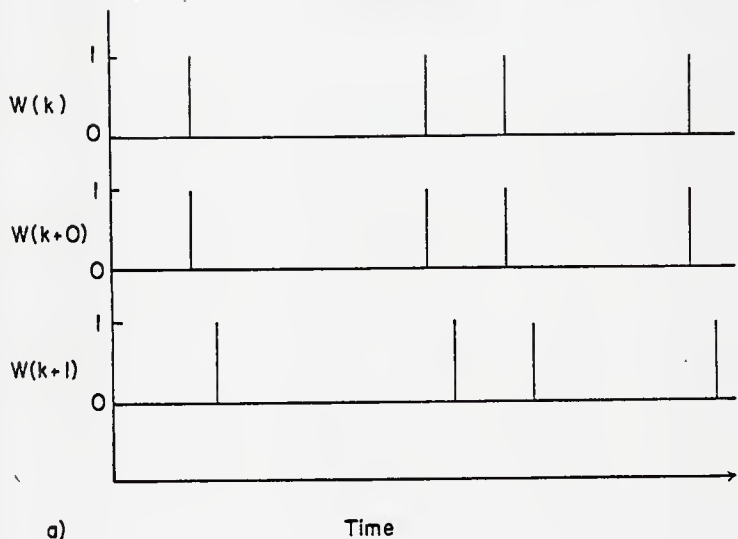


Fig. 3. a) Time Series $W(k)$ with One Observation Per Pulse.
b) Autocorrelation Function for $W(k)$.

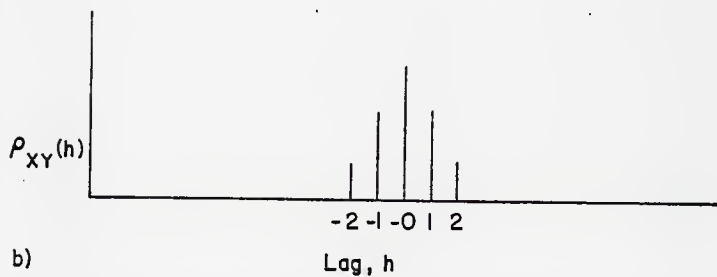
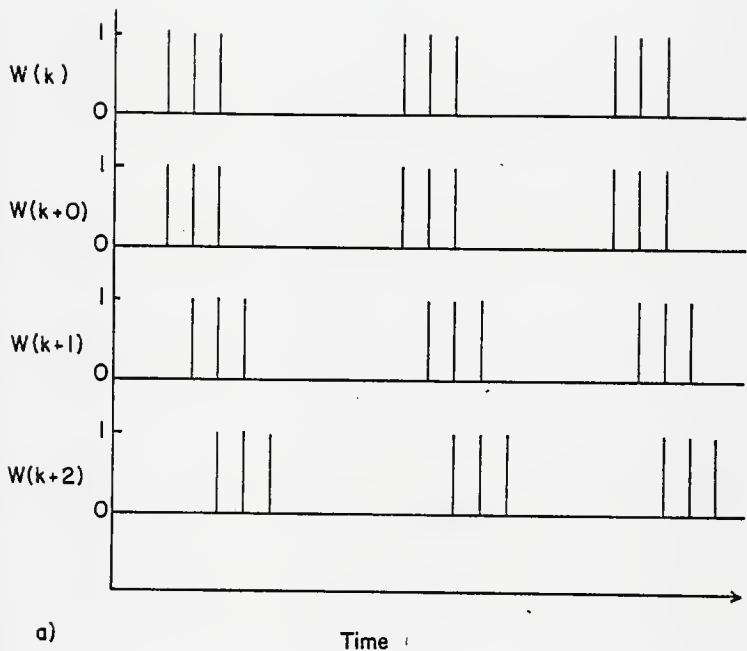


Fig. 4. a) Time Series, $W(k)$, with Three Observations Per Pulse.
 b) Autocorrelation Function for $W(k)$.

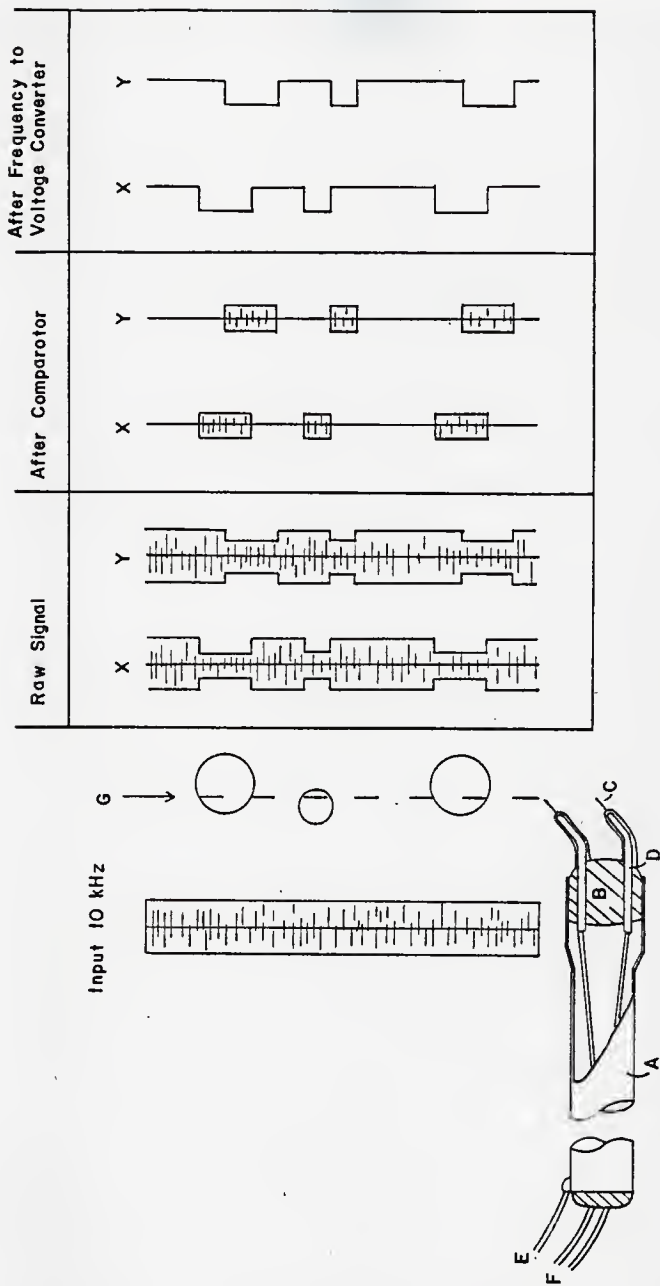


Fig. 5. Details of Resistivity Probe and Response Signals for Uni-directional Bubble Flow; A. Stainless Steel Tube, B. Epoxy, C. Platinum 10% Rhodium Needles, Insulated with Varnish Except at the Tip, D. Copper Supporting Tube, E. Lead from Common Ground, F. Leads from the X and Y Needles, G. Direction of Bubble Flow.

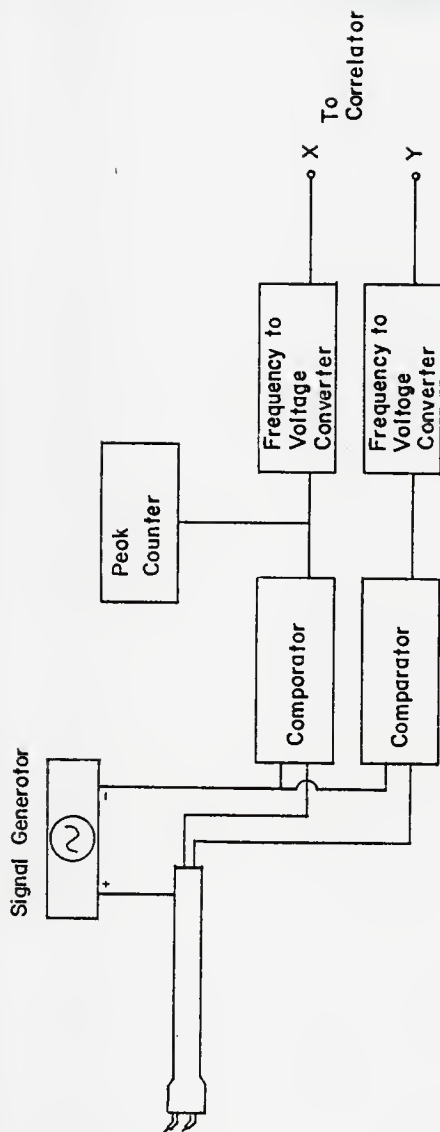


Fig. 6. Block Diagram of Resistivity Probe Analysis System.

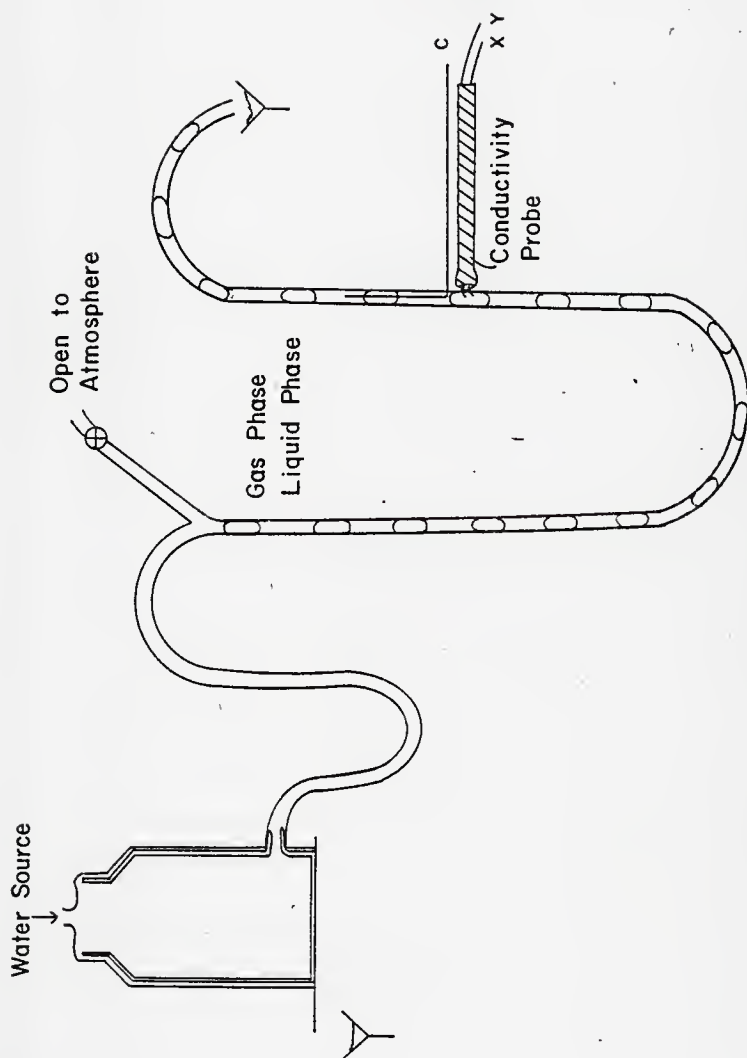


Fig. 7. Schematic Diagram of Equipment Used to Study Unidirectional Slug Bubble Flow in a Tube.

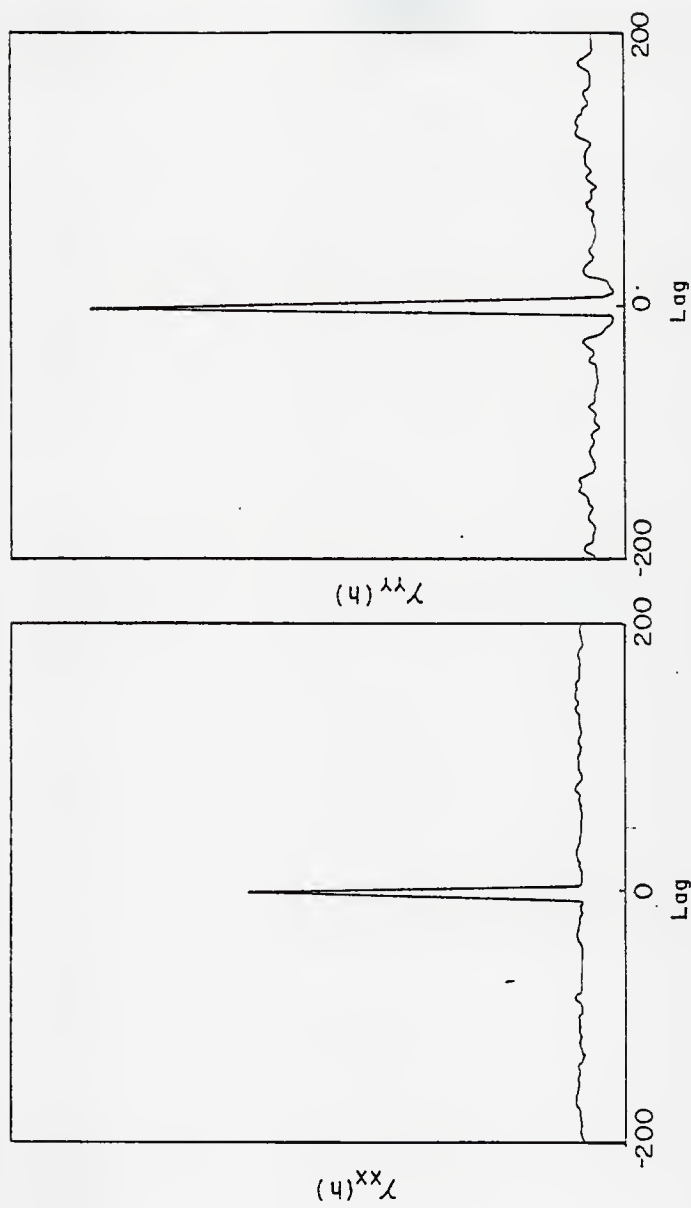


Fig. 8. Autocovariance of $X(t)$ and $Y(t)$ for Bubble Flow in a Tube. ($\Delta t = 1$ ms).

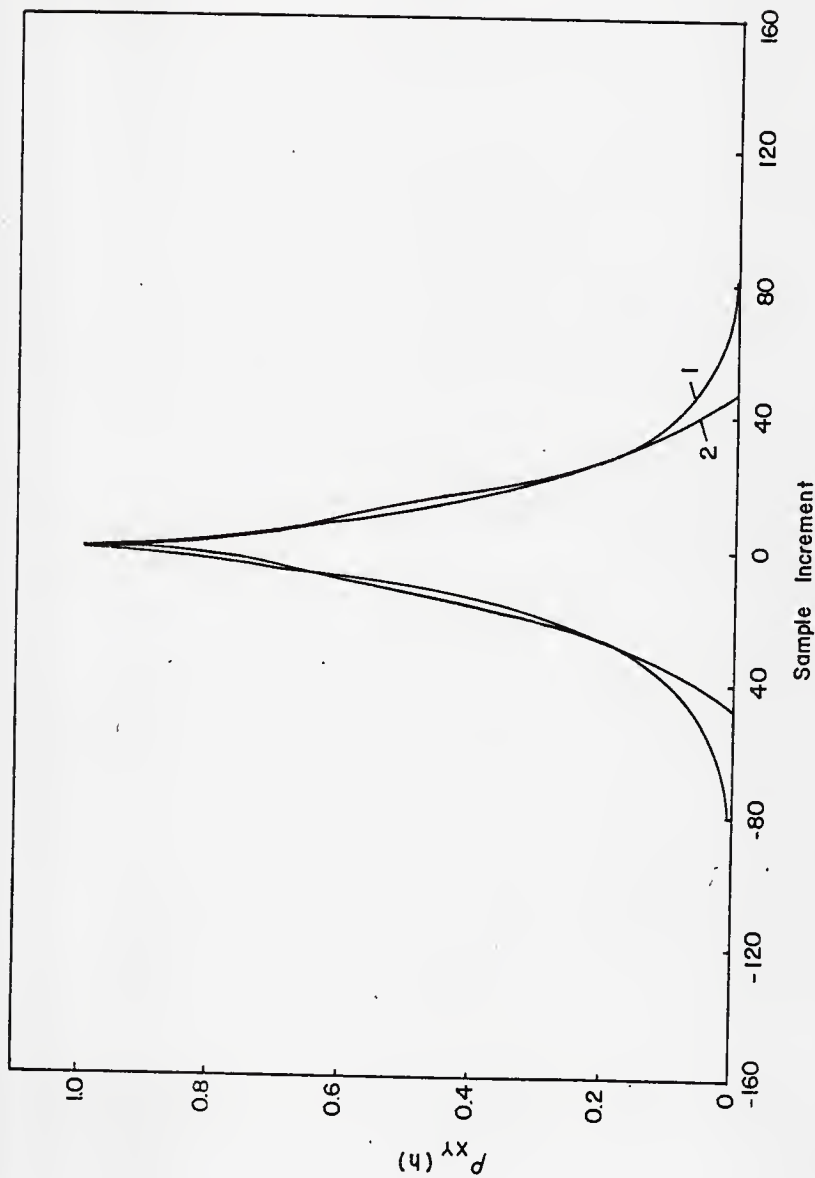


Fig. 9. Autocorrelation Values as a Function of Sample Increment. 1. Estimated Value from $\left(\frac{k-1}{k}\right)(d-h)$ with $k = 18$, 2. Observed value for unidirectional flow.

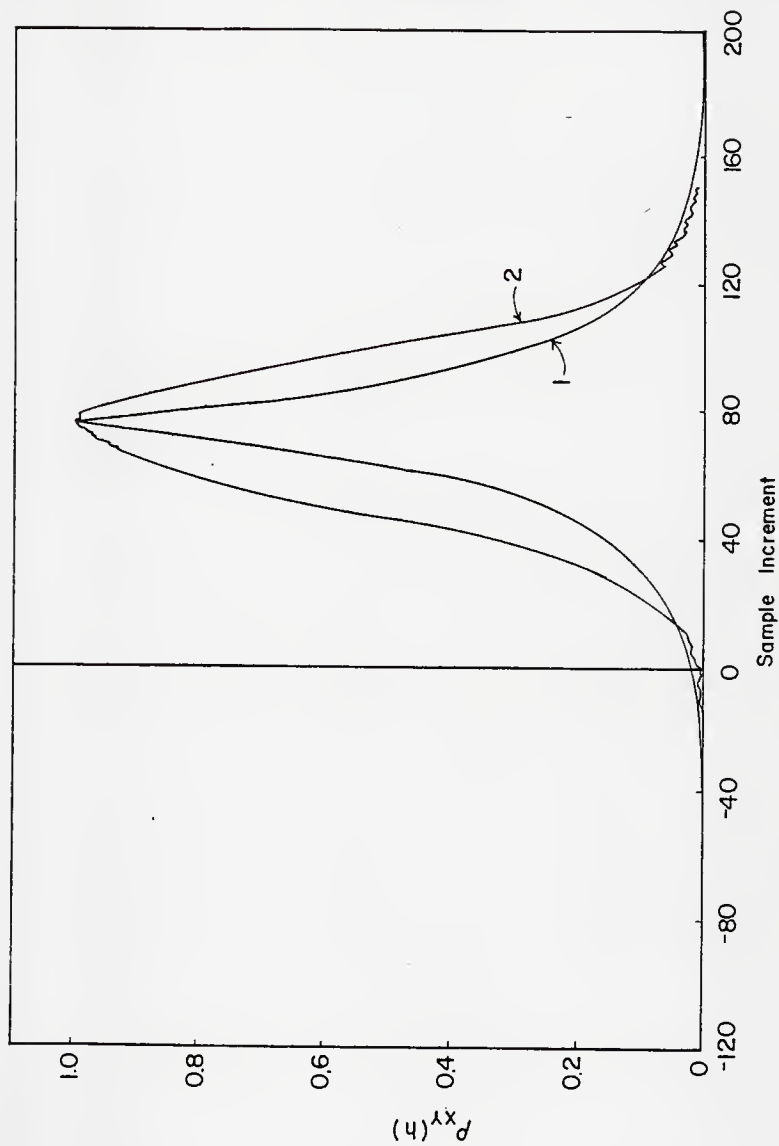


Fig. 10. Crosscorrelation Value as a Function of Sample Increment. 1. Estimated Value from $(\frac{x-h}{\ell})|d-h|$ with $\ell = 20$, 2. Observed Value for Unidirectional Flow.

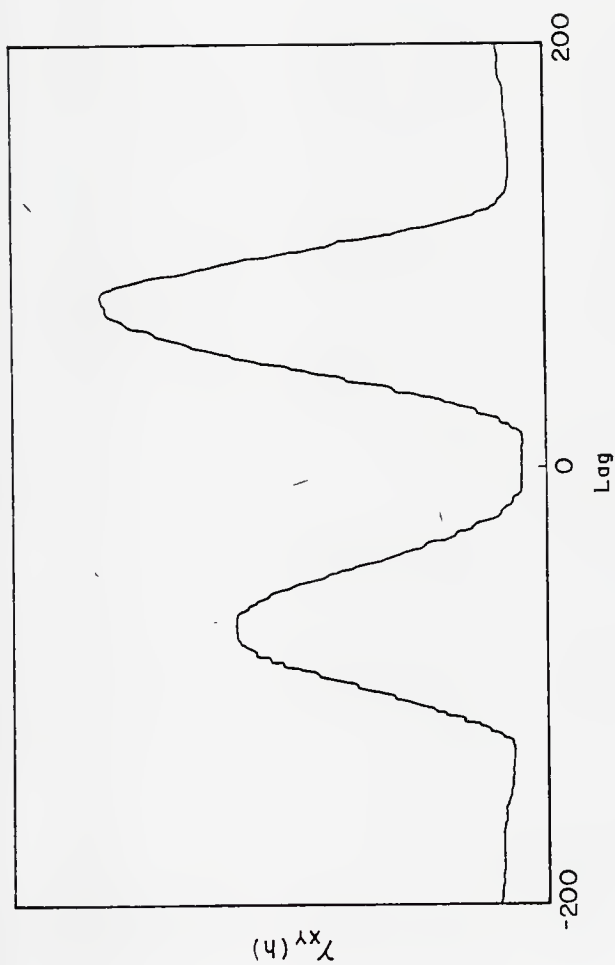


Fig. 11. Cross Covariance of $X(t)$ and $Y(t)$ for a Time Fraction of 0.625 Upward Flow and 0.375 Downward Flow of Bubbles in a Tube. ($\Delta t = 0.1$ ms)

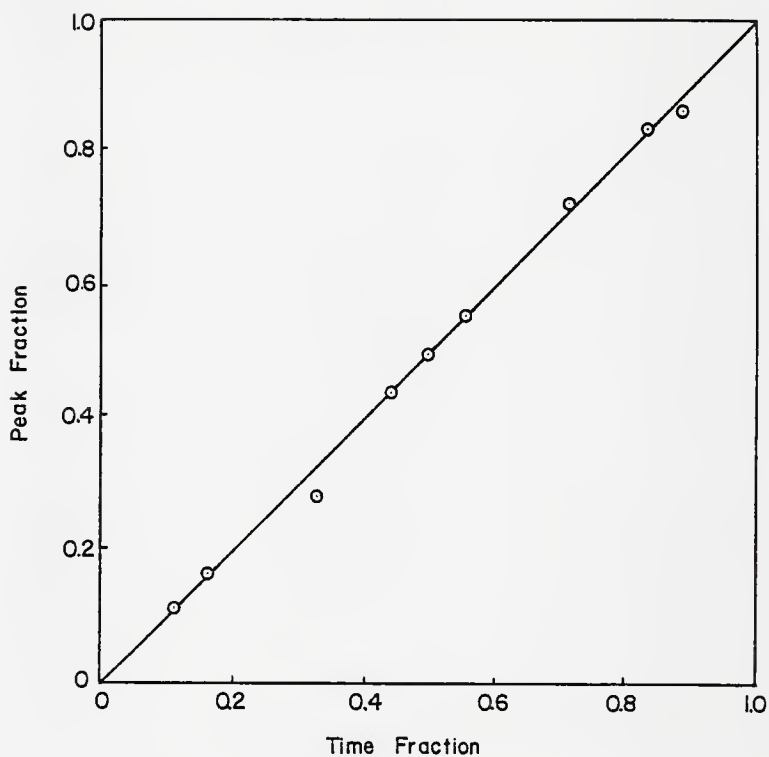


Fig. 12. Fraction of Cross-Covariance Peak Height as a Function of Time Fraction of Bubble Flow.

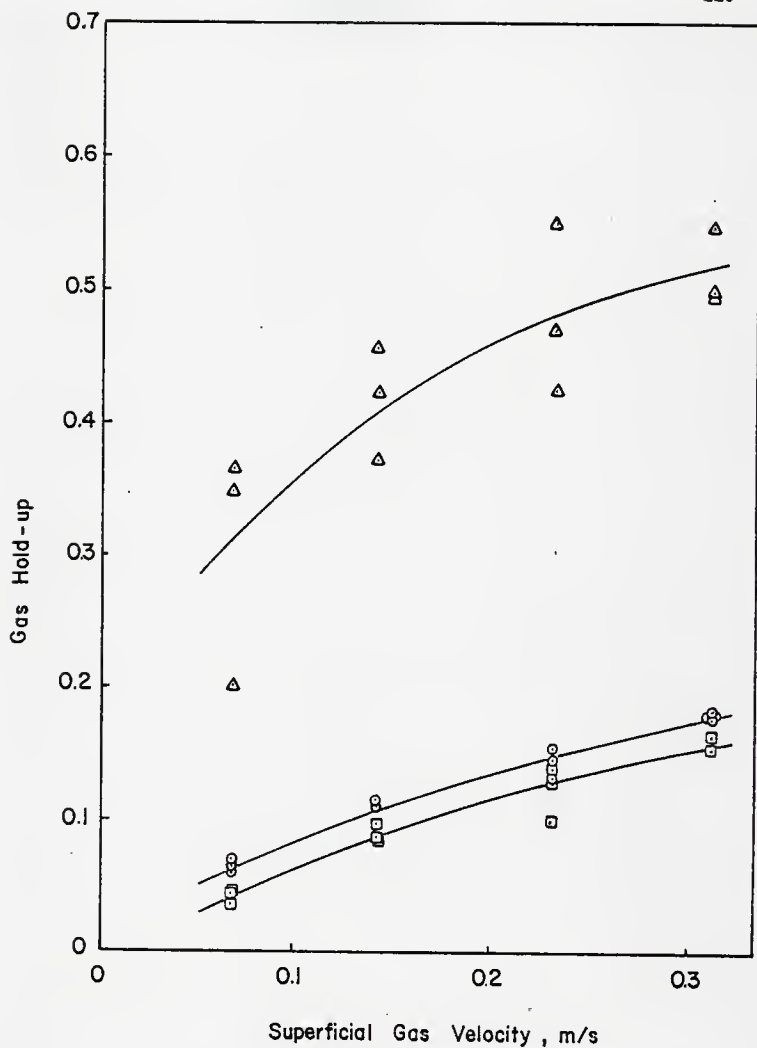


Fig. 13. Gas Hold-Up as a Function of Superficial Gas Velocity, Δ Head Region, \circ Upflow Region, \square Downflow Region.

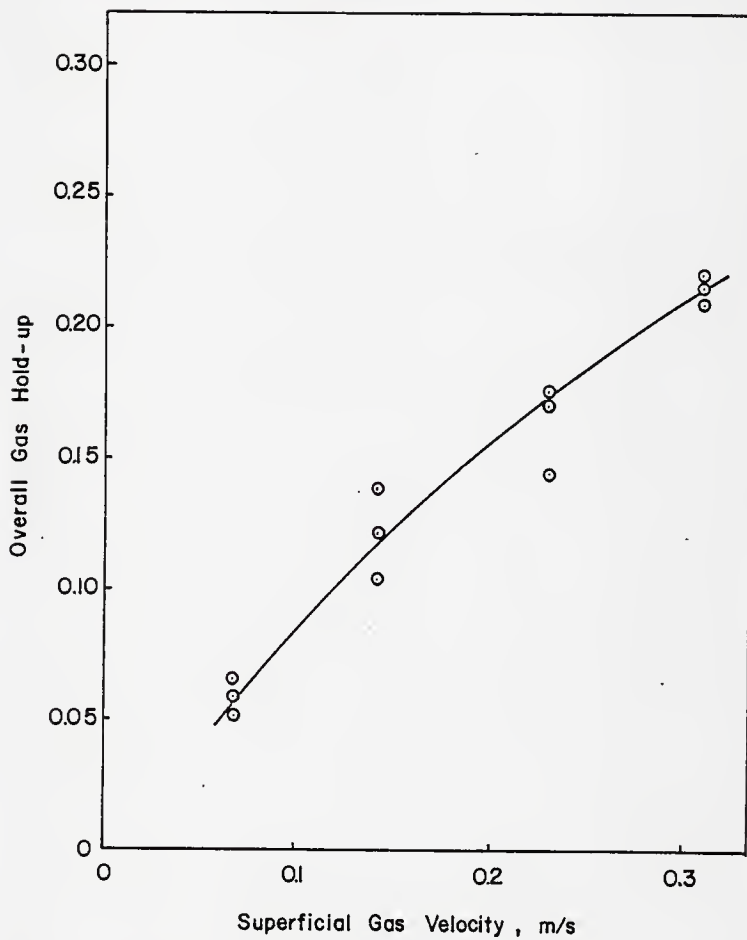


Fig. 14. Overall Gas Hold-Up as a Function of Superficial Gas Velocity.

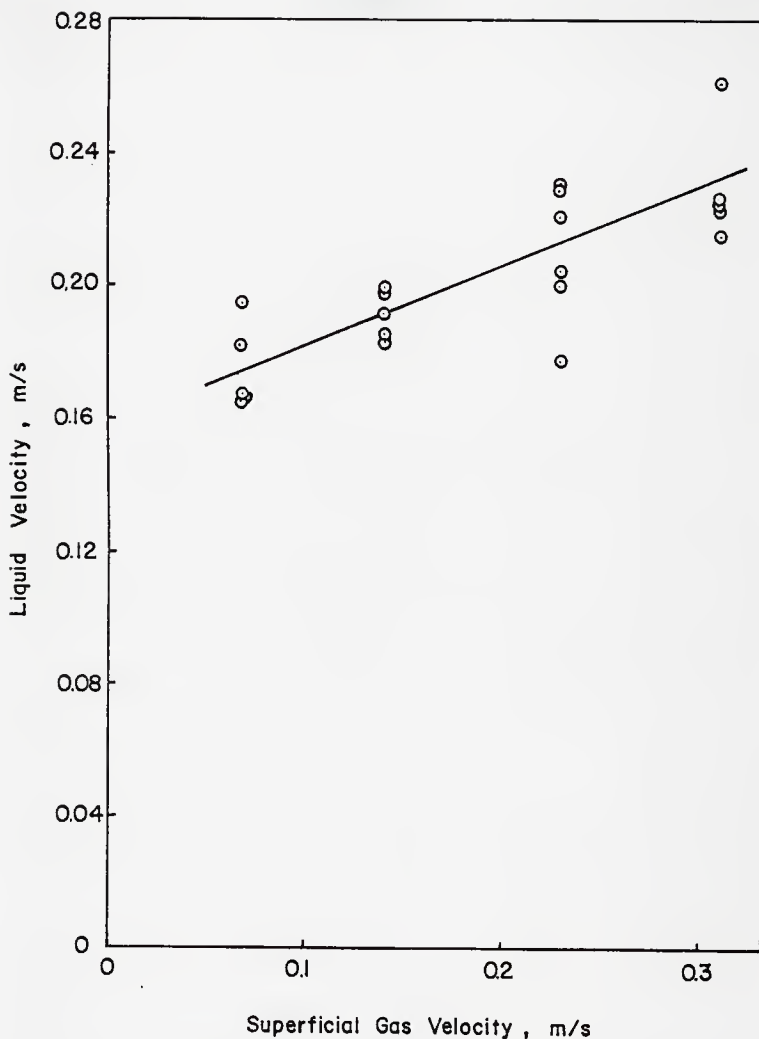


Fig. 15. Liquid Velocity in the Downflow Section as a Function of Superficial Gas Velocity.

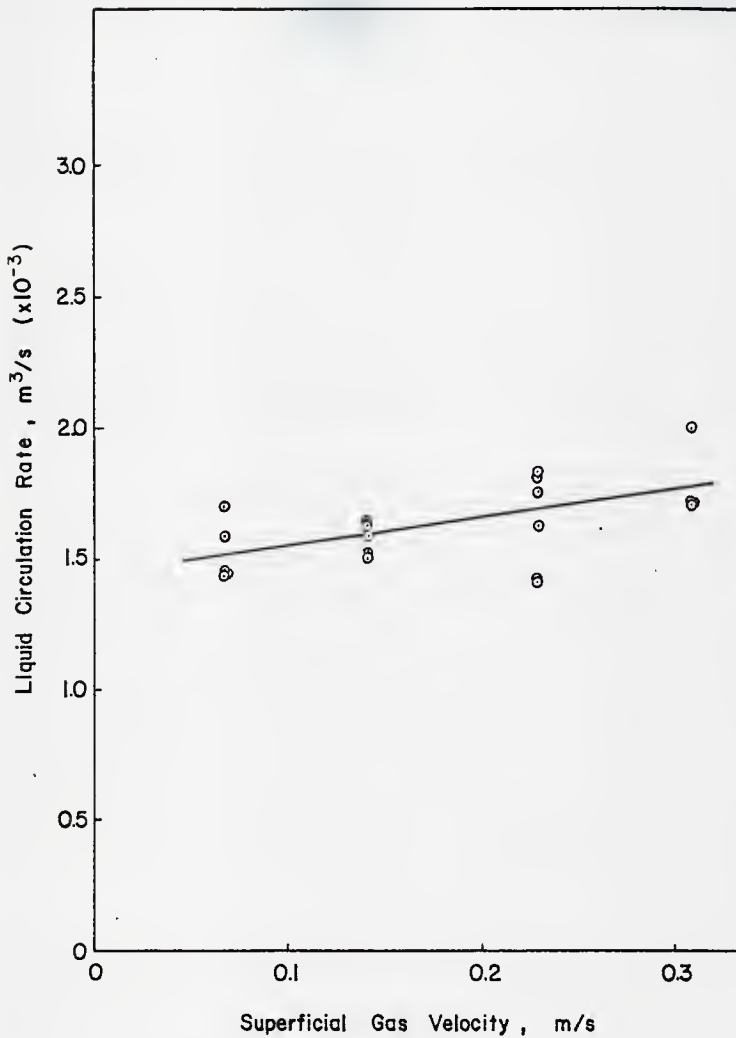


Fig. 16. Liquid Recirculation Rate as a Function of Superficial Gas Velocity.

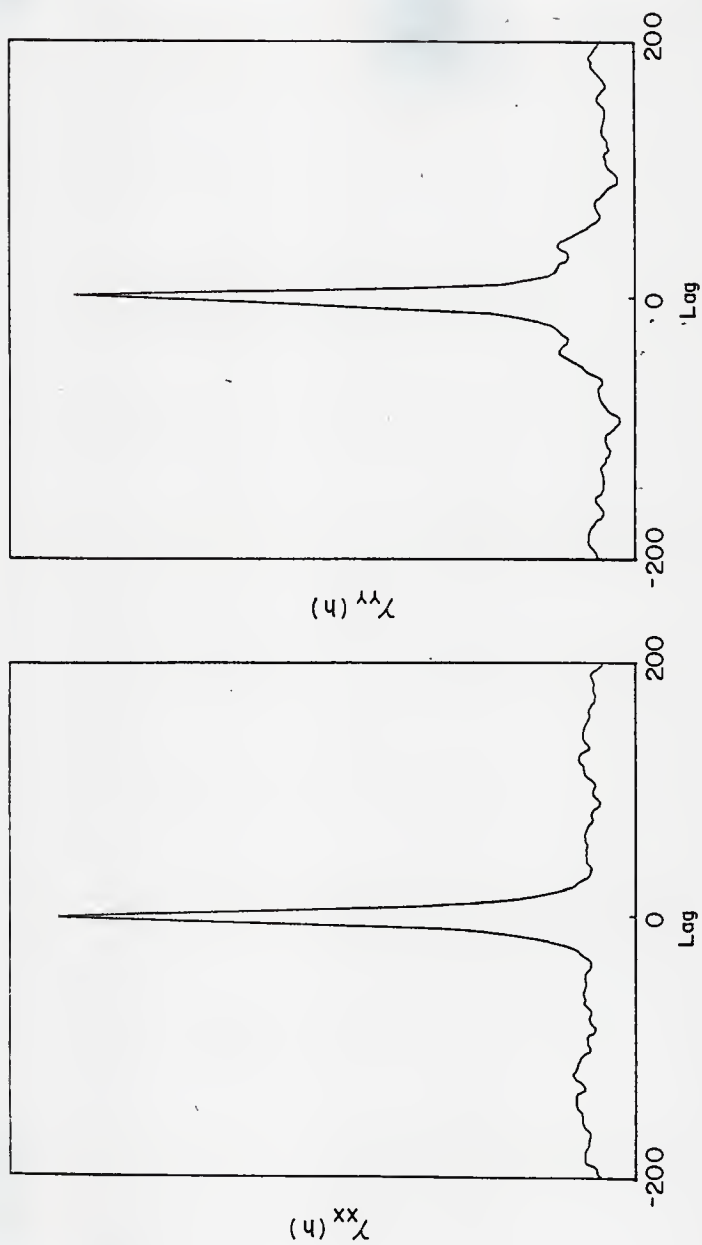


Fig. 17. Autocovariance of $X(t)$ and $Y(t)$ for Bubble Flow in the Downflow Section of the Airlift Tower. ($\Delta t = 1$ ms)

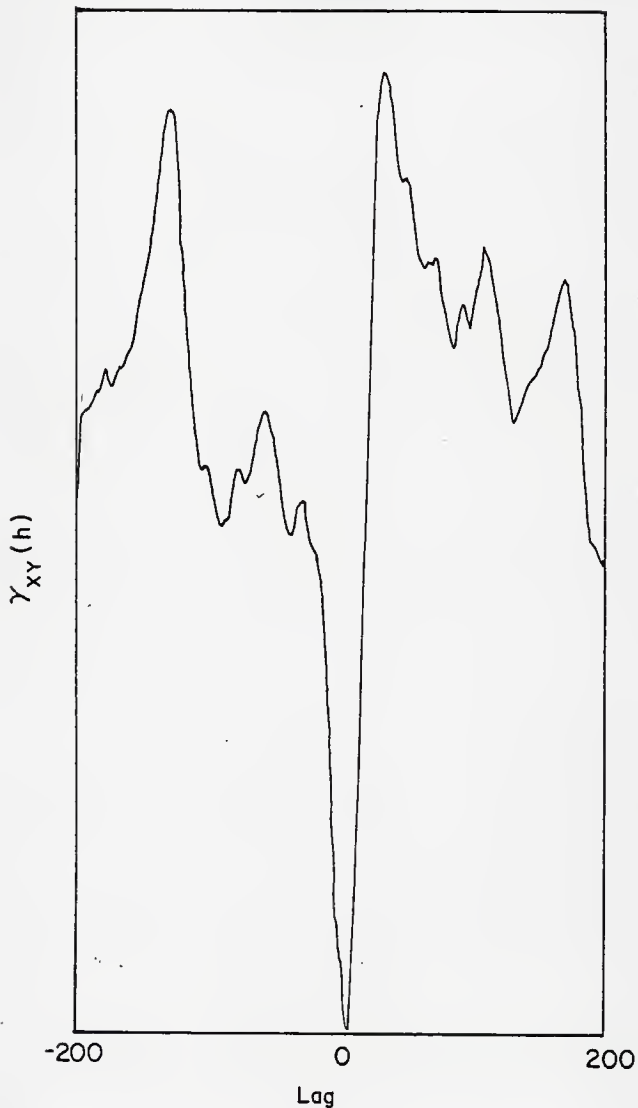
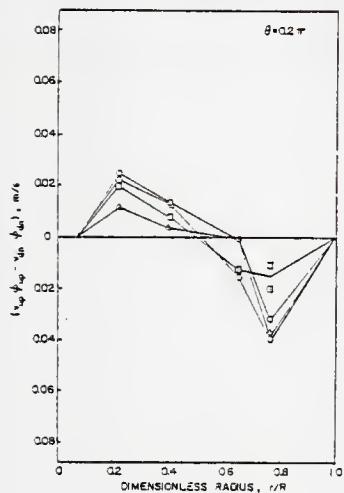
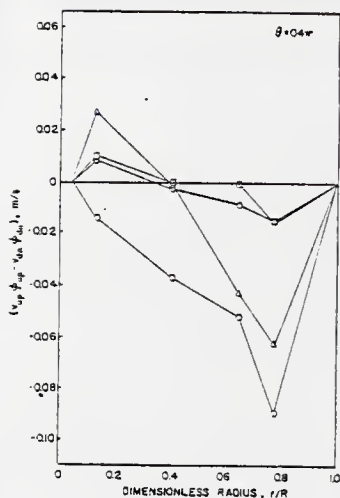


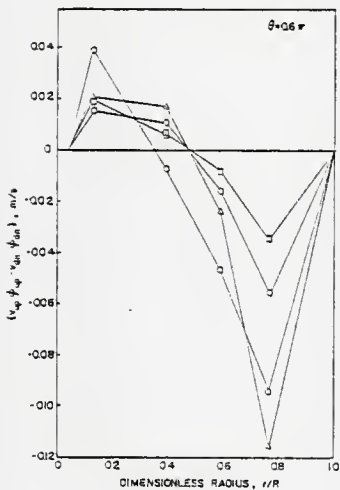
Fig. 18. Cross Covariance of $X(t)$ and $Y(t)$ in the Downflow Section of the Airlift Tower. ($\Delta t = 0.5$ ms)



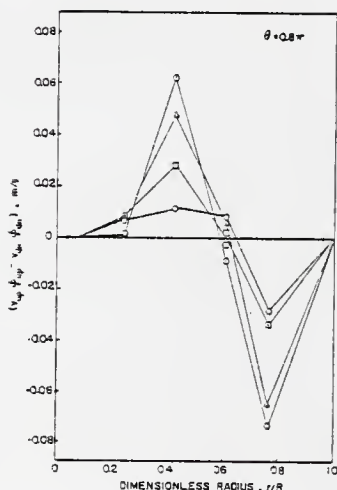
$\theta = 0.2\pi$



$\theta = 0.4\pi$

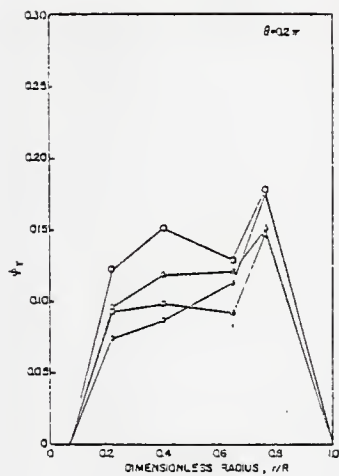


$\theta = 0.6\pi$

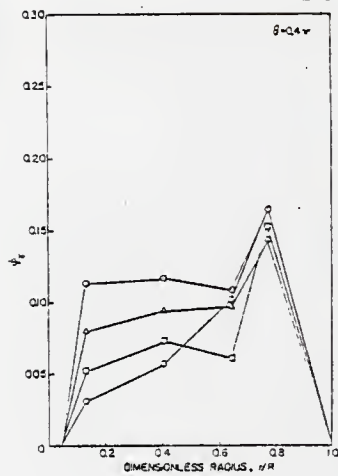


$\theta = 0.8\pi$

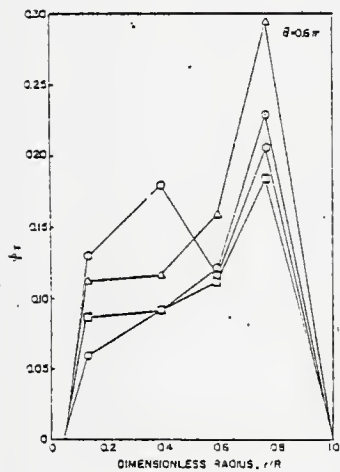
Fig. 19. Net Bubble Velocity as Functions of Dimensionless Radius for Level 1, with Superficial Gas Velocity as a Parameter;
 ○ 0.0683 m/s, □ 0.1412 m/s, △ 0.2307 m/s,
 ◇ 0.3115 m/s.



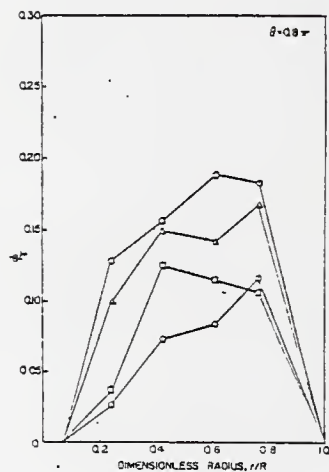
$$\theta = 0.2\pi$$



$$\theta = 0.4\pi$$

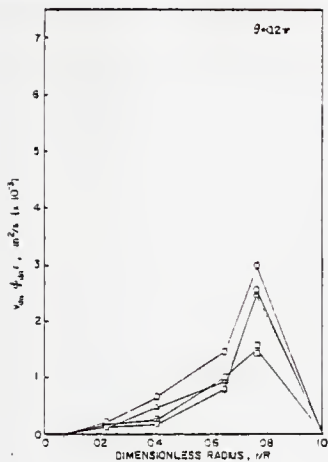


$$\theta = 0.6\pi$$

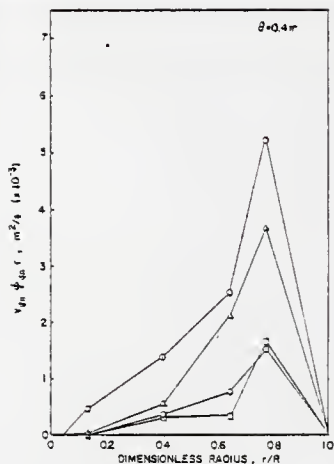


$$\theta = 0.8\pi$$

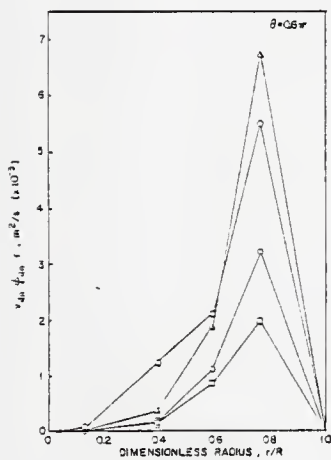
Fig. 20. Void Fraction as Functions of Dimensionless Radius for Level 1 with Superficial Gas Velocity as a Parameter,
 ○ 0.0683 m/s, □ 0.1412 m/s, △ 0.2307 m/s,
 ◇ 0.3115 m/s.



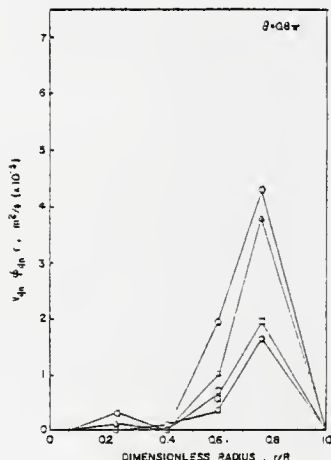
$$\theta = 0.2\pi$$



$$\theta = 0.4\pi$$

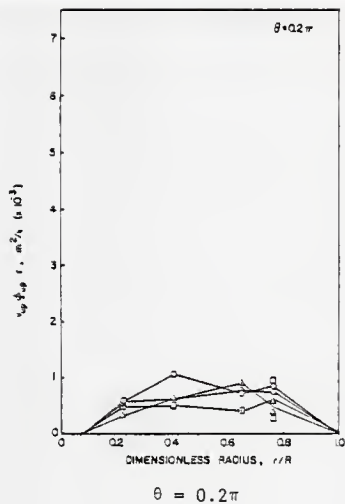


$$\theta = 0.6\pi$$

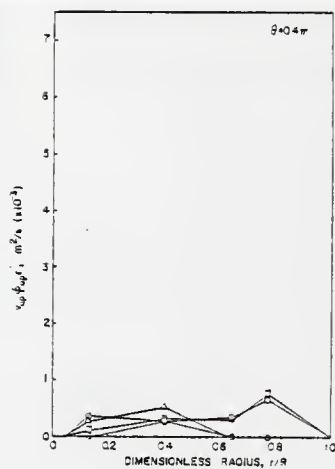


$$\theta = 0.8\pi$$

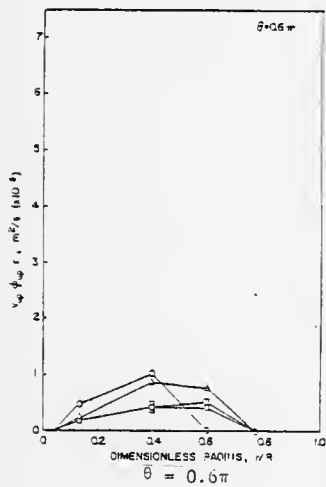
Fig. 21. $V_{dn} \phi_{dn} r$ as a Function of Dimensionless Radius for Level 1 with Superficial Gas Velocity as a Parameter; \odot 0.0683 m/s, \square 0.1412 m/s, \triangle 0.2307 m/s, \diamond 0.3115 m/s.



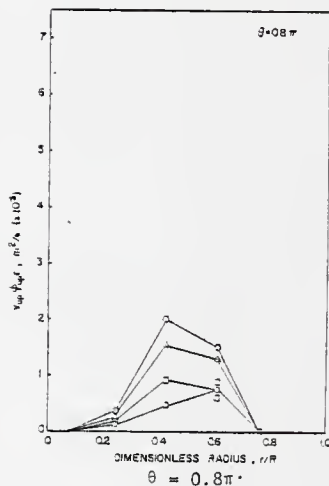
$$\theta = 0.2\pi$$



$$\theta = 0.4\pi$$

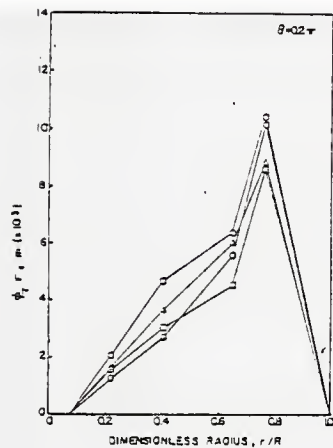


$$\theta = 0.6\pi$$

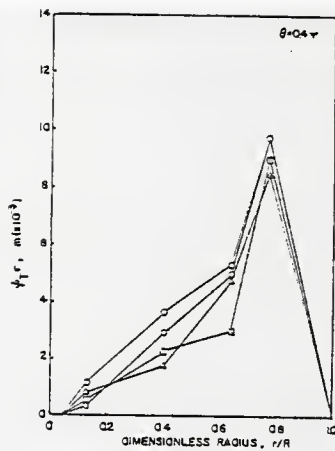


$$\theta = 0.8\pi$$

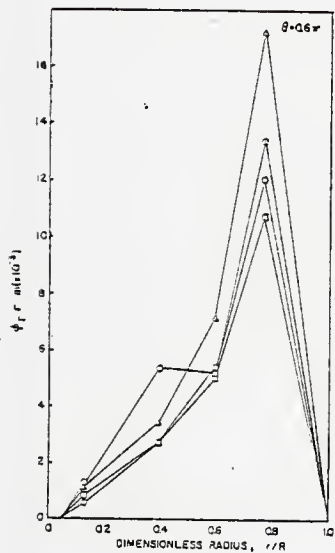
Fig. 22. $V_{up}\phi_{up}r$ as a Function of Dimensionless Radius for Level 1 with Superficial Gas Velocity as a Parameter; \odot 0.0683 m/s, \square 0.1412 m/s, \triangle 0.2307 m/s, \ominus 0.3115 m/s.



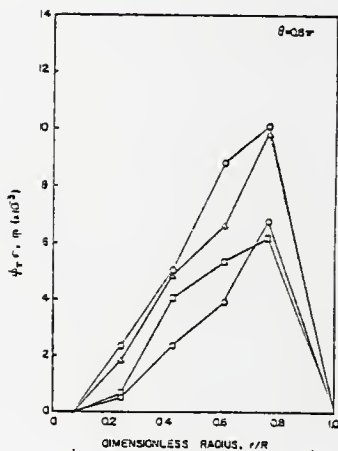
$$\theta = 0.2\pi$$



$$\theta = 0.4\pi$$



$$\theta = 0.6\pi$$



$$\theta = 0.8\pi$$

Fig. 23. $\psi_r r_m$ as a Function of Dimensionless Radius for Level 1 with Superficial Gas Velocity as a Parameter, \odot 0.0683 m/s, \square 0.1412 m/s, \triangle 0.2307 m/s, \ominus 0.3115 m/s.

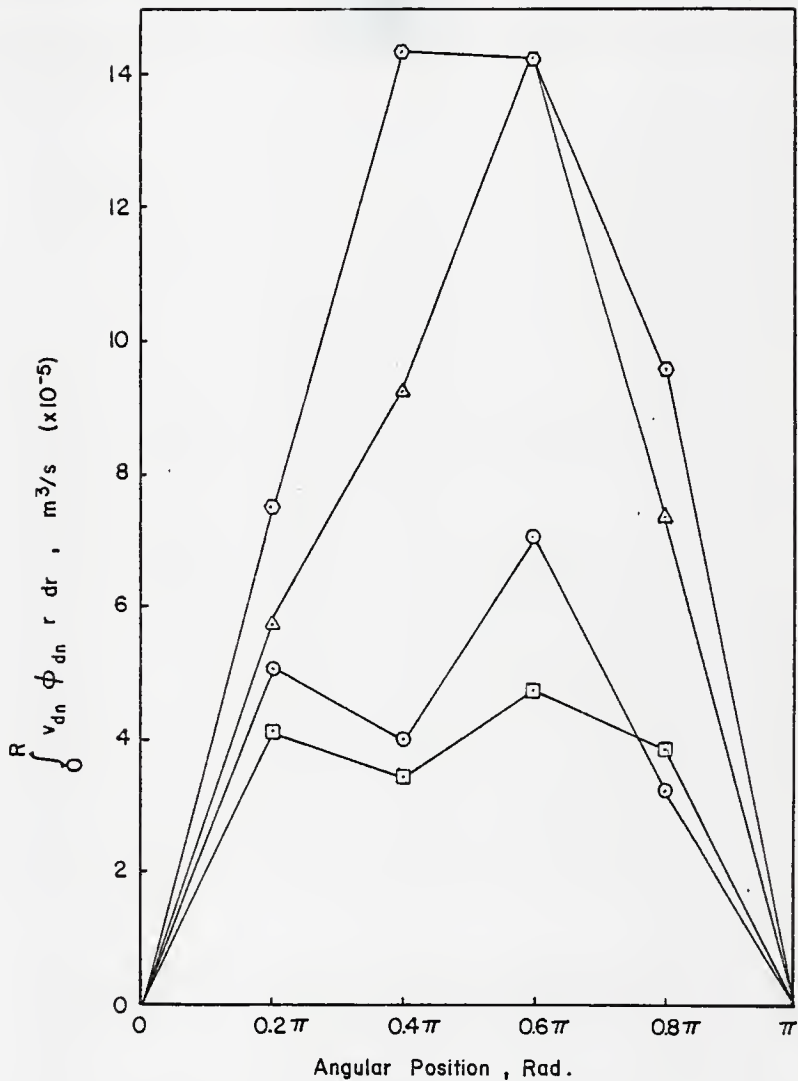


Fig. 24. $\int_0^R v_{dn} \phi_{dn} r dr$ as a function of Angular Position for Level 1 with Superficial Gas Velocity as a Parameter; ○ 0.0683 m/s, □ 0.1412 m/s △ 0.2307 m/s, ◇ 0.3115 m/s.

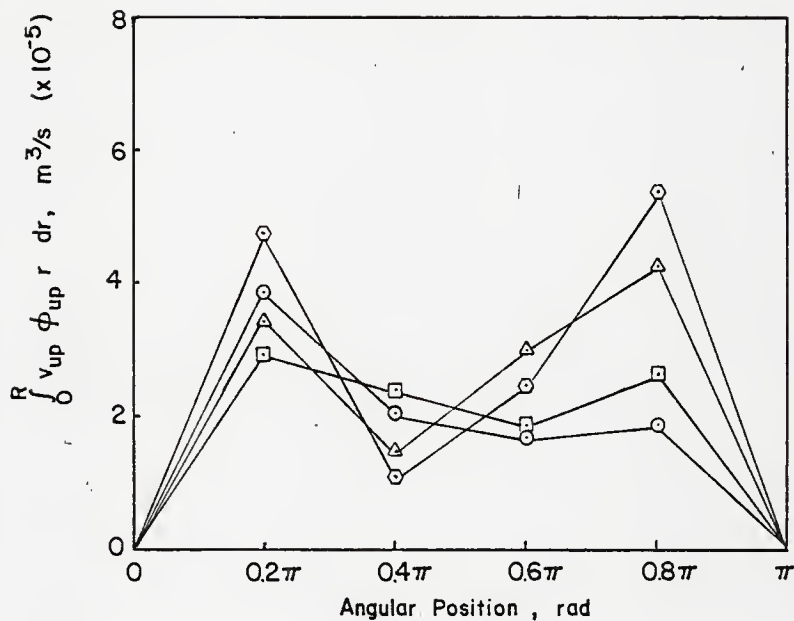


Fig. 25. $\int_0^R v_{up} \phi_{up} dr$ as a Function of Angular Position for Level 1 with Superficial Gas Velocity as a Parameter; ○ 0.0682 m/s, □ 0.412 m/s, △ 0.2307 m/s, ◇ 0.3115 m/s.

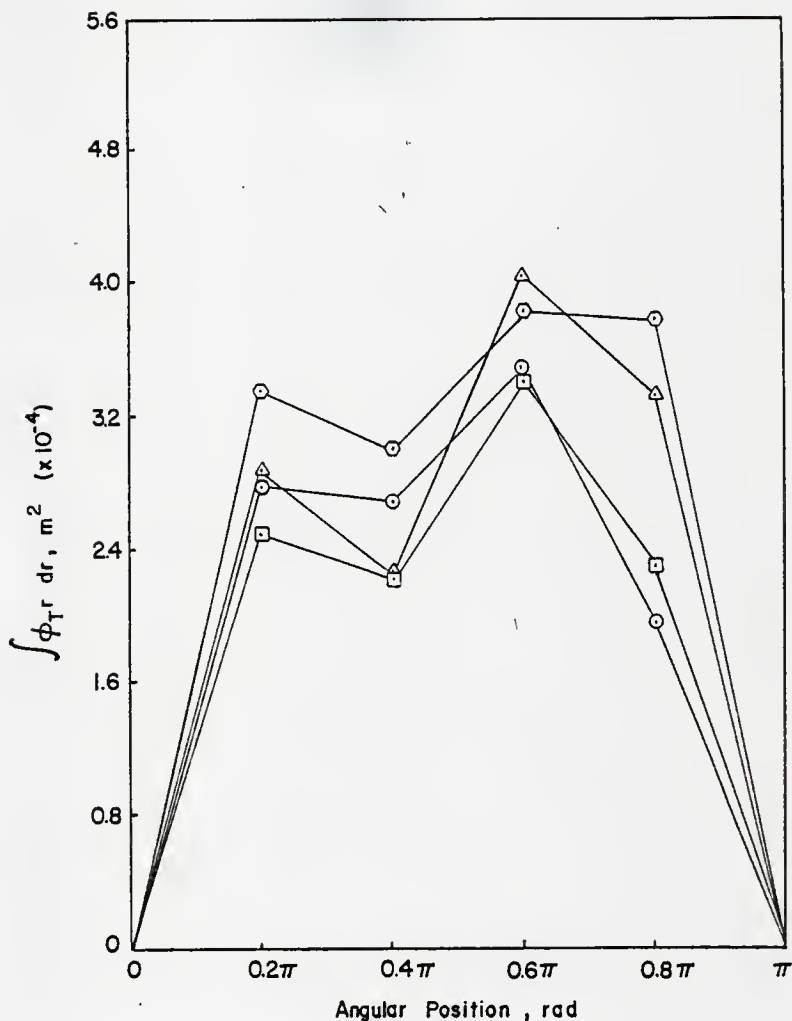


Fig. 26. $\int_0^R \phi_T r dr$ as a Function of Angular Position for Level 1 with superficial Gas Velocity as a Parameter; ○ 0.0682 m/s, ◻ 0.1412 m/s, △ 0.2307 m/s, ◇ 0.3115 m/s.

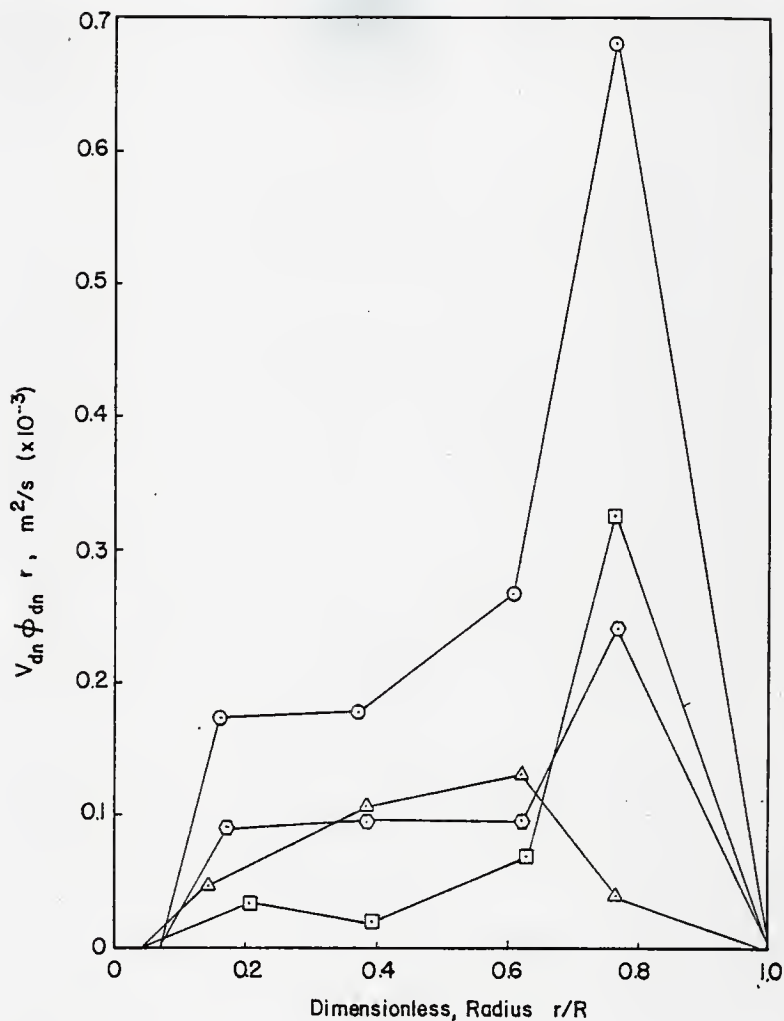


Fig. 27. $V_{up} \phi_{up} r$ as a Function of Dimensionless Radius for Level 2 with Superficial Gas Velocity of 0.3115 m/s and Angular Position as a Parameter; \odot 0.2π , \square 0.4π , \triangle 0.6π , \diamond 0.8π .

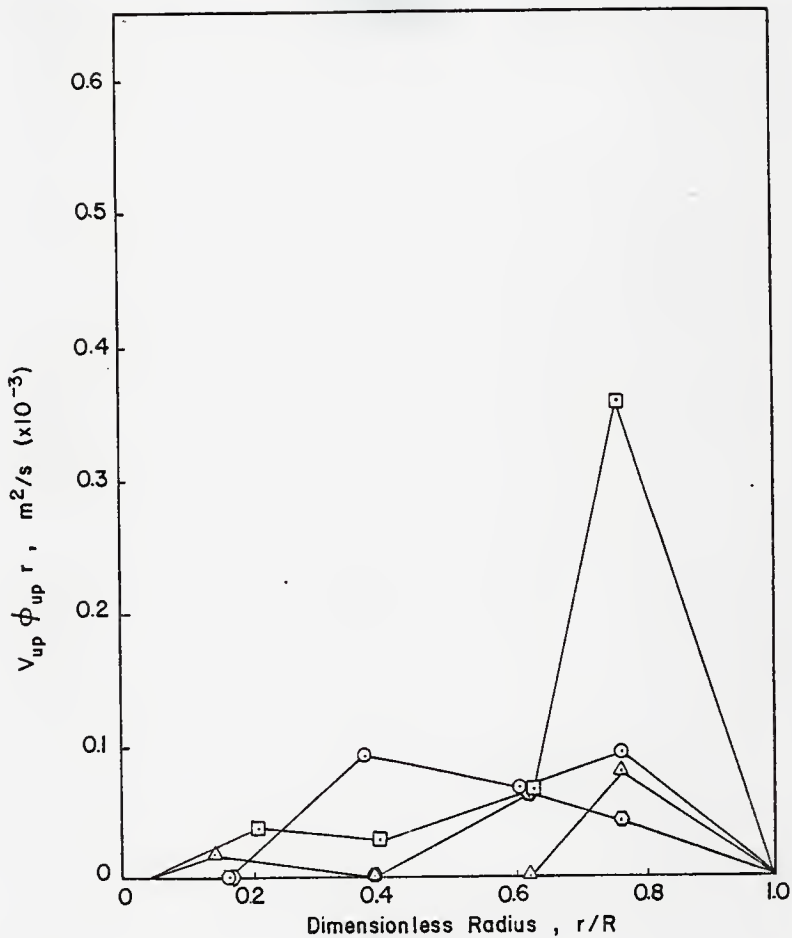


Fig. 28. $V_{up} \phi_{up} r$ as a Function of Dimensionless Radius for Level 2 with Superficial Gas Velocity of 0.3115 m/s and Angular Position as a Parameter; \circ 0.2π , \square 0.4π , \triangle 0.6π , \diamond 0.8π .

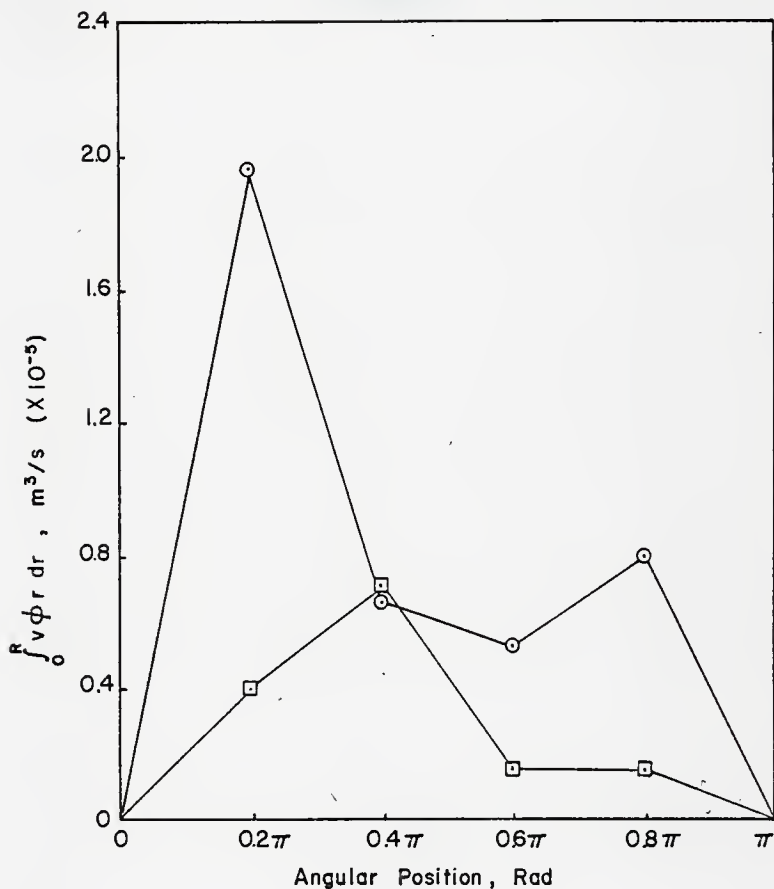


Fig. 29. $\int_0^R v_\phi r dr$ as a Function of Angular Position for Level 2 with a Superficial Gas Velocity of 0.3115 m/s.
 ○ Downward Component, □ Upward Component.

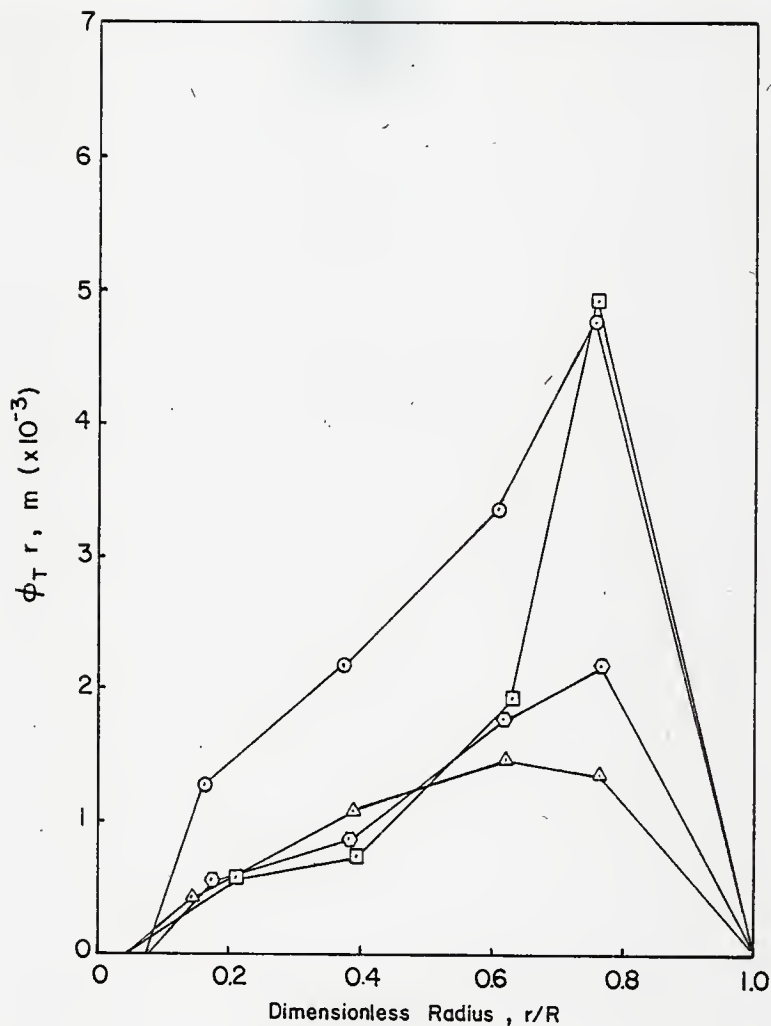


Fig. 30. $\phi_T r$ as a Function of Dimensionless Radius for Level 2 with a Superficial Gas Velocity of 0.3115 m/s and Angular Position as a Parameter; \odot 0.2π , \square 0.4π , \triangle 0.6π , \diamond 0.8π .

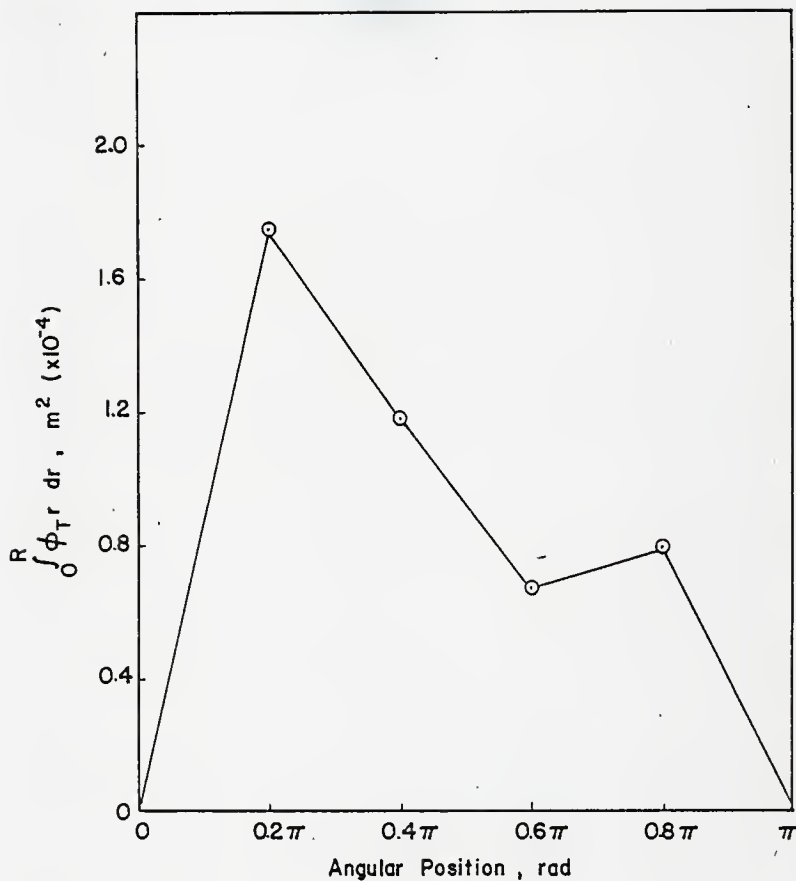


Fig. 31. $\int_0^R \phi_T r dr$ as a Function of Angular Position for Level 2 with a Superficial Gas Velocity of 0.3115 m/s.

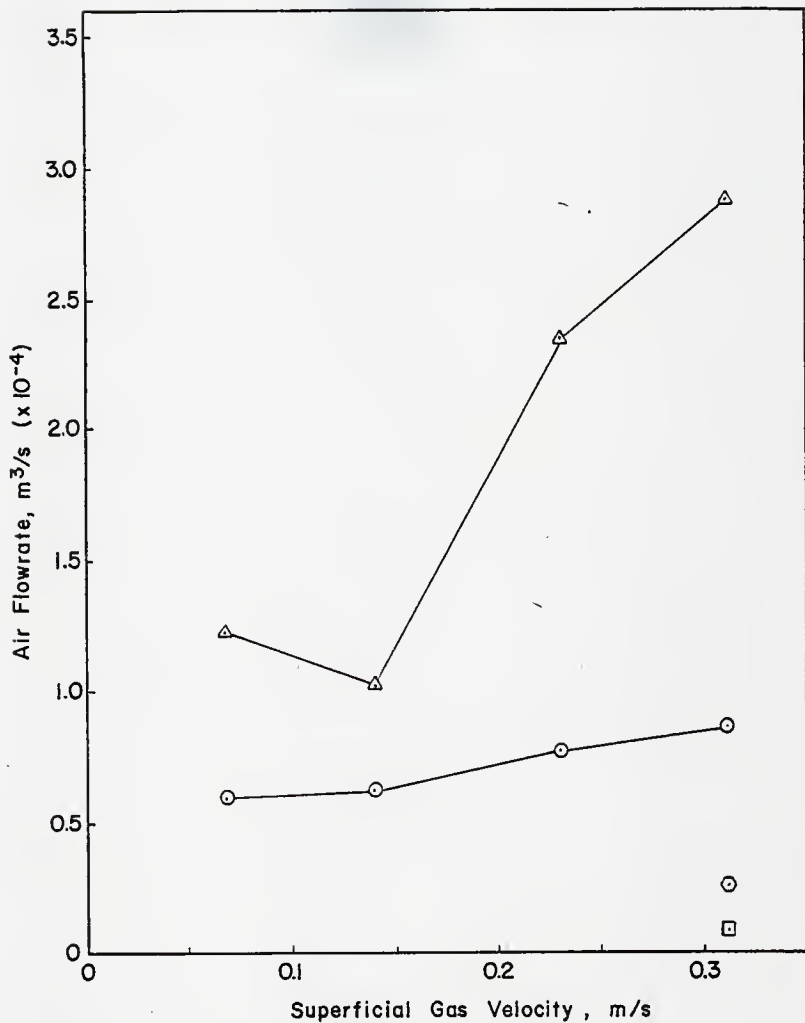


Fig. 32. Air Flowrate as a Function of Superficial Gas Velocity in the Downflow Section of the Split Cylinder Airlift Tower; Level 1: ○ Flow Upward, △ Flow Downward, Level 2: ◻ Flow Upward, ⊙ Flow Downward.

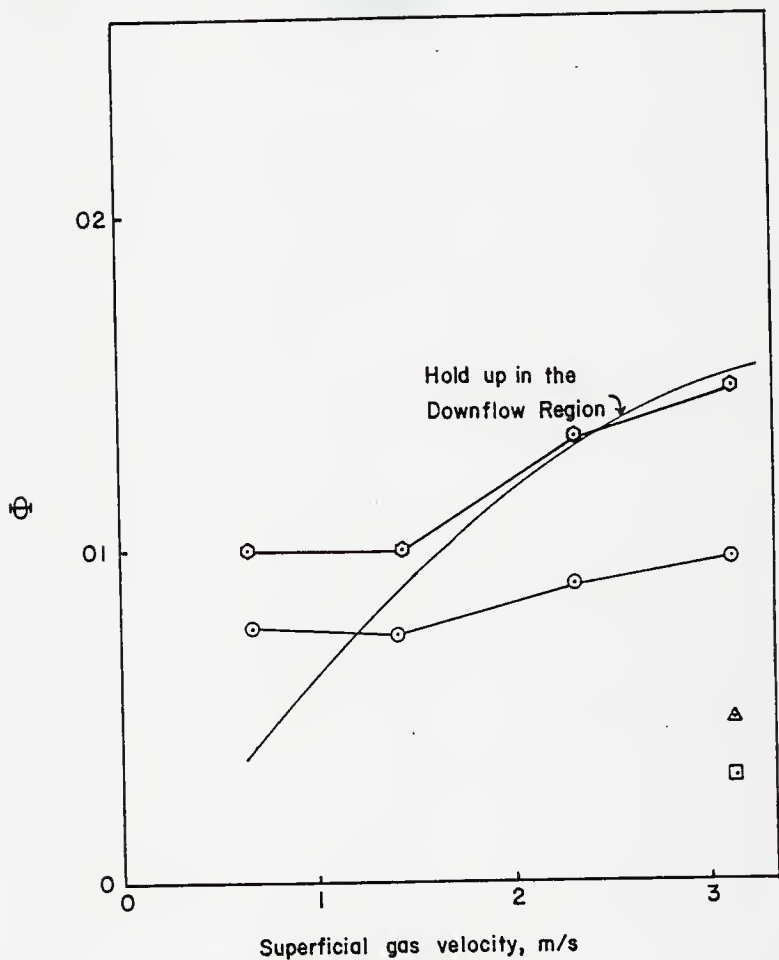


Fig. 33. Total Integrated Void Fraction as a Function of Superficial Gas Velocity: Assuming a Zero Void Fraction at the Walls; \circ Level 1, \square Level 2, Assuming a Nonzero Void Fraction at the walls, \odot Level 1, \triangle Level 2.

APPENDIX A: Construction of Conductivity Probes

The presence of a gas or liquid phase at a point can be detected by observing the difference in conductivity between the two phases. The probe used to detect this difference, as shown in Fig. 7, employs two sharp needles and a stainless steel tube as electrodes. The stainless steel tube serves both as a housing for the needle electrodes, and as a common electrode. The needles are insulated except at the tips, and a 10 kHz alternating current is allowed to flow between the common electrode and the two needle electrodes. As shown in Fig. 7, when a bubble envelops an electrode, the resistance to current increases instantaneously, and the amplitude of the response signal from the electrode decreases. The time interval for which the signal amplitude is decreased is the time interval in which the bubble "insulates" the electrode.

Design Factors

Four major factors need to be considered in the design of a two-needle conductivity probe.

- 1) The two needles and the tube body need to be electrically insulated. This also means that the probe must be water tight.
- 2) The probe should be capable of detecting the bubbles which enter the detection path. The needles should be sharp enough to pierce the bubbles which come into contact with it. The best piercing action occurs when the surface area initially contacting the bubble is minimized. A suitable probe configuration is shown in Fig. 1A.

The total surface area of the needles contacting the bubble should be minimized to reduce the effect of the probe on bubble velocity. The drag exerted by the probe on the bubble is greater for the configuration shown

in Fig. A1a than for the configuration shown in Fig. A1b. The probe shown in Fig. A1b, however, will not pierce the bubbles effectively. A compromise configuration, shown in Fig. A1c, is chosen to provide good piercing and a small amount of drag.

3) The needles should maintain their geometric integrity. The distance between the probe tips should be constant, and the material used should be corrosion resistant. Herringe and Davis⁽¹³⁾ used stainless steel surgical needles as electrodes; however, severe corrosion problems were encountered when they were used in the present study. The large current density at the needle tips makes the use of a more noble metal desirable. Both Platinum and Platinum 10% Rhodium performs well. The platinum alloy is selected because of its superior resistance to deformation.

4) The distance between the tips of the needles should be large enough to be accurately measured, yet small enough that a bubble contacting one needle could be expected to contact the other. For the probe described here the distance ranges from 0.41 to 0.51 cm. The distance can be measured by photographing the probe tips along with a micrometer which provided a reference length.

Procedure

1) Preparation of tube body. In the present probe the tubular body is fashioned from a stainless steel tube with a 0.635 cm O.D, 0.508 cm I. D. length, approximately 15 cm long, is cut from a straight section of tubing. The length of the tube used is dependent upon the size of the system for which the probe is intended.

As shown in Fig. A2a, an electrical connection is attached to the tube at one end. This is done by wrapping the wire around the tube and soldering

it, or by drilling a hole in the tube and inserting the wire into it before soldering. A resin-core solder with a zinc chloride flux is used for all connections.

The compression fitting is placed on the tube with the threaded end facing the end of the tube that is not used for the electrical connection. This end was placed in a vise and the last centimeter of the tube was pinched slightly. The pinching of the tube, shown in Fig. A2a gives the end of the tube an elliptical cross-section. This shape allowed the needle to be placed farther apart than they could be with an unflattened tube. For a given distance between needles a smaller diameter tube can be used for the body if the end is flattened. This, along with the streamlining effect of the flattened section, minimizes the disturbance of flow.

2) Construction of needle support assembly. The needle support tubes are assembled as a separate unit which is then inserted into the tube body. The needle support tubes, with 0.165 cm O.D. and 0.089 cm I. D., are 2.5 cm in length. A 33 degree bend is formed 0.5 cm from the end of each support tube. The exact angle is not critical as long as both tubes have the same angle.

The electrical leads are attached to the straight ends of these tubes. This is done by coating the wires with molten solder and inserting them into the support tubes. The two support tubes are clamped by the connected wires in a table vise. Quick setting epoxy is used to join the support tubes together and insulate them from each other. The finished product, shown in Fig. A2b, should be small enough to fit into the tube body.

3) Joining of needle support tube assembly and tube body. The electrical leads to the support tube assembly were threaded into the tube body, and the

assembly is inserted into the elliptical end of the tube body as shown in Fig. A2c. Epoxy is used to join the support tube assembly to the tube body to avoid leakage of water into the probe, and to insulate the support tubes from the tube body.

4) Insertion of Platinum 10% Rhodium needles. Platinum 10% Rhodium 0.051 cm O. D. wire is honed to a 0.0012 cm tip radius to form the needle electrodes. The needle support tubes are filled with molten solder and the platinum alloy needles inserted. A thin layer of quick-setting epoxy is applied to the exposed needle support tubes and to the solder connection. The result is shown in Fig. A2d. The use of support tubes in the probe assembly makes the exchange of new needles for damaged ones an easy process.

5) Insulation of needle electrodes. The final step in the construction of the conductivity probe is to spray the probe needles with Krylan Crystal Clear Protective Spray Coating No. 1302. This coating insulates the needles. The surface tension is large enough that the sharp tips of the needles remained uncoated. As needed, the spray coating is reapplied during use.

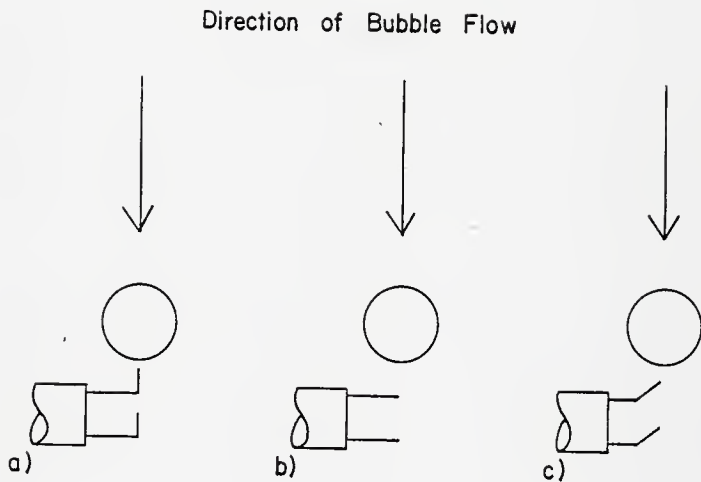


Fig. A1. The Effectiveness of Probe Configurations;
a) Good Piercing Action, Large Amount of Drag,
b) Poor Piercing Action, Small Amount of Drag,
c) A Compromise Between a) and b).

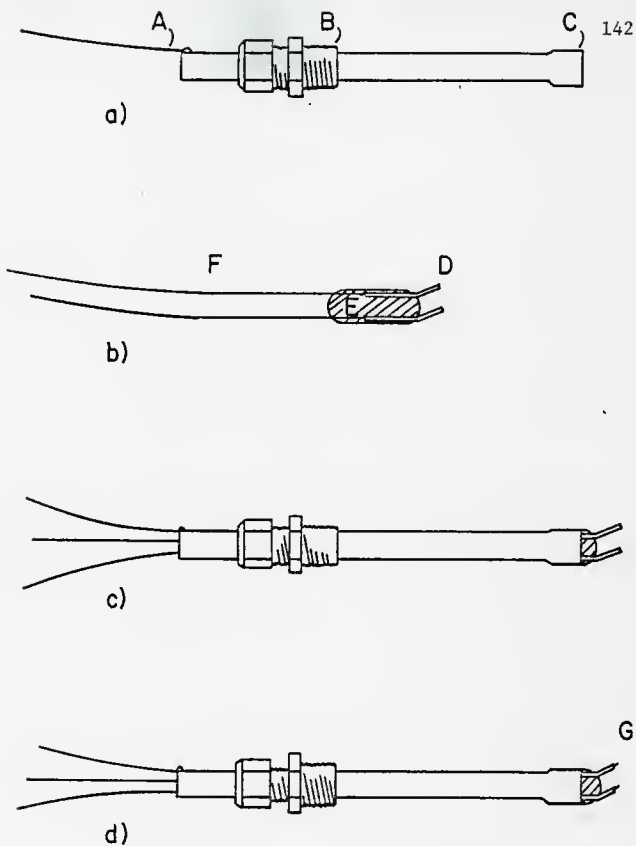


Fig. A2. Schematic Diagram of Systematic Conductivity Probe Construction;

- a) Preparation of Tube Body,
- b) Construction of Needle Support Tube Assembly,
- c) Joining of Support Tube Assembly and Tube Body,
- d) Insertion of Platinum 10% Rhodium needles.

A. Electrical Connection to Tube Body, B. Compression Fitting, C. Flattened End of Tube Body, D. Copper Needle Support Tubes, E. Epoxy, F. Electrical Connections to Support Tube, G. Platinum 10% Rhodium needles.

APPENDIX C. Data Summary for Airlift Tower

Table Cl. Physical Description of Airlift Tower

Liquid Volume	10.25 l
Diameter	15.2 cm
Baffle Height	51.0 cm
Baffle Width	0.635 cm
Distance from Bottom of Column to Bottom Edge of Baffle	5.5 cm
Sparger Tube Height	5.5 cm
Sparger Tube I.D.	0.95 cm ²
Upflow Cross-Sectional Area	90.7 cm ²
Level 1 Position	52.0 cm
Level 2 Position	7.3 cm

Table C2. Data Summary for Level 1 with an Angular Position of 0.2π

No.	Radial Position, r/R_s	v_s m/s	ϕ_T	ϕ_{up}	ϕ_{dn}	Time Lag up (ms)	Time Lag dn (ms)	v_{up} (m/s)	v_{dn} (m/s)
49	0.768	0.0683	0.174	0.030	0.144	12.0	16.2	0.412	0.305
50	0.768	0.1412	0.147	0.055	0.092	16.8	16.8	0.294	0.294
51	0.768	0.2307	0.151	0.024	0.127	59.0	18.5	0.084	0.267
52	0.768	0.3115	0.178	0.031	0.147	18.0	14.5	0.274	0.341
53	0.650	0.0683	0.113	0.041	0.072	13.0	22.0	0.380	0.225
54	0.650	0.1412	0.092	0.025	0.067	15.0	16.0	0.329	0.309
55	0.650	0.2307	0.121	0.053	0.068	14.4	17.5	0.343	0.282
56	0.650	0.3115	0.129	0.035	0.094	11.8	15.6	0.419	0.317
57	0.407	0.0683	0.087	0.074	0.013	18.2	10.8	0.271	0.457
58	0.407	0.1412	0.098	0.063	0.035	18.6	19.8	0.266	0.249
59	0.407	0.2307	0.118	0.060	0.058	19.5	22.5	0.253	0.220
60	0.407	0.3115	0.151	0.094	0.057	14.8	18.0	0.334	0.274
61	0.223	0.0683	0.074	0.047	0.027	13.4	13.0	0.369	0.380
62	0.223	0.1412	0.093	0.049	0.034	7.0	16.6	0.706	0.298
63	0.223	0.2307	0.096	0.076	0.020	10.0	18.0	0.494	0.274
64	0.223	0.3115	0.122	0.094	0.028	19.4	13.2	0.255	0.374
						13.2	10.6	0.374	0.466

Table C3. Data Summary for Level 1 with an Angular Position of 0.4π

No.	Radial Position, r/R	v_s (m/s)	ϕ_T	ϕ_{up}	ϕ_{dn}	Time Lag up (ms)	Time Lag dn (ms)	v_{up} (m/s)	v_{dn} (m/s)
33	0.774	0.0683	0.165	0.066	0.099	29.0	19.0	0.170	0.260
34	0.774	0.1412	0.153	0.062	0.090	23.8	15.8	0.280	0.313
35	0.774	0.2307	0.144	-	0.144	-	11.4	-	0.433
36	0.774	0.3115	0.165	-	0.165	-	9.2	-	0.537
37	0.643	0.0683	0.102	0.030	0.072	20.8	22.6	0.238	0.219
38	0.643	0.1412	0.061	0.030	0.031	23.0	22.8	0.215	0.217
39	0.643	0.2307	0.097	-	0.097	-	11.2	-	0.441
40	0.643	0.3115	0.109	-	0.109	-	10.4	-	0.475
41	0.407	0.0683	0.057	0.031	0.026	16.4	10.6	0.301	0.466
42	0.407	0.1412	0.073	0.038	0.035	18.6	17.4	0.266	0.284
43	0.407	0.2307	0.094	0.035	0.059	10.0	16.0	0.494	0.309
44	0.407	0.3115	0.117	0.015	0.102	8.8	11.2	0.561	0.441
45	0.131	0.0683	0.031	0.031	-	18.6	-	0.266	-
46	0.131	0.1412	0.052	0.046	0.007	18.6	21.6	0.266	0.229
47	0.131	0.2307	0.080	0.078	0.002	14.0	22.0	0.353	0.225
48	0.131	0.3115	0.113	0.057	0.057	8.0	5.8	0.618	0.852

Table C4. Data Summary for Level 1 with an Angular Position of 0.6π

No.	Radial Position, r/R	v_s (m/s)	ϕ_T	ϕ_{up}	ϕ_{dn}	Time Lag up (ms)	Time Lag dn (ms)	v_{up} (m/s)	v_{dn} (m/s)
17	0.768	0.0683	0.229	-	0.229	-	20.4	-	0.242
18	0.768	0.1412	0.184	-	0.184	-	26.6	-	0.186
19	0.768	0.2307	0.294	-	0.294	-	12.6	-	0.392
20	0.768	0.3115	0.206	-	0.206	-	10.8	-	0.457
21	0.591	0.0683	0.121	0.038	0.083	20.8	16.4	0.238	0.301
22	0.591	0.1412	0.112	0.040	0.072	17.0	18.0	0.291	0.274
23	0.591	0.2307	0.159	0.042	0.117	12.0	14.0	0.412	0.353
24	0.591	0.3115	0.116	-	0.116	-	12.2	-	0.405
25	0.394	0.0683	0.092	0.070	0.022	21.0	19.4	0.235	0.255
26	0.394	0.1412	0.092	0.049	0.043	17.2	30.0	0.287	0.165
27	0.394	0.2307	0.116	0.077	0.039	20.5	47.5	0.241	0.104
28	0.394	0.3115	0.180	0.073	0.107	13.0	15.6	0.380	0.317
29	0.131	0.0683	0.060	0.060	-	19.4	-	0.255	-
30	0.131	0.1412	0.087	0.061	0.026	22.2	-	0.223	-
31	0.131	0.2307	0.112	0.094	0.018	19.5	29.0	0.253	0.170
32	0.131	0.3115	0.130	0.117	0.013	12.0	7.0	0.412	0.706

Table C5. Data Summary for Level 1 with an Angular Position of 0.6π

No.	Radial Position, r/R	v_s (m/s)	ϕ_T	ϕ_{up}	ϕ_{dn}	Time Lag up (ms)	Time Lag dn (ms)	v_{up} (m/s)	v_{dn} (m/s)
1	0.768	0.0683	0.116	-	0.116	-	20.2	-	0.245
2	0.768	0.1412	0.106	-	0.106	-	15.6	-	0.317
3	0.768	0.2307	0.168	-	0.168	-	12.8	-	0.386
4	0.768	0.3115	0.173	-	0.173	-	11.6	-	0.426
5	0.610	0.0683	0.084	0.058	0.026	17.4	15.6	0.284	0.317
6	0.610	0.1412	0.115	0.076	0.039	28.4	12.4	0.174	0.398
7	0.610	0.2307	0.142	0.084	0.058	19.0	16.0	0.260	0.309
8	0.610	0.3115	0.189	0.088	0.101	13.2	12.8	0.338	0.386
9	0.427	0.0683	0.073	0.056	0.017	18.6	25.0	0.266	0.198
10	0.427	0.1412	0.125	0.125	-	21.6	-	0.229	-
11	0.427	0.2307	0.149	0.149	-	15.4	-	0.321	-
12	0.427	0.3115	0.156	0.156	-	12.4	-	0.398	-
13	0.243	0.0683	0.027	0.027	-	20.2	-	0.245	-
14	0.243	0.1412	0.037	0.037	-	21.4	-	0.231	-
15	0.243	0.2307	0.099	0.065	0.034	21.6	24.0	0.229	0.206
16	0.243	0.3115	0.128	0.084	0.044	21.2	12.0	0.233	0.412

Table C6. Data Summary for Level 2 with a Superficial Gas Velocity of 0.3115 m/s

No.	Angular Position, rad	Radial Position, r/R	ϕ_T	ϕ_{up}	ϕ_{dn}	Time Lag up (ms)	Time Lag dn (ms)	v_{up} (m/s)	v_{dn} (m/s)
18	0.2π	0.755	0.083	0.021	0.062	54.0	22.0	0.078	0.191
19	0.2π	0.610	0.072	0.022	0.050	65.0	36.5	0.065	0.115
20	0.2π	0.374	0.076	0.033	0.043	43.0	29.0	0.098	0.145
21	0.2π	0.164	0.101	-	0.101	-	30.5	-	0.138
6	0.4π	0.761	0.085	0.048	0.037	33.0	27.5	0.128	0.153
7	0.4π	0.630	0.040	0.024	0.016	75.5	46.5	0.056	0.091
8	0.4π	0.394	0.024	0.014	0.010	63.5	65.0	0.066	0.065
9	0.4π	0.210	0.035	0.016	0.019	30.0	37.0	0.140	0.114
10	0.6π	0.768	0.023	0.014	0.009	44.5	55.5	0.095	0.076
11	0.6π	0.623	0.031	-	0.031	-	47.5	-	0.089
12	0.6π	0.387	0.037	-	0.037	-	42.5	-	0.099
13	0.6π	0.144	0.038	0.013	0.025	36.5	24.5	0.115	0.172
14	0.8π	0.768	0.037	0.010	0.027	60.0	27.5	0.070	0.153
15	0.8π	0.623	0.037	0.020	0.017	65.5	34.5	0.064	0.122
16	0.8π	0.387	0.029	-	0.029	-	37.0	-	0.114
17	0.8π	0.171	0.042	-	0.042	-	25.5	-	0.165

Table C7. Intermediate Integrated Values

Level	Angular Position, rad.	v_s (m/s)	$\int_0^R v_{up} \phi_{up} r dr$ (m ³ /s)	$\int_0^R v_{dn} \phi_{dn} r dr$ (m ³ /s)	$\int_0^R \phi_T r dr$ m ²
1	0.2 π	0.0683	3.88×10^{-5}	5.10×10^{-5}	2.79×10^{-4}
1	0.2 π	0.1412	2.93	4.15	2.52
1	0.2 π	0.2307	3.43	5.73	2.88
1	0.2 π	0.3115	4.72	7.50	3.37
1	0.4 π	0.0683	2.01	4.01	2.70
1	0.4 π	0.1412	2.37	3.43	2.23
1	0.4 π	0.2307	1.45	9.24	2.36
1	0.4 π	0.3115	1.09	14.32	3.02
1	0.6 π	0.0683	1.63	7.07	3.50
1	0.6 π	0.1412	1.83	4.75	3.03
1	0.6 π	0.2307	2.99	14.33	4.49
1	0.6 π	0.3115	2.46	14.26	3.84
1	0.8 π	0.0683	1.83	3.21	1.96
1	0.8 π	0.1412	2.60	3.88	2.32
1	0.8 π	0.2307	4.24	7.35	3.34
1	0.8 π	0.3115	5.33	9.60	3.79
2	0.2 π	0.3115	0.395	1.960	1.753
2	0.4 π	0.3115	0.703	0.657	1.180
2	0.6 π	0.3115	0.157	0.521	0.671
2	0.8 π	0.3115	0.155	0.791	0.797

Table C8. Integrated Flowrate and Void Fraction

Level	v_s (m/s)	$Q_{A\text{ up}}$ (m^3/s)	$Q_{A\text{ dn}}$ (m^3/s)	ϕ_T
1	0.0683	0.602×10^{-4}	1.23×10^{-4}	0.0773
1	0.1412	0.632	1.03	0.0742
1	0.2307	0.780	2.35	0.0895
1	0.3115	0.875	2.88	0.0974
2	0.3115	0.0898	0.2508	0.0306

APPENDIX D: Data Summary for Verification of Cross-Covariance Technique

Table D1 Cross-Covariance Function Peak Fractions and Time Fractions of Bubble Flow For Bubble Flow in a Tube.

Cross-Covariance Function Peak Fraction			Time Fraction of Bubble Flow				
Chord up, cm	Chord dn, cm	Fraction up	Fraction down	tape length up, ft	tape length dn, ft	Fraction up	Fraction dn
8.91	8.70	0.506	0.494	50	50	0.50	0.50
3.33	4.16	0.445	0.555	40	50	0.444	0.556
0.35	0.91	0.278	0.722	20	50	0.286	0.714
1.57	8.10	0.162	0.838	10	50	0.167	0.833
1.09	6.81	0.138	0.862	10	80	0.111	0.889
3.20	1.25	0.719	0.281	70	30	0.700	0.300
8.90	1.80	0.832	0.168	50	10	0.833	0.167
7.62	0.95	0.889	0.111	80	10	0.889	0.111
4.44	3.48	0.561	0.439	50	40	0.556	0.444

Chapter V

CONCLUDING REMARKS

This chapter summarizes the conclusions presented in Chapters III and IV. Recommendations for future work are presented.

Conclusions

The comparison of one and two-stage airlift towers based on mass transfer rates and efficiencies yielded the following conclusions:

1) The use of a multi-stage airlift tower has merit in gas-liquid contacting. Oxygen transfer coefficients ($K_L a$) of over 25 min^{-1} (1500 hr^{-1}) were obtained at a superficial gas velocity of 2728 cm/min for a sodium sulfite-air system in a two-stage tower. At a superficial gas velocity of 2262 cm/min the $K_L a$ for the two-stage tower was 54 percent higher than in the one-stage system.

2) The use of a multi-stage airlift tower requires more reactor volume than the single stage tower of equal liquid volume, but the oxygen transfer coefficient based on dispersion volume is still 27 percent higher than in the one stage tower at a superficial gas velocity of 2262 cm/min.

3) At low gas velocities the two-stage and one-stage towers have equivalent mass transfer characteristics. At a superficial gas velocity of 1300 cm/min the $K_L a$ levels off for the one-stage tower, while the $K_L a$ for the two stage tower increases linearly with superficial gas velocity in the range studied.

4) The two-stage tower becomes more efficient than the single stage tower at oxygen transfer rates larger than 180 m mole/l hr .

Bubble flow in the downflow section of the airlift tower has net upward and downward components. A technique based on time series analysis was developed to obtain the velocity and time fraction of bubble flow for each component. Resistivity probes were employed to obtain dependent time series indicating the presence of the gas or liquid phase at a point. The cross-covariance function of these series was bimodal with local maxima giving rise to the time lag characteristics of each component of flow. The time fraction of flow was found to be equal to the peak fraction of the bimodal cross-covariance function, linearly translated so that the function at zero lag has a value of zero. This technique was developed theoretically and verified experimentally. A number of significant conclusions can be drawn concerning the technique.

1) The appearance of bubbles at a point in a gas-liquid flow field is a random occurrence.

2) The autocorrelation function for random bubble flow is modeled by equation (13).

3) The cross-correlation function is distinguished from the autocorrelation function in that the theoretical lag may be non/zero and is not constant. A reasonable model for the cross-correlation function is prescribed as equation (41).

The technique developed was employed in a study of the downflow section of the airlift tower. The significant conclusions are:

1) Bubble flow in the downflow section of the airlift tower has upward and downward components of velocity.

2) The downflow of air at a level of 4.5 cm below the top edge of the baffle ranged from $1.23 \times 10^{-4} \text{ m}^3/\text{s}$ at a superficial gas velocity of 0.0683 m/s to $2.88 \times 10^{-4} \text{ m}^3/\text{s}$ at a superficial gas velocity of 0.3115 m/s.

3) The flowrate of air carried from the downflow section into the upflow section was $0.2508 \times 10^{-4} \text{ m}^3/\text{s}$ at a superficial gas velocity of 0.3115 m/s .

4) The bubble flow field was essentially symmetric about the angular position.

5). The bubble flow at the upper level of the airlift tower was downward at a large radius and upward near the center of the tower.

The velocities and time fractions of flow in complex two phase flow systems can be found through an analysis of the cross-covariance functions characteristic of the flow field. The techniques developed in this work to extract this information from bimodal cross-covariance functions is general, and should be employed in other multi-phase system.

Recommendations

The scale-up of one-stage and multi-stage airlift towers needs to be examined. The magnitude of improvement of mass transfer characteristics observed with 20 l staged airlift towers may be different than that observed in larger systems.

The motivations for staging in fermentation systems are to increase mass transfer rates and to achieve greater cell yields by employing partial mixing. The one-stage and two-stage towers should be examined under continuous fermentation. The organisms chosen for this study should have high growth rates with large oxygen consumption rates. The effect of staging on mass transfer is more apparent under large oxygen transfer rates.

Some preliminary studies of the one-stage tower under batch fermentation were conducted. The tower dimensions are described in Chapter

III. A mixed culture, obtained from a soil sample, was grown on a glucose and salts medium as shown in Table 1. The fastest growing organisms in the soil sample were selected for use.

A paramagnetic oxygen analyzer was used to measure the oxygen concentration of the exit gas. The dissolved oxygen concentration was measured in the upflow and downflow sections of the airlift tower. An oxygen balance yielded the values of the oxygen transfer coefficient which is shown in Fig. 1 as a function of cell concentration for the one-stage airlift tower. The surface tension was measured to be 47.5 dynes/cm, and the liquid density was 1.015 g/cm³. Foaming problems were controlled by use of Dow Corning silicone Antifoam agent. The culture was in the exponential growth phase. This technique was workable in the 20 l system.

Turbulent two-phase flow can be characterized by its statistical properties. T. Y. Chen⁽²⁾ observed bimodal cross-covariance functions in solid flow through a tube. The technique developed in Chapter IV for the analysis of gas-liquid flow can be applied to gas-solid and liquid-solid flow.

The airlift tower should be investigated more thoroughly, increasing the number of data points obtained at each level and increasing the number of levels investigated. The statistical methods developed can be employed in the investigation of larger airlift towers.

The bubble flow was analyzed in this study along the net upward and downward directions of flow. The turbulent nature of the flow is such that a horizontal component of flow exists. This can be examined using similar techniques.

References

1. Bauer, S. and J. Shiloach, "Maximal Exponential Growth Rate and Yield of E. Coli Obtainable in a Bench Scale Fermentor," Biotech. and Bioengg., 16, 933 (1974).
2. Chen. T. Y., personal communication (1977).

Table 1. Composition of Fermentation Medium

$C_6H_{12}O_6$	30 g/l
Nutrient Broth	3 g/l
Na_2HPO_4	3.8 g/l
KH_2PO_4	3.5 g/l
$(NH_4)_2SO_4$	3.5 g/l
$MgSO_4 \cdot 7H_2O$	1 g/l
Trace Metal Solution	3 ml/l

Trace Metal Solution

$FeCl_3 \cdot 6H_2O$	27 g/l
$Na_2MoO_4 \cdot 2H_2O$	2 g/l
$CoSO_4 \cdot 7H_2O$	2 g/l
$ZnSO_4 \cdot 7H_2O$	2 g/l
$CaCl_2$	0.8 g/l
H_3BO_3	100 ml/l

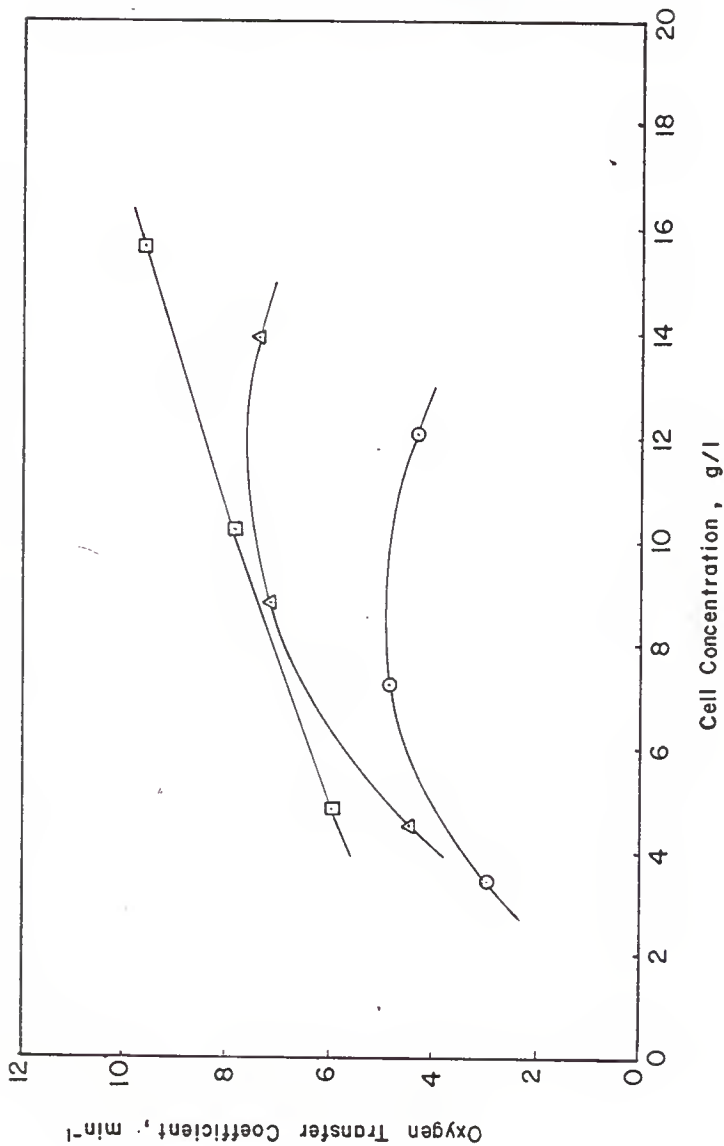


Fig. 1. Oxygen Transfer Coefficient as a Function of Cell Concentration for the One Stage Air-Lift Tower with Superficial Gas Velocity as a Parameter; ○ $V_s = 736$ cm/min, △ $V_s = 1431$ cm/min, □ $V_s = 1996$ cm/min.

Acknowledgement

The author expresses his sincere gratitude to his advisor, Dr. L. E. Erickson, for his support and guidance throughout the course of this work.

The guidance of Dr. K. Oki, Dr. D. Hasza and Dr. L. T. Fan was very valuable in the work presented as Chapter IV. The aid of D. Beardmore in Chapter III and J. Feldhausen in Chapter IV is also gratefully acknowledged.

This work was partly funded by NSF grants ENG 74-11531 and ENG 77-16999.

OXYGEN TRANSFER AND BUBBLE FLOW
IN SPLIT CYLINDER AIRLIFT TOWERS

by

MARK E. ORAZEM

B.S., Kansas State University, 1976

.

AN ABSTRACT OF A MASTER'S THESIS

submitted in partial fulfillment of the

requirements for the degree

MASTER OF SCIENCE

Department of Chemical Engineering

KANSAS STATE UNIVERSITY
Manhattan, Kansas

1978

One of the more promising contactor designs for high mass transfer rates with low power consumption is the airlift tower. The mass transfer coefficients reported in the literature for the airlift tower were compared to the bubble column, agitated vessel, staged bubble column and stage agitated vessel. Staging has been shown to improve the mass transfer characteristics of bubble columns and agitated vessels.

The oxygen transfer characteristics of a two stage split cylinder airlift tower were investigated and compared to those of a similar single stage airlift tower of equal liquid volume using a sodium sulfite-air system. At superficial gas velocities from 0.120 to 0.200 m/s no difference in $K_L a$ was apparent. The $K_L a$ was significantly larger in the two stage tower for a gas velocity between 0.200 and 0.455 m/s. At 0.455 m/s a $K_L a$ of 25.2 min^{-1} was achieved in the two stage system, and at 0.377 m/s the two stage tower had a 54 percent larger $K_L a$ than the single stage. A comparison of dispersion volume based $K_L a$ showed a 27 percent larger value at a gas velocity of 0.377 m/s. The performance ratio for the two-stage tower was larger than that for the single stage tower at oxygen transfer rates greater than 180 m mole/l hr.

Bubble flow in the airlift tower has both upward and downward components. A technique based on time series analysis was developed to obtain the velocity and time-averaged void fraction for each component of bubble flow. This technique was derived theoretically and verified experimentally.

The technique was employed in a study of the downflow section of an airlift tower for an air-water system. The downflow of air at the upper level of the tower ranged from $1.23 \times 10^{-4} \text{ m}^3/\text{s}$ at a superficial gas velocity in the upflow section of 0.0683 m/s to $2.88 \times 10^{-4} \text{ m}^3/\text{s}$ at 0.3115 m/s.

The flow rate of air carried from the downflow section into the upflow section was $0.2508 \times 10^{-4} \text{ m}^3/\text{s}$ at a superficial gas velocity of 0.3115 m/s .